UNIVERSITA' DEGLI STUDI DI PISA

Facoltà di Ingegneria

Corso di Laurea in Ingegneria Biomedica

Tesi di Laurea Magistrale

STUDY AND DEVELOPMENT OF A SENSORIZED PLATFORM FOR THE MONITORING OF LVAD-IMPLANTED PATIENTS

Relatori:

Prof.ssa Arianna Menciassi

Dr.ssa Monica Vatteroni

Candidato:

Maura Cuppone

24 Settembre 2013

Anno Accademico 2012-2013

A mio nonno

TABLE OF CONTENTS

INTRODUCTION

Diseases of the heart and circulatory system are the main cause of death in Europe, accounting for over 4 million deaths each year. In particular, heart failure by itself accounts for almost 1.1 million deaths each year and it is more common among old people, in fact approximately 6% to 10% of people older than 65 years are affected by this disease.

Heart failure is an abnormal health condition characterized by the inability of the heart to supply sufficient blood-borne nutrients for the body's metabolic demands. It is caused by heart-related factors, above all myocardial infarction, cardiogenic shock and myocardial infection, but also valve deformity, progressive coronary artery diseases, congenital defects diseases or external factors, such as hypertension, increased cardiac demands or increased volume load.

The last chance for heart failure has been cardiac transplantation but the disparity between availability and demand of heart donors leads to the death of a significant number of patients while waiting for a new heart. In fact, the number of patients in the European Union who potentially could benefit from cardiac transplantation in 2011 was estimated to be about 4,000, whereas the number of patients dying on waiting lists was estimated to be 5,500.

As a consequence, the mechanical support is considered as a viable option by taking over the pumping functions of the natural heart. The principal requirements for such support systems are that the mechanical components must be necessarily small and operate without failing under highly stressful conditions.

Nowadays, different mechanical ventricular assist devices (VADs) are in use. A VAD is a mechanical circulatory device used to partially reduce the payload of a failing heart. The last generation of VAD system consists of a pump, partially performing the fluid actuation work, a control unit and a power supply.

VADs are currently used as a bridge to heart transplantation, working as a temporary support for patients awaiting for a new organ. More recently, a revolutionary approach has been proposed, which regards the possibility to recur to the device therapy also as destination therapy for patients who are not candidates for transplantation (like old

people or patients who show the ability to recover the cardiac functions thanks to the pump help).

In order to enhance the VADs applicability for a long-term therapy usage, current research is going towards VADs miniaturization, sensorization and development of more comfortable devices able to dynamically respond to the support needs, depending on the subject activity.

A control system for continuous-flow LVAD able to automatically respond to physiologic cardiac demands is required. The current methodology makes use of pumps that operate at a fixed speed set according to the patient's activity level. This control is carried out by the physician, by setting the desired flow. Then, a VAD controller can have the capability to automatically adjusts the current and voltage applied to the pump to achieve and maintain the desired flow. Thus, it is clear that a continuous remote automatic monitoring system could guarantee much more consistency and safety. Especially to reach the goal of a long-term therapy, which needs at least the reduction of patient dependence on clinical management allowing her/him to return home, the development and integration of an automatic, robust and adaptive physiological control strategy is mandatory. The system should be able for fast response to physiologic cardiac demand by an automatic feedback mechanism which is directly based upon physiologic indicators of cardiac demand.

An innovative system for the implementation of all these features could be an integrated platform which aims for helping the physician to easily monitor the VAD and for giving a better life quality to the patient.

This intelligent platform is at the basis of this thesis and its components and their behavior are described in the following chapters.

CHAPTER 1

1.1 AN INNOVATIVE APPROACH FOR LVAD

Heart failure and related pathologies are the most frequent cause of death in the industrialized countries. The ageing of the world population and the low availability of heart donors with respect to the demand have led to the develop and experimentation of device therapy for patients with heart failure, not only as bridge to transplant, but also as destination therapy.

Heart failure (HF), also known as a cardiac or myocardial failure, is an abnormal health condition characterized by the inability of the heart to supply sufficient blood-borne nutrients for the body's metabolic demands. End-stage HF is the leading cause of mortality, morbidity and disability worldwide.

In fact, diseases of the heart and circulatory system (cardiovascular disease or CVD) are the main cause of death in Europe, accounting for over 4 million deaths each year. Nearly half (47%) of all deaths are from CVD (52% of deaths in women and 42% of deaths in men). The main forms of CVD are coronary heart disease (CHD) and HF. HF by itself accounts for almost 1.1 million deaths in Europe each year. More than one over seven women (15%) and one over ten men (10%) die from the disease.

The annual rate of hospital discharges for CVD in Europe in 2008 and 2009 was just under 2,500 per 100,000 population. HF, in particular, is estimated to cost the EU economy over €38 billion a year: around one-fifth of the overall cost of CVD.

Reported case fatality rates in 21 European countries show also more than three-fold differences in acute myocardial infarction case fatality rates, from 2.3% in Denmark to 8.6% in Belgium.

In developed European countries, 17% of all DALYs (Disability Adjusted Life Year) lost were due to CVD, making it the second largest single cause after neuropsychiatric disorders [1].

Furthermore, HF is more common among old people, in fact approximately 6% to 10% of people older than 65 years have HF, and approximately 80% of patients hospitalized with HF are more than 65 years old [2].

HF is caused by both heart-related factors, above all myocardial infarction, cardiogenic shock and myocardial infection but also valve deformity, progressive coronary artery diseases, congenital defects diseases or external factors, such as hypertension, increased cardiac demands or increased volume load.

The myocardial infarction, often called heart attack, is predominantly a condition of the left ventricle and occurs when the blood flow through one or more of the coronary arteries is obstructed. Leaving the area of the myocardium previously fed by the occluded coronary artery without oxygen, the result is the necrosis, or tissue death, of the heart involved area. After a myocardial infarction, the ability of the heart to function as a mechanical pump is directly related to the extent of the myocardial damage.

Cardiogenic shock is characterized by a decreased pumping ability of the native heart, causing a shock like state characterized by inadequate tissues perfusion. It usually occurs in conjunction with, or as a direct result of, ischemic damage to the heart muscle and is most often initiated by an acute myocardial infarction. The damaged heart muscle loses its contractility, reducing, on a mechanical level, the ejection fraction and cardiac output.

Finally, the latest of the main HF cause is the myocardial infection. This is usually the result of acute myocarditis, or infection of the heart muscle. Infection may also affect the endocardium, native or prosthetic valves, or the cardiac conduction system [3].

The last chance for HF has been cardiac transplantation, since Barnard successfully transplanted a human heart for the first time in 1967. But the disparity between availability and demand of heart donors leads to the death of a significant number of patients while waiting for a new heart. In fact, the number of patients in the European Union who potentially could benefit from cardiac transplantation in 2011 was estimated to be about 4,000, whereas the number of patients dying on waiting lists was estimated to be 5,500 [4]. As a result, the mechanical support results as a viable option: it has to take over the pumping functions of the natural heart and the principal requirements are that the mechanical components are necessarily small and must operate without failing under highly stressful conditions.

Nowadays different mechanical ventricular assist devices (VADs) are in use. A VAD is a mechanical circulatory device used to partially reduce the payload of a failing heart. It is different from an artificial heart, which is designed to completely replace cardiac function and generally require the removal of the patient's heart.

VADs are currently used as a bridge to heart transplantation, working as a temporary support for patients awaiting a new organ or, more recently, as destination therapy for patients who are not candidates for transplantation. It was observed that VADs could double survival at 1 year from implant and triple survival at 2 years [6].

Experiments and clinical experiences show that, if the heart is chronically unloaded, there is the possibility to recover the cardiac functions to the extent that the patient could be weaned from the device and a transplantation could be avoided. According to the clinical experience, the incidence of recovery, allowing left VAD (LVAD) explantation in patients affected by chronic cardiomyopathy, ranges from 18 to 72% [2]. But heart recovery mechanisms and related time are still unknown since today VADs are mainly implanted on patients in heart failure end stage with multiorgan failure. However, it has been observed in some of these patients a dramatic reduction of left ventricular size during unloading with a LVAD with improvement or even restoration of cardiac function. It is worth mentioning that it is necessary to study heart recovery even in younger patients in which LVAD would allow good functional recovery, but with low probability to be transplanted and high probability for the need of long term assistance.

In order to enhance the VADs applicability and to improve patient life quality, current research is going towards VADs miniaturization, sensorization and development of more comfortable devices able to dynamically respond to the support needs, depending on the subject activity. A control system for continuous-flow LVAD able to automatically respond to physiologic cardiac demands is required. The current methodology makes use of pumps that operate at a fixed speed that could be set according to the patient's activity level. This control is carried out by the physician, by setting the desired pump revolutions per minute (rpm) or flow. Then, a VAD controller can have the capability to automatically adjusts the current and voltage applied to the pump to achieve and maintain the desired flow.

Thus, it is clear that a continuous remote automatic monitoring system could guarantee much more consistency and safety. Especially to reach the goal of a long-term therapy, which needs at least the reduction of patient dependence on clinical management allowing her/him to return home, the development and integration of an automatic, robust and adaptive physiological control strategy is mandatory. It would be able to fast

respond to physiologic cardiac demand by an automatic feedback mechanism which is directly based upon physiologic indicators of cardiac demand.

An innovative system for the implementation of all these features could be an integrated platform which aims for helping the physician to easily monitor the VAD and for giving a better life quality to the patient.

As described in Figure 1, the platform proposed in this thesis will be composed by different blocks: a central control unit (ARU), pressure (PRS) and flow (FLW) sensors, a transcutaneous energy transfer system (TET) and a telemetry system (TEL). Each component is introduced in the following paragraphs.

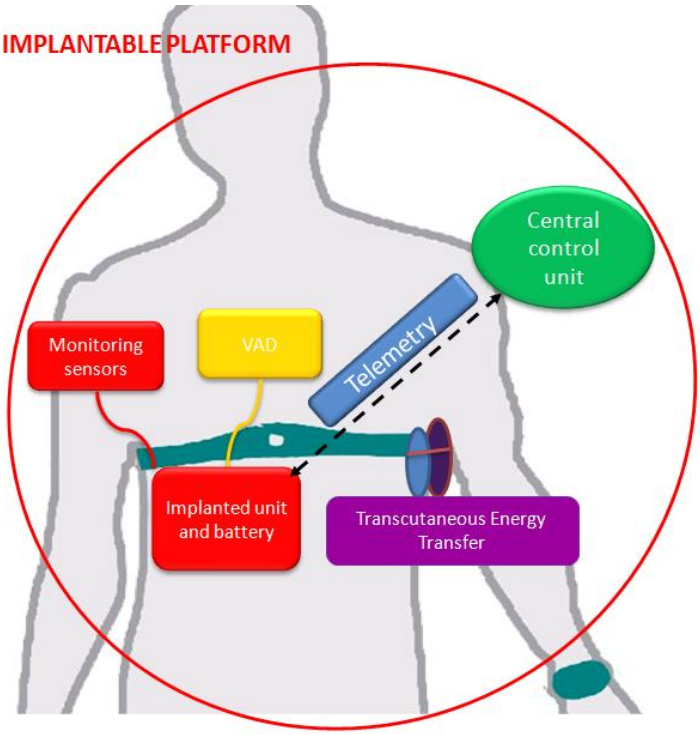

Figure 1 – Overview of the implantable platform within the SensorART system.

1.2 VENTRICULAR ASSIST DEVICE

Ventricular Assist Devices (VADs) are mechanical pumps used to reduce the payload of a deceased heart. VADs are implanted primarily in late stage congestive heart failure patients, in order both to facilitate cardiac recovery and, most often, to take time to the availability of a suitable heart. Nowadays, VAD systems have been proposed as a long term therapy alternative to heart transplantation.

In heart failure patients, therapy may include the need to reduce the cardiac workload and sustain systemic and coronary circulation by assisting mechanically the heart. In particular, mechanical pumps are usually used for this purpose in three different situations:

- *bridge-to-transplant:* in end stage heart decease, the heart cannot be saved and the patient is supported by circulatory assist to sustain systemic circulation, while waiting for a donor heart, suitable for transplantation.
- *bridge-to-recovery:* in patients with cardiogenic shock, myocardial infection or after a myocardial infarct, it is possible to try and save the heart by reducing the workload and/or increasing coronary circulation. In this way the heart may have sufficient time and circulation to recover.
- *destination therapy* or *alternative-to-transplant:* this is an embryonic therapeutic field designed for end stage heart failure patients, that are ineligible for other therapies such as a heart transplant, and the only solution is a permanent circulatory heart.

About the history of mechanical circulatory devices, the first bio-engineering objective was to facilitate cardiac surgery. In 1952, Dr. Dodrill reported the first use of mechanical support to perform a mitral commissurotomy with left heart bypass. The addition of an oxygenator for cardiopulmonary bypass by Dr. Gibbon, in 1953, marked the beginning of open heart surgery. Use of circulatory support then expanded outside of the operating room, and in 1963, Dr. DeBakey, together with Dr. Liotta, implanted the first left ventricular assist device as acute support for a patient in cardiogenic shock [7]. In 1969, Dr. Cooley was the first to use an artificial heart to bridge an acutely deteriorating patient to transplantation 3 days later. In 1982, Dr. DeVries performed the permanent implant of an artificial heart as destination therapy. Recognizing that many patients would benefit from just left ventricular support instead of heart transplant, the

National Heart, Lung, and Blood Institute (NHLBI) established the Clinical VAD program in 1975.

In the 1970s and 1980s, several ventricular assist systems were developed and they are collectively referred to as first generation VADs. They were large devices characterized by pulsatile flow, artificial heart valves, and typical rates between 80 and 100 times per minute with the use of either forced air or electricity. The first generation VADs with FDA (Food And Drug) approval in the USA are the Thoratec PVAD/IVAD, the Heartmate IP/VE/XVE, and the Novacor LVAD.

The Thoratec PVAD (paracorporeal) and IVAD (implantable) employ a pneumatic pulsatile VAD and mechanical valves, in the inflow and outflow ports to ensure unidirectional flow. The pump alternates positive and negative air pressure states that actuate a flexible blood sac within the rigid casing. Its stroke volume is 65 ml, providing an output between 1,3 and 7,2 l/min at rates between 20 and 110 beats per minute (bpm). Thoratec PVAD received FDA approval as a bridge to transplant in 1995 and as a bridge to recovery in 1998. It has been implanted in over 1700 patients since its introduction but it is still too large for pediatric support.

The Heartmate IP (implantable pneumatic) was similar to the Thoratec PVAD and it received the approval as a bridge to transplant by the FDA in 1994. This model was later supplanted by the Heartmate VE (Vented Electric) and then the Extended Vented Electric (XVE) in 2001. The main characteristic of its design is a textured titanium and polyurethane blood contact surface, which limits thromboembolism. It provides, also, a complete unloading of the left ventricle in refractory heart failure patients. A multicenter review of 146 VE and 98 XVE implants demonstrated the XVE decreased the major device malfunction at 1 year from 76% to 97%. The XVE received FDA approval for use as bridge to transplantation and destination therapy in 2003.

The Novacor LVAD is composed by two push-plates, electrically controlled, that compress a blood sac, forcing the blood to eject and two valves to prevent back flow. The technique used to pump the blood makes it possible to fill the pump without applying a negative pressure from outside. Novacor is characterized by a pump volume of 70 ml and a maximum flow of 10 l/min. It was demonstrated that the 75% of the implanted patients survive till transplant. Novacor received the FDA approval as a bridge to transplantation in 1988.

The need of increased durability, total implantability and smaller sizes brought to the development of the second generation VADs. These devices provide a continuous flow by using of a rotary axial pump which operates at high revolutions per minute (typical range: 8000–10 000 rpm). Compared to pulsatile VADs, the second-generation pumps are smaller, quieter, easier to implant, last longer and simpler in design with a fewer moving parts and no valves. The main disadvantage is the increased probability of suction events and gastrointestinal bleeding.

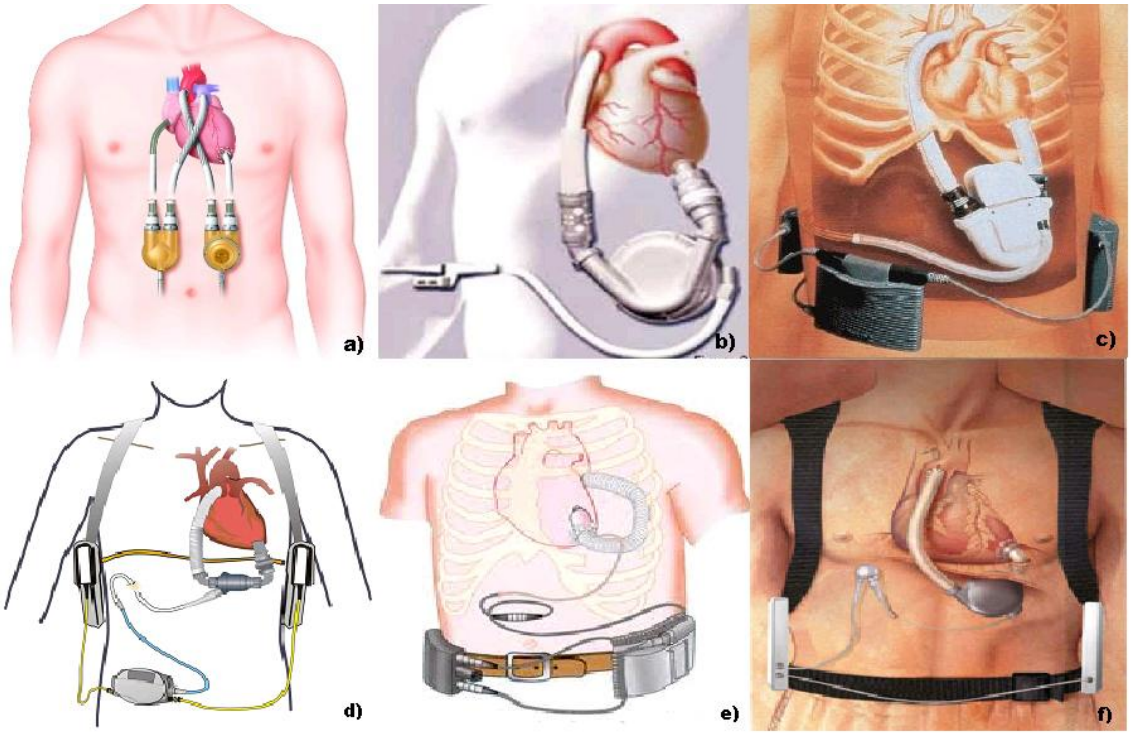

Figure 2 – a) Thoratec PVAD; b) Heartmate VE; c) Novacor LVAD; d) Heartmate II; e) Jarvik 2000; f) Levacor VAD.

From the second generation class, only the Heartmate II has been FDA approved as a bridge to transplant in 2008. The pump utilizes rotor flow to propel blood, its rate ranges from 6,000 to 15,000 rpm and produces flows up to 10 lpm. It is exceptionally durable, dependable, and thromboresistant. The internal pump is placed in the preperitoneal space, also in smaller patients due to its smaller size. An external controller, with the size of an adult's hand, monitors the pump and allows the patient to leave the hospital and do most daily life activities.

Another second generation VAD example is the Jarvik 2000 FlowMaker. It is a titanium pump with a direct current motor and a size of a C battery. The normal operating range

for the control system is 8000 to 12000 rpm, which generates an average pump flow rate of 5 l/min. The external controller is responsible for the control of the pump speed and the monitoring of the pump function and the remaining power in the batteries. Currently, the Jarvik 2000 does not have full FDA approval, but only for bridge-to-transplant use investigational studies. In Europe, the Jarvik 2000 has earned CE Mark certification for both bridge-to-transplant and lifetime use.

Ongoing research and development has led to so called third generation VADs. These pumps utilize a design that is bearingless, for a more durable system, and centrifugal, for a flatter and more sensitive pressure flow curve at lower rpms, reducing the risk of suction events. Currently approved VADs are implanted just below the diaphragm in the abdomen, or can sit outside the body on top of the abdomen. A driveline that contains the power wires exits the skin, usually on the right side of the abdomen, and connects to a controller that is worn on a belt. This controller is then connected to either a power-based unit, that plugs into the wall, or a large batteries, that can be worn in a holster, or a vest for portable use. The controller is the brain of the pump, and provides important information to the patient, caregivers, and medical team about VAD function and battery life [8].

The Levacor VAD is one of the next-generation blood pumps. It is a compact, centrifugal pump, with a completely magnetically levitated impeller that guarantee greater clearances and more optimized blood flow. Levacor VAD is also characterized by enhanced blood compatibility, multi-year reliability and durability and imperceptible noise and vibration.

There are also multiple other ventricular assist devices developed for short-term support. The Abiomed circulatory support system is one of the most widely used and provides temporary support for one or both sides of the natural heart in circumstances where the heart has failed, giving the patient's heart the opportunity to rest and potentially recover. Patients implanted of this device must remain in the hospital during the support phase. The AB5000 Ventricle is vacuum assisted technology, allowing the patient to be mobile. Multiple studies have shown that patient ambulation, or walking, greatly assists the recovery process. So the ventricle is equipped with a console that allow patients to leave their hospital rooms and walk on hospital grounds.

More in general, a VAD system, today, consists of a pump, partially performing the fluid actuation work, a control unit and a power supply. Traditionally, the pumps

employed in these systems are either displacement based pumps or radial-flow pumps. A displacement pump produces a pulsating outflow, inducing a mechanical force on a fluid, contained within a defined space, hence giving it motion. They are very large in size, excluding many patients from use, but easy to control due to their relative insensitivity to changes pre- and after- load conditions. Radial-flow pumps impart momentum to a fluid by a rotating device in the fluid, allowing for counter pulsation operation. They are generally much smaller, even suitable for pediatric use, but more difficult to control due to their high sensitivity to changing pre- and after-load conditions. The control unit monitors a number of physiological and physical parameters in order to control the way the pump works. The power supply is used to power the VAD and it may be external, requiring transcutaneous wires or tubes, or implanted (such as a battery) [3].

The VAD may be implantable or located outside the patient's body. VADs may also be used for assisting the left heart, LVADs, or the right heart, RVADs, or simultaneously both the left and right heart, BIVADs (Bi-Ventricular Assist Devices). In LVADs, the inlet of the VAD is connected to the heart via a cannula and the blood is returned to the heart by another cannula, usually connected to the ascending aorta (Figure 3).

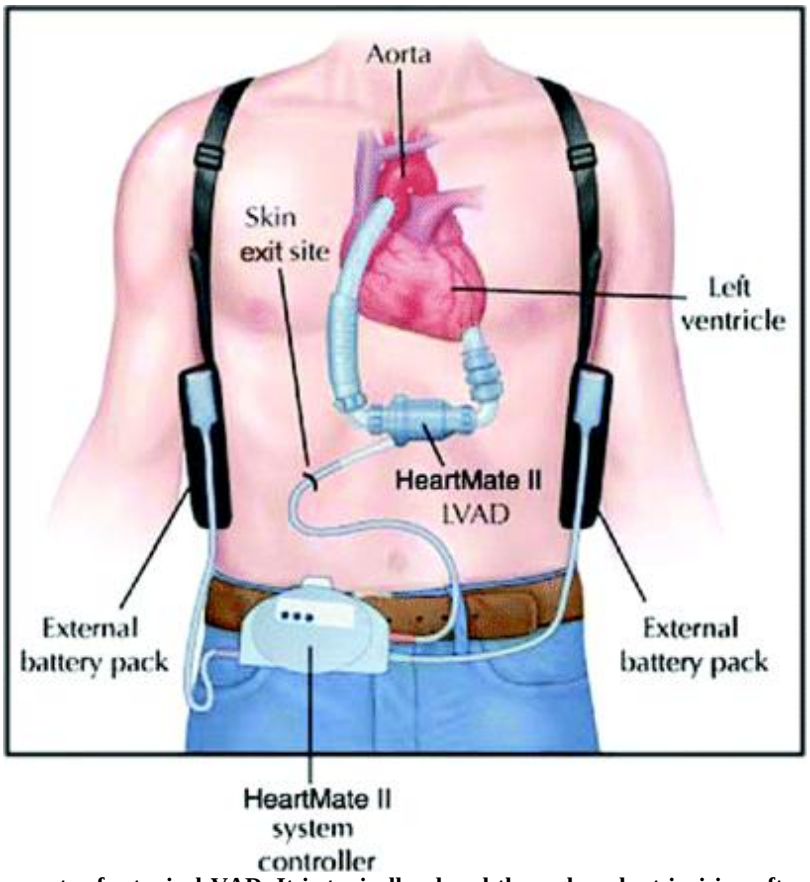

Figure 3 - Components of a typical VAD. It is typically placed through a chest incision after the patient has been positioned on a heart-lung bypass machine. A continuous-flow LVAD consists of a pump connected to the heart and aorta via an inflow and outflow cannula and a system controller that is typically worn on a belt. Power to the controller and pump is provided by external batteries or a power-based unit.

1.2.1 SYNERGY™ DEVICE

The Synergy™ Device (Figure 4) is a LVAD pump by CircuLite (Aachen, Germany).
The system is composed by CircuLite's proprietary micro-pump, an inflow cannula and an outflow graft, a percutaneous lead that is connected to a wearable external controller and a lightweight, rechargeable dual battery pack system. The pump has the size of a AA battery and provides up to 4.25 liters of blood flow per minute and it can be set to respond to the patient's cardiac output demands. The system is surgically implanted using a non-invasive mini-thoracotomy and the pump is placed in a pacemaker-like pocket.
The Micro-pump is characterized by a magnetically and hydrodynamically levitated and stabilized rotor motor and the design allows the avoidance of the contact between the blood and the motor and the minimization of the potential of thrombus formation.

The dual battery pack system is connected to the micro-pump via a percutaneous lead that exits the body in the abdominal area and power the SYNERGY system. The controller provides the patient with information on the battery status and alerts the patient to any change that needs attention.

An important feature of the SYNERGY system is its ability to work in conjunction with the patient's remaining native heart function. In the event of accidental power disconnection, patients may be supported by their remaining cardiac output until power can be restored to the system.

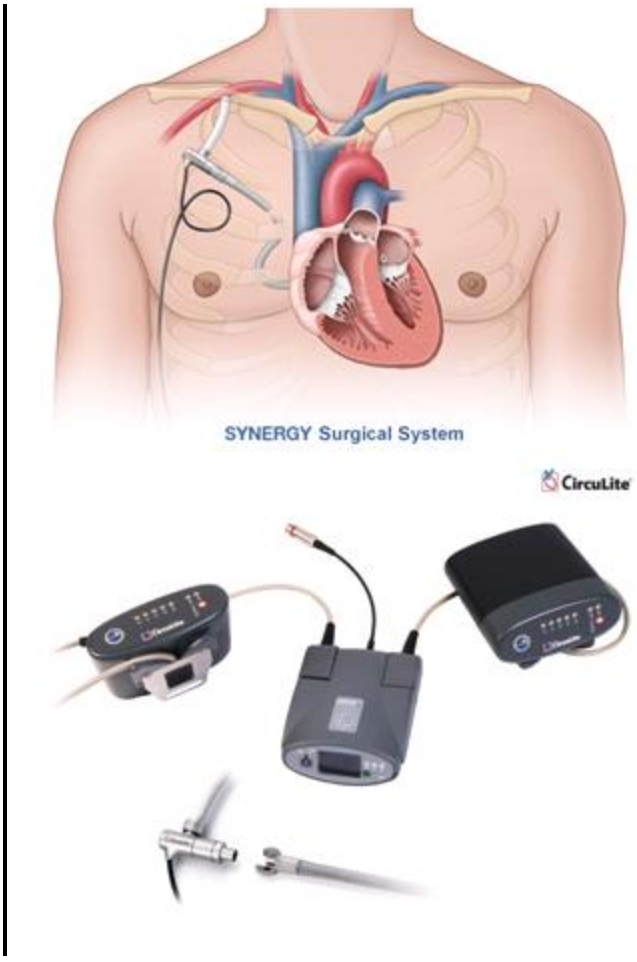

Figure 4 – SYNERGY device from Cyrculite

In the in-vitro setup for testing and validation, the device is fastened to an homemade hydraulic circuit made by a silicone tube, 3/8x1/16” inches (internal diameter x wall thickness) in size, connected to a tank filled with the fluid to be pumped into the flow

loop. The fluid contained the 48.3% of glycerine and the 51.7% of water to simulate the viscosity of blood and to avoid the bearings damage of the pump.

This LVAD has been used in the *in-vitro* scenario, which is exploited as test-bench to design and test the implantable platform proposed in this thesis.

1.3 CENTRAL CONTROL UNIT

Although the patients are well educated about the management of the device before the discharge, a continuous remote automatic monitoring system could add far more reliability and safety to the management of the device and the patient.

Together with the reduction of the ventricle workload, the pump also improves its oxygen supply, by increasing systemic arterial pressure. In the heart, the control is provided by the so called Frank–Starling mechanism [5], whereby stroke volume increases in response to the increased diastolic filling as a result of increased venous pressure. This behavior, which is mediated by the contractile properties of the myocardium, ensures a cardiac response to increased physiological demand. This local control is normally overcome by the central response, which acts by neural and/or humoral mediators and leads to an increased strength of contraction, reducing the endsystolic volume and increasing the heart rate. In heart transplant the central neural humoral responses are absent, as well as in VAD patients is absent. In this cases, the Starling mechanism alone suffices to regulate heart action. In this situations, there is not the same elastic ability of the organ to vary the stroke volume as in the natural ventricle anymore, so the control response is usually based on the control of the pump rate [9].

Thus, a recent aim of the physiological control system of rotary LVADs is to bring the patients' abnormal haemodynamic variables back to the normal range. Different variables have been proposed as criteria of normal condition. Some are critical and must be satisfied, such as:

A1) providing normal blood flow,

A2) maintaining arterial pressure within normal physiological range,

A3) avoiding pulmonary congestion,

A4) avoiding left ventricular suction.

A3 means that the left atrial pressure (LAP) or the left ventricular end diastolic pressure (LVPED) is less than an upper limit. The violation of this limit over extended period can cause severe problem like pulmonary congestion. This limit may be patient specific, but 15 mmHg is a general good reference. A4 implies that the LAP or LVPED must be maintained above a time-critical lower limit, usually the pleural pressure, so that the collapse of left ventricle will not happen. It is worth noting that all the key criteria are

about hemodynamic variables, which are co-dependent on each other. These criteria are satisfied at the same time for a normal person, but may not for a CHF patient with a LVAD, due to the remodeling and compensation mechanism of the body. A1 and A2 are treated with equivalently importance. There is no conclusive remark about which one should be selected if A1 is in conflict with A2. A3 is not as time critical as A1, A2, and A4, and usually deem to be true if A1 or A2 are satisfied.

Other proposed criteria, which are desired but not critical, are classified as secondary, such as:

B1) maintaining nonzero left ventricular outflow

B2) maintaining positive pump flow

B3) robust performance.

B1 is to make sure that aortic valve is open for a portion of the heart cycle, preventing the blood stagnation on the backside of the aortic valve. If the natural heart is too weak, this criterion may not be achieved when A1 is satisfied, but can be compensated by anti-coagulation drugs. B2 is to prevent the regurgitation of blood back from the aorta to the left ventricle in diastole, which in fact is acceptable at small amount. B3 is to guarantee the reliable performance of rotary LVADs in the presence of physiological state variations. This one is particularly important for long term application of rotary LVADs.

Some examples of control algorithm used over the years will be discussed in the following.

Parnis *et al* [10] used a proportional controller for the Jarvik 2000 VAD. Heart rate was obtained from the fundamental frequency of the motor current (I) waveform and set as a linear function with the pump rotational speed (ω). A limitation for this approach is the fact that a linear relation was supposed between the heart rate and the angular speed of the pump. In CardioWest C-70 and in the Utah Electrohydraulic Total Artificial Heart, the measured heart inflow pressure was used as the parameter to control cardiac output. The correlation between in-flow pressure and pumped volume has been well established and it is depicted in Figure 5.

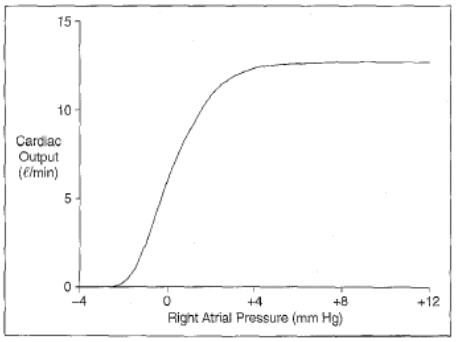

Figure 5 - Cardiac output vs Right atrial pressure

The same could be done with mechanical blood pump: a commutator controls the motor speed at a constant level that is requested from the physiological controller. The control law for the last one is implemented to duplicate the curve in Figure 5 is duplicated. The atrial pressure reference input can be changed to shift the curve along the x-axis depending on individual patient requirements.

Another example is given by Giridharan *et al* [11]. They proposed a different approach to physiological control of rotary blood pumps. Their method allows to implement an automatic response to changes in demands of physiological perfusion by maintaining a constant average pressure difference between the left ventricle and the aorta. Such system requires the implantation of two pressure sensors and the development of a gain scheduled proportional integral (PI) feedback controller.

The target of the control strategy is to achieve the physiological perfusion and this is done when the blood pump maintain and average pressure difference (ΔP) between the left ventricle and the aorta, close to a reference pressure (ΔPr). The feedback control algorithm will regulate ω within physiologically acceptable limits while minimizing the difference between ΔPr and ΔP.

Moreover , it is very important to keep oscillations of ω as low as possible in order to guarantee a longer pump life and patient's comfort. The electrical current of the pump (I) is used as a control input and it is subject to an inequality constraints $\omega_{\min} \leq \omega(I) \leq \omega_{\max}$, such that the quadratic objective function is minimized.

$$J = \int_0^t [(\Delta \mathrm{Pr} - \Delta P)^2 + r\dot{\omega}^2]dt$$

Where ω_{min} and ω_{max} are functions of the blood volume in the left ventricle, $\dot{\omega}$ is the rate of change of ω where this should satisfy the system of nonlinear hybrid equations which describes the circulatory system assisted by rotary blood pump. In order to maintain

ΔPr as much constant as possible, a proportional integral controller was selected to manipulate I according to the following control law:

$$I = Kp(\Delta \mathrm{Pr} - \Delta P) + Ki \int_0^t (\Delta \mathrm{Pr} - \Delta P)dt$$

where ΔP is the measured head pressure. The proportional (Kp) and integral (K_I) constants were selected to minimize J for different weighting. Different values for Kp and K_I to minimize J were obtained for two different types of rotary blood pumps: for an axial pump and a centrifugal pump. Tests were done using this controller and results showed that maintaining a constant average pressure difference between the left vetricle and aorta resulted in physiological perfusion over a wide range of physiological conditions including rest, light and strenuous exercise levels.

Another example of control algorithm was the one proposed by Bullister *et al* in 2002 [12]. It is a hierarchical algorithms whose aim is to control and monitor the blood pumps using pressure inputs measured by APEX pressure sensors (APSs) at pump inlet and outlet. The control algorithms has two level in order to adapt to various left ventricular diastolic filling pressure (LVDFP). The main goal of level 1 is to keep the LVDFP within a physician-programmable range. This was done by means of an integral control algorithm implemented with pump inlet pressure (*P*in) where this was used as an input and the pump speed control signal as the output. Moreover, level 1 outer loop control is also charged to maintain the arterial pressure within programmed limits and has a slower response time than the inner control loop. In particular, the outer loop changes the LVDFP set point of the nested inner loop when the arterial pressure reaches the programmed limit values.

On the other hand, level 2 control algorithm was implemented as an outer control loop around the inner level 1 control loop. The control input is the outlet pressure (*P*out), while the control output is the modified target LVDFP, that is sent to the level 1 control loop. When level 2 is active and the pulse rate is above a certain threshold, the desired target value for LVDFP is continuously updated to provide the feedback control for the target arterial pressures. So, the mean arterial pressure controlled by level 2 is kept constant thanks to an intermediate mechanism that actively adjust the level 1 effective target value of the LVDFP within its working ranges.

A very common problem that must be prevent in continuous LVADs is the collapse of the left ventricle. For this reason, Wu *et al* proposed a proportional integral controller

whose target is to minimize the sum of the aortic pressure tracking error and weighted head tracking error. In fact, during heart cycle, aortic pressure should be maintained relatively constant. However, during dramatic physiological disturbances such as a sudden change from rest to exercise, the left ventricular collapse may occur even if aortic pressure is maintained as constant as possible. When ventricular collapse occurs, the pressure and blood volume in the left ventricle decreases; as a consequence, a very efficient way to detect the onset of the ventricular collapse could be the monitoring of the difference of pressure across LVAD. This explains the necessity of controlling both the aortic pressure and the difference in pressure between the ventricles.

However, for invasive and non-invasive techniques, control algorithm had been developed over the years in order to control physiologically and adaptively the left ventricle assist devices and to avoid undesired phenomena, such as pumping states of left ventricular in which a collapse is caused by suction. The main requirements for this automatic control system are to ensure stable, reliable operation and to work at high power efficiency. Moreover, for long-term use, the control algorithm must stabilize the operation of the blood pump and meet changes in physiological demand.

The most frequent strategies, used to sense and monitor the relevant parameters for heart assisting devices, are based on:

- measurements during the act of driving the pump electrically,
- measurements of fluid-mechanical variables by incorporation of transducers,
- solutions in which the fluid-mechanical variables of pressure drop and flow-rate have been estimated indirectly,
- solutions in which suction and/or valve non-opening are detected,
- solutions in which the measurements available to the pump controller can be used to assess natural heart function,
- use of other sensors for miscellaneous purposes (such as fault detection).

The pressure transducer method is the most used one both because the sensors would allow the real time adjustment of the assistance device performance, thanks to a feedback loop, and because this method is used as a standard of comparison for other proposed control methods.

1.4 MONITORING SENSORS

The selection of suitable sensors that detect the changes in the body's metabolic demands is one of the important goals in designing LVADs control systems.

Presently, most of the pumps derive all their information from the pump's power consumption but use this information predominantly to monitor (to detect suction, low flow conditions, pump stoppage) and to trigger alarms. If the pump would be sensorized, it can take advantage also from physiological signals acquired by a set of sensors, all communicating with the auto-regulation unit, in order to monitor not only the status of the LVAD but also the patient.

Physical sensors could also allow assessing patient/LVAD hemodynamics relationship during assistance, in order to detect the contribution of the native heart. This issue may become important when the effect on recovery of drugs or other therapy (e.g. stem cells) has to be evaluated. Finally, monitoring native heart function during daily activity may give information about the effect of skeletal muscle endurance on myocardial recovery.

The sensors that can be used in the physiological control system of VADs are limited by the market and physical constraints. Physiological sensors are those sensors that can directly measure the cardiovascular physiological variables. Potential physiological sensors used in LVADs include oxygen saturation sensor, pressure sensor, flow rate sensor, and acceleration sensors [14].

Because of their high flow impedance and complication of blood clotting, the conventional flow sensors have never been used in any implantable LVAD. But, in this case, the flow rate information is highly desired, so the high accuracy ultrasonic flow meters are used. This type of flow sensor can be clamped outside the LVAD pump outlet cannula to measure the flow rate without surface contact with blood. Thus, they are totally impedance and thrombosis factor free.

Pressure sensors are also very important, in fact they have been suggested as an effective method for controlling a LVAD. As discussed in the previous paragraph, several control algorithms are based on the directly measured pressure feedback. Conventional pressure sensors are mainly used in LVAD applications only for the short term because they are responsible of drift and thermal problems. Fortunately, in the last years, they have been developed in a manner that might provide a longer working

period. For example, Apex Medical Inc. has designed what they have claimed to be a long-term implantable pressure sensor, called APS [15]. This pressure sensor uses a pressure-sensing diaphragm that can be built into the wall of any titanium pump or inlet cannula.

Physiological sensors are also grouped into two classes: the ex-body sensors for patient monitoring, and in-body sensors for VAD and patient monitoring. The in-body sensor data and VAD pump data will be sent through the body using a medical standard wireless protocol like MICS. In the case of continuous powering through an inductive link, it is also an option to retrieve the data through a load-modulated uplink, or send data to the VAD by power carrier modulation. Ex-body sensors for patient monitoring can be hardwired to the hardware unit, or connected through the same wireless protocol. By using hardwired sensors the problem is to overcome and to foresee a separate power supply for every sensor node.

1.5 TRANSCUTANEOUS ENERGY TRANSFER SYSTEM

The purpose of a transcutaneous signal transmission is to develop a system that transmit signals to and from a left ventricular assist device, leading to a decrease of the amount of cable through the skin. In the first project of the LVAD, the percutaneous cables were 23 with a diameter of 8mm. Over the year, the design process allowed to decrease the number to 7 cable and the cable diameter to 2.7 mm. This was possible by changing the placement of components as well as implementing a communication protocol, SPI, capable of transmitting and receiving the required signals through the same cable. Moreover, this cables are very stiff and they cause discomfort, limited range of motion and many health risks to the patient, because the exposure of the tissue to the cable increases the risk of infections.

For all these reasons, a transcutaneous energy transmission system was designed in order to exploit the capacity of time varying magnetic fields to transfer power across the skin to drive implantable biomedical devices without the use of any percutaneous wire.

Using inductive coupling, a primary coil located on the outside of the body would transfer the required energy to a secondary coil located on the inside of the body. In order to induce a magnetic field between the two coils, an AC power source is added. The only power supply available is a DC battery; therefore an inverter is designed to convert the energy. The power efficiency is found to be 10% over the system and 27% over the coils [18].

To bring some example, it is possible to mention the TET system proposed by Carr et al [18] (Figure 6). Here, a PWM controller was used to create a different frequency square wave. The coils used were 7 cm in diameter and made of 20 and 75 turns respectively. This ratio was determined in order to compensate the voltage drop across the coupled coils. It was also added a supplementary battery pack in order to prevent accidental power failure. For this reason, a switch was added and it is capable to read the input voltage of the pump. In this way, if the TET voltage dropped below 14.8V, the backup battery would power the system until the TET power reached a suitable level. The controller used for this TET is an open-loop system and its setting can be adjusted only by human intervention.

Future development could oversee the implementation of a feedback network to close the control loop in order to fulfill in every moment the desired condition.

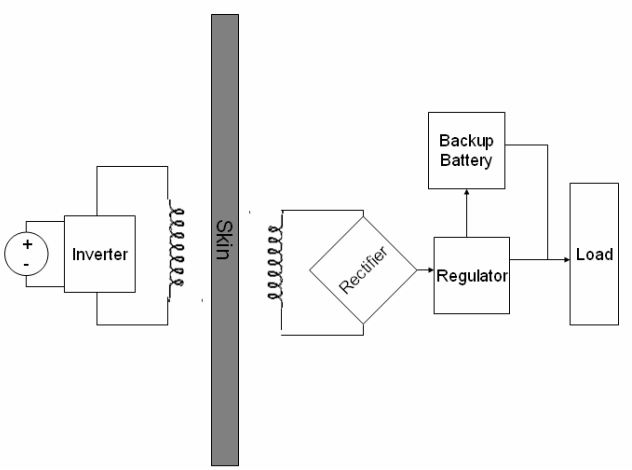

Figure 6 - Schematic of Carr et al. TET

An other example is the TET system designed by Dissanayake et al [19], it is used a DC voltage that is supplied by an external battery pack. A current resonant converter is then used to generate a high frequency sinusoidal current across the primary coil in order to produce a sinusoidal voltage in the secondary coil that is then rectified by the power conditioning circuit to provide a stable DC output in the implanted device. As shown in Figure 7, a DC inductor is added to the secondary pick up following the rectifier bridge in order to maximize the power transfer to the load. The DC inductor is important to sustain a continuous current flow in the pick up.

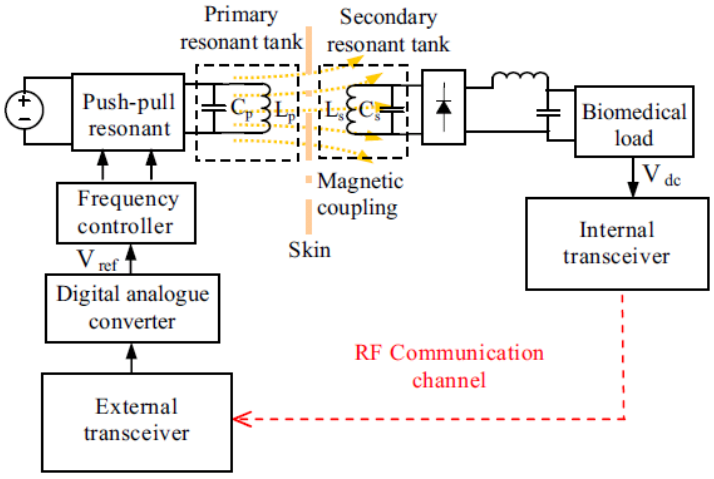

Figure 7 - Dissanayake et al. system architecture

Two transceivers are also integrated for data communication. The internal transceiver send the detected DC output voltage of the pickup to the external transceiver, through a RF communication channel. Then, the external transceiver task is to process the data and adjusts the duty cycle of the output PWM signal. In this way, the reference voltage (Vref) of the frequency control circuitry is adjusted and a Digital to Analogue Converter (DAC) is used for the PWM signal in order to obtain a variable reference voltage. By this variable reference voltage the frequency of the primary resonant converter is varied and, as a consequence, also the power delivered to the implantable system changes.

With respect to the state of the art, one of the main improvements of the proposed platform is the replacement of wired with wireless links to maintain not just two way data transmission, but also power support for the implant.

A TET system is basically a DC-DC converter built around a loosely coupled transcutaneous transformer. The primary coil, placed outside the body, is driven by a switching amplifier and it generates a magnetic field, which is partly picked up by the secondary coil, hereby, inducing a current. After rectification, a regulator or a feedback loop are used to ensure a constant output voltage despite variations in coupling factor or power drain.

From a technical standpoint, the transmitted power amount can vary from a few mW up to several W in the appropriate coupling conditions. The TET system will be used in synergy with an implantable rechargeable battery pack that will serve as a backup solution in case TET will fail or whenever the patient will need to stop TET (e.g. to take a shower), as safety norms request. Adoption of an implantable battery pack will drastically reduce failure risks related to the platform and give to the patient the opportunity to be free from cables for a while.

Furthermore, some issues about change in energy delivering have to be solved. For example the coupling between the external and internal coils will vary according to their orientation and posture or other potential sources of power delivery variations, arise from changes in circuit parameters and loading conditions. In order to maintain correct device function, the power delivered must be regulated to face these variations.

For these reasons, compared to percutaneous wires, TET systems is more complex to be managed and to operate under variable coupling conditions, because, in the majority of the cases, it result in a variation of the power transferred to the device. The typical

separations between the internal and external coils are in the range of 10-20 mm. If insufficient power is delivered to the load then the implanted device will not operate properly. If excessive power is delivered, then it must be dissipated as heat with the potential for causing tissue damage. Therefore, it is important to deliver the right amount of power matching the load demand.

The design of an inductive link for the supply of high power consuming implants is far from being a trivial task because it is necessary to include high efficiency, stability, reliability and patient's safety. A continuous compromise between power transfer efficiency, system dimensions and respect of safety standards, is the biggest challenge. Most relevant parameter is the implant power consumption: the higher the required power, the stricter becomes the freedom in the magnetic design. In high power systems all the possible sources of power loss have to be drastically reduced, and must include a feedback loop to constantly adjust the externally applied power.

From the regulatory standpoint, a specific energy absorption rate (SAR) up to 10W/kg is considered safe for operational exposure of head or trunk for an operating frequency below 10MHz. This SAR value is unlikely to produce any detrimental health effects on humans. By properly selecting the carrier frequency and by accurately design the TET system, a SAR below 10W/kg is considered a feasible threshold to comply with in order to supply an average of 11 W to the implanted system. It must be said the ICNIRP norms [20] are to be intended as a preliminary margin of a matter that is still to be investigated by the scientific community. This indication is really strict at the moment but the real tolerability limit is probably higher. Theoretical study and *in-vivo* testing will help in defining how this limit can be extended. On the other hand, improving the energy transfer efficiency (e.g. using a ferrite core in the secondary coil) will allow transmitting the target power amount, limiting the external magnetic field, fully complying the current limits.

1.6 TELEMETRY

Biomedical telemetry has been used primarily for the measurement of physiological signals at a distance, through wireless communication technologies. Physiological signals are acquired by means of a transducer, then post-processed and transmitted to an exterior monitor or a control equipment. But, one of the latest developments of biomedical telemetry is in the field of implantable medical devices (IMDs). Millions of people worldwide depend upon implantable medical devices. In fact, RF-linked implantable medical devices are already in use for a wide variety of applications, such as temperature monitors, pacemakers and defibrillators, functional electrical stimulators (FES), blood-glucose sensors, and cochlear and retinal implants. Usually they work on the MICS (Medical Implant Communication Service: 402 – 405 MHz) band, because of its advantages of being available worldwide and being feasible with low-power and low-cost circuits. This band reliably supports high-data-rate transmissions, falls within a relatively low-noise portion of the spectrum, lends itself to small antenna designs and acceptably propagates through human tissue. The critical point of the RF-linked implantable medical devices is the integrated implantable antenna, which enables the bidirectional communication with the exterior [22].

High frequency antennas dedicated to medical implants are rare in the literature but there is a number of different antenna designs that may be adapted for IMDs. Coil antennas are used for biomedical telemetry at low frequencies because they are compact when used in short distance links. One classic design is to use the tuning coil of the oscillator as the antenna, and thus get the antenna for free. Modern IMDs use far-field radio-frequency (RF) telemetry, which mainly are resonant electric antennas, in contrast to the coil antenna, which is a magnetic antenna. The implant and the base station contain a RF transceiver and use radio-frequency for communication. The communication range for RF telemetry is much longer than inductive telemetry (Figure 8). However, the implanted battery also needs to power the RF transceiver, so RF telemetry consumes much more energy than inductive telemetry.

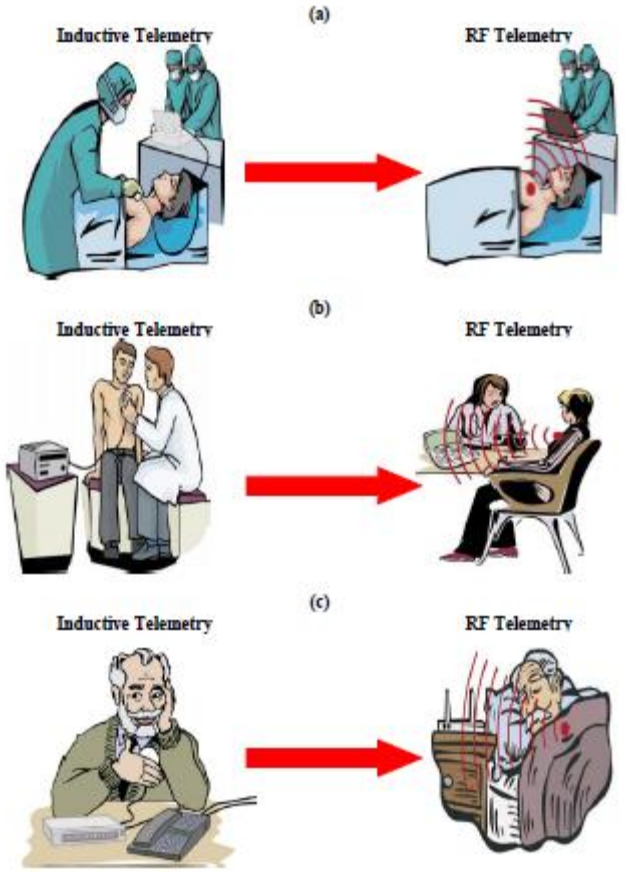

Figure 8 - Inductive Telemetry vs. RF Telemetry: (a) – During/Post Surgery, (b) – Follow-up Clinics, (c) – Home Monitoring

An interesting telemetry system was developed for a wireless endoscope by Shirvante et al. [21]. The system consists of a thermally stable low power transceiver, a microcontroller, a balun, and an antenna. In particular, a wide band antenna for transmitter and a narrow bandwidth antenna for receiver were designed. The receive antenna is a compact spiral monopole antenna with an area less than $100mm^2$. The overall length of the wire is approximately a quarter wavelength: $\lambda air /4 = 187mm$ at 402MHz for air medium. For the transmit antenna, it is necessary to consider the environmental variations. The pill experiences a change of relative permittivity and conductivity in the range of 40 to 70 and 0.08 S/m to 1.9 S/m, respectively, as it travels from mouth to intestine. A permittivity ε_r of 55 and a conductivity of 0.7 S/m have been used for simulation. The overall length of the antenna is selected in order to have $\lambda body/4=\lambda air/4\sqrt{\varepsilon r}= 26mm$.

An other example is the one from Kiourti *et al.*[22] who proposed patch design for implantable antenna and did numerical and experimental investigations in order to demonstrate its biocompatibility. This type of antenna are highly flexible in design and

shape, thus relatively simple to miniaturize and integrate into the shape of the IMD. For example, the hardware can be mounted on the existing hardware of the device to serve also as the ground plane. Patch antennas are also patient safe and guarantee high-quality communication with exterior equipment.

However, antennas for implantable telemetry systems are generally electrically small antennas, like most of antennas for wireless applications, but the implant will be located in a complex lossy medium and this influences their performance. Thus, it is necessary to investigate the electromagnetic properties of the human body in order to design a suitable antenna. Classical antenna theory mainly deals with radiating structures placed in vacuum or in air; this means that they are placed in a non-conducting environment with a permittivity of ε_0 = 8.854 * 10^-12 F/m. While, when the antenna is placed in a material with a higher permittivity, and with non-zero conductivity, the usual simplifications cannot be used [23].

The general challenge of an implantable antenna design is that the behavior of an free-air antenna is radically different from an implantable antenna due surrounding tissue with different electrical properties. Indeed, the human body consists of different tissue types as skin, muscle, fat, bone, blood (

Figure **9**).

Tissue	ε_{er}	σ_e (S/m)
Muscle	57.1	0.797
Fat (non infiltrated)	5.6	0.041
Lung	23.8	0.375
Skin (dry)	46.7	0.690
Skin (wet)	49.8	0.670
Bone Cancellous	22.4	0.235
Brain grey matter	57.4	0.739
Brain white matter	42.0	0.445

Figure 9 - Dielectrical properties for tissue at 403.5 MHz [23].

Due to the fact that the wavelength of electromagnetic wave in dielectric matter prolongs, the dimensions of an implantable antennas can be designed shorter. The shortening factor could be expressed by the following equation:

$$\lambda_m = \frac{\lambda_f}{\sqrt{\varepsilon_r}}$$

where
λ_m = wavelength in material,
λ_f = wavelength in free space,
ε_r = relative permittivity

By applying this equation a shortening factor between 2.3 (fat) till 7.5 (muscle, blood) can be calculated.

Furthermore, the analysis of the radio link has to consider a wave propagating not only from the antenna through the body but also into the air and over to the base-station antenna. It is hard to characterize this propagation, especially the radiation pattern from the implant one. Another complication is that the radiation characteristics are influenced by the tissues in the near-field of the antenna, and thus vary between different patients.

It is necessary to consider the following design challenges and restrictions in order to design an implantable antenna:

- size limitations mean that careful considerations in design must be made,
- power consumption must be minimal during data transmission,
- for the MICS band, a limited ERP (effective radiated power) of 25μW is required outside of the body,
- materials for biomedical implantation are limited to titanium, platinum or PEEK (Polyether ether ketone) (system can be encased as well),
- cannot have DC potential to the system nor the body,
- RF Losses in tissue (see Figure 10).

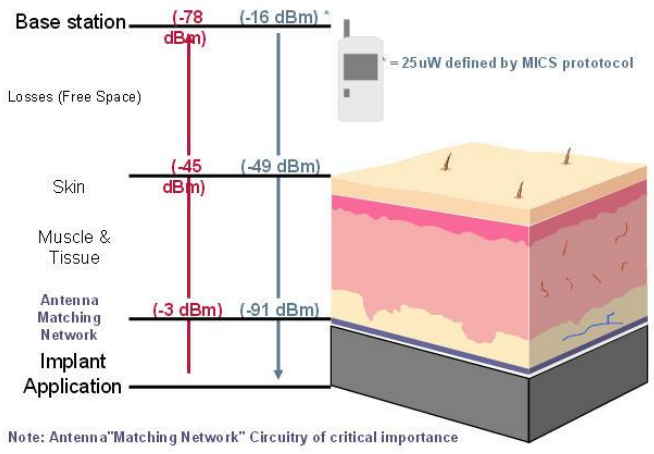

Figure 10 - Upstream and downstream RF losses due to tissue [24].

The main objective has not been to find the best antenna for use in a medical implant, but to get a valid figure for a reasonable antenna performance to be expected from a medical implant.

The simpler way to perform a successful design is following these steps:

- Choose an antenna type to be used (dipole, helix, loop antenna), depending on the required bandwidth, the communication electronics and the volume available.
- Perform an initial design considering a homogeneous lossless medium surrounding the antenna. In this way, the advantages are speeding up the simulation time and ensuring that the bandwidth reached by the antenna is "real" bandwidth and not due only to losses in the body.
- Miniaturize the design.
- Re-tune the antenna, after adding the losses in the homogeneous body model and the cover.
- Add a more realistic body phantom as the medium surrounding the antenna. Re-tune the antenna.

1.7 PROPOSED IMPLANTABLE PLATFORM

A revolutionary approach to reach the aforementioned aim could be the development of a implantable platform integrating on the VAD miniaturized innovative flow and pressure sensors and implementing a continuous monitoring strategy, with the purpose to optimize and personalize the heart unloading degree.

This implantable platform is one of the topics introduced in the framework of the European project SensorART (a remote controlled Sensorized ARTificial heart enabling patients empowerment and new therapy approaches).

The main goal of this project is to better understand patient-device interactions by providing technological improvements centered on the development of: wearable sensors, artificial intelligent algorithms, light-weight portable hardware controllers and "smart" signal processing algorithms. The advantages of such platform could be the steering and optimization of the pump function without intervention of a care-taker, thus leading to a greater independence of the patient and to the reduction in costs for personnel to realize home support. It could also be possible to study the biohumoral signals during the assistance and cellular changes before and after the assisting therapy and to measure the natural heart delivery capacity according to the assisting time.

The different hardware and software components, included in SensorArt, could lead to the development of an open, interoperable, extendable system that improves the quality of the patients treatment as well as the workflow of the specialists.

In particular this system will include different modules (Figure 11). It integrates sensors, signal acquisition module, hardware controller, a remote control framework and a decision support system.

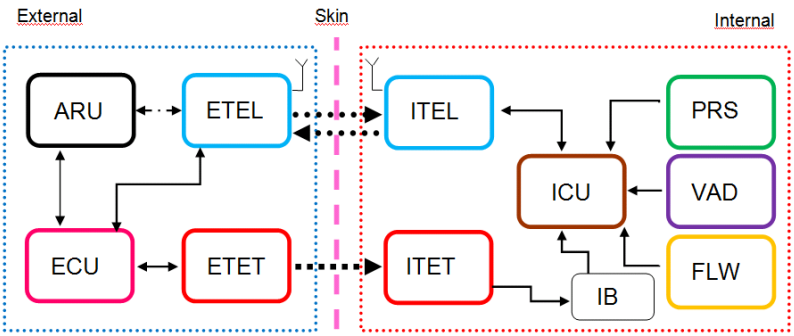

Figure 11- Block diagram of the proposed platform.

Overview of the implantable platform within the SensorART system.

Therefore, the main components of the implantable platform are: the LVAD, the implanted flow and pressure sensors embedded on the pump, a transcutaneous energy transfer system, a telemetry system, for data transfer to the external unit, and a remote data management for the wireless transfer of data collected by the implanted sensors.

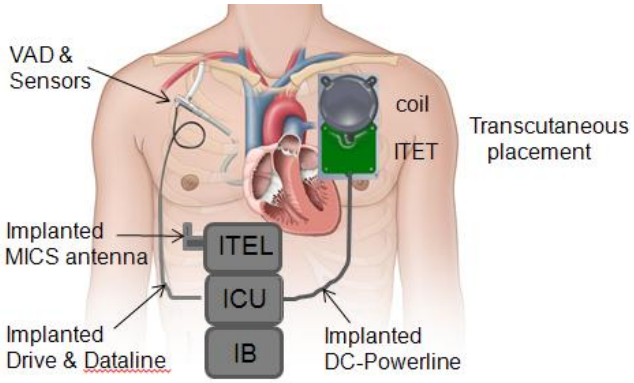

Figure 12 - Implantable components and units

The sensor module, measuring pressure and flow, is used to monitor both the status of the LVAD and of the patient. The LVAD and the embedded monitoring sensors will be integrated in the self-contained implantable platform. This platform is in a closed loop with a central control unit, namely Auto-Regulation Unit (ARU), that ensures a continuous monitoring and a feedback control of the parameters. The ARU is an external and wearable hardware unit wirelessly linked to the implanted sensors and to the VAD actuators, which implements the control algorithms; in particular, it acquires and stores data, controls the status of the VAD and it is able to set the pump by direct intervention of the cardiologist or in an auto-regulation loop based on sensors data output. The transcutaneous energy transfer (TET) is able to deliver a stable DC power for VAD driving, including additional power for charging batteries. The RF link is a bidirectional telemetry operating in the worldwide accepted frequency range from 402 – 405 MHz (Medical Implant Communication Service: MICS), that allows wireless communication between the implantable platform and the extracorporeal system components.

Some development steps and measurements for the evaluation about each component of the implantable platform will be described in the following chapters.

CHAPTER 2

2.1 THE AUTO-REGULATION UNIT

As previously said, the ARU is the unit that implement an intelligent control algorithm, with the purpose to optimize and personalize the heart unloading degree.

In the proposed sensorized platform, the auto-regulation control algorithm will be implemented in an external and wearable hardware unit, wirelessly linked to implanted sensors and to VAD actuators. This unit will allow to auto-adjust the blood flow, provided by the VAD to the patient's heart, according to signals coming from sensors. It is based on control algorithms able to work in real-time by using adjustable thresholds and control parameters. Moreover, this unit will monitor the energy consumption, as well as the VAD functionality, thus generating the appropriate crucial and vital alert messages.

As stated in the first chapter, currently known methodologies for adjusting pump parameters imply a manual setting of the pump speed until the patient perceives a comfortable level of perfusion.

In this particular case, the physician chooses a proper level of perfusion and sets the corresponding flow value through a dedicated interface. According to this value, the implemented control algorithms automatically send to the pump controller the proper command to change the rpm. The target value is reached by the implementation of a Proportional-Integrative (PI) control that dynamically and precisely changes the pump speed in order to achieve the desired flow value. This control method has been implemented since it allows a fast, fine and stable reaching and maintaining of the desired flow.

A second kind of control algorithms has been implemented to monitor the pump status through checking drops in pressure values. The aim of this check is to monitor if high, fast and/or repetitive changes in the pressure values occur. In particular, these changes could be the signal for a LVAD malfunctioning such as the presence of a suction event that could negatively affect the patient condition and suddenly provoke thrombus formation. To avoid this problem, a threshold control on drop pressure variation has

been implemented in order to reset the pump if pressure oscillations are detected.
The control algorithm was implemented using the LabView development environment and run, in a first phase, on one PC. Then, for problems related to computational load, it has been split on two different and dedicated PCs, thus simplifying suitability and feasibility test of the proposed control method. The hardware components of the platform are connected only to the first PC, named “Acquiring PC” which has the task to acquire and store all the data. While on the second PC the algorithms run, processing these data and creating the command that have to be send to the pump controller. This second PC is named "Control PC". The logic work flow used to implement the control unit and all the communications are showed in Figure 13.

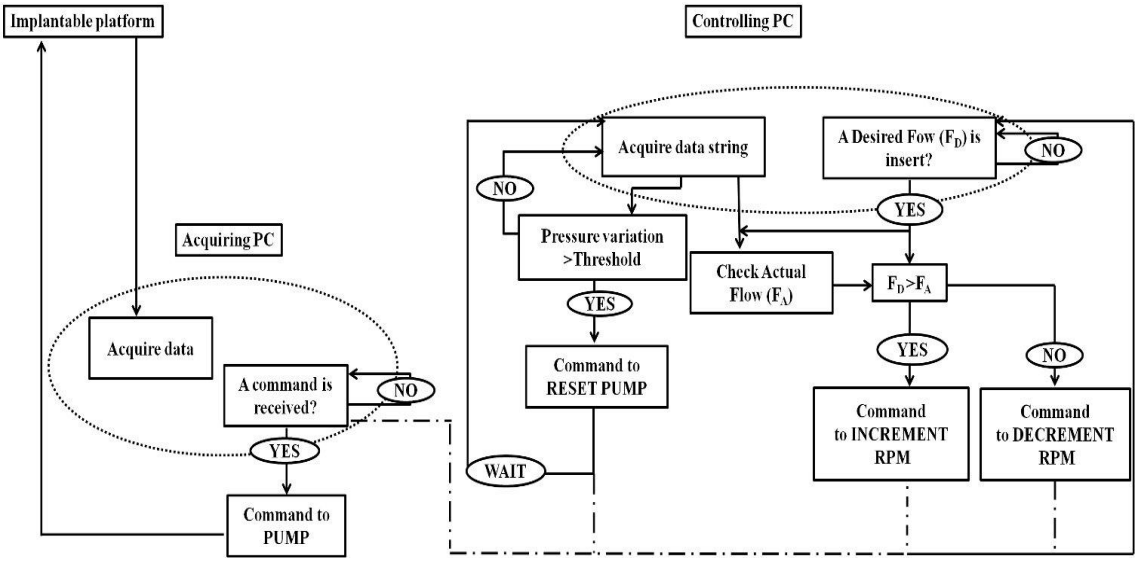

Figure 13 - Logical work flow of the ARU

A first functionality for the ARU is implemented in the Acquiring PC, which continuously acquires, visualizes and stores both flow and pressure data and the values of speed and current from the pump controller. These data are constantly collected and converted into format strings in order to be transmitted to the Control PC. For every running cycle the latter continuously controls pressure and flow values. In particular, as regards the flow control, the algorithm checks, at every cycle, if a new desired flow value is set into the interface. When a new value is inserted, the system compares it to the current flow value and, through a case structure, discerns two different conditions:

1. the desired flow is higher than the actual read;
2. the desired flow is lower than the actual read.

A PI controller was selected in order to obtain the increment or decrement needed for reaching the desired flow, and directly change the pump speed. The theoretic basis of the PI controller are reported in [13]. The PI controller was implemented in LabView with the transfer function form according to the following law (1):

$$\frac{U(s)}{E(s)} = Kp\ (1 + 1/Tis)$$

where K_P and T_i represent respectively the proportional gain and the integral time. A manual tuning was used to define their proper values. U(s) represents the Laplace transform of the controller output and E(s) the Laplace transform of the inlet. In our implementation E(s) is calculated depending on the situation detected by the case structure. Considering F_D the desired flow value insert by the clinician and F_A the actual read flow value:

1. E(s) is the Laplace transform of (F_D - F_A) when F_D is higher respect to F_A;
2. E(s) is the Laplace transform of (F_A - F_D) when F_A is higher respect to F_D.

In order to minimize the difference between flow values, the PI will return in output U(s), which is the quantity in rpm that must be added or subtracted to the actual value.

As explained above, the activation of the PI controller depends on the insertion of a flow value into the interface. Conversely, the control on pressure is a really automatic control, continuously active for every running cycle of the program. A threshold control on the standard deviation of the average pressure drop values is implemented. More in detail, a 100-samples-long dynamic array is assembled and updated as soon as a new pressure value is available, and its standard deviation (σ) is calculated according to the following law (2):

$$\sigma = \sqrt{\sum_{i=0}^{n-1} (x_i - \mu)^2 / n - 1} \qquad (2)$$

where n is the number of samples (n=100 in our case) and μ their mean value. The standard deviation of the dynamic array is continuously monitored and compared to a pre-defined threshold. In order to define an accurate and suitable threshold value for the implemented pump, a specific test was carried out keeping the pump in a steady condition (i.e. no suction or any instable events occurring). The standard deviation in these conditions has been evaluated in order to define the pressure variation during normal working operations of the pump. Then, the same test was carried out simulating a suction event to define the typical standard deviation in this case. By these measurements

it was possible to define a proper threshold which must be higher than the one associated to the normal working condition of the pump and, at the same time, lower with respect to the one measured during a suction event. The typical value of standard deviation to foresee a suction event has been found to be approximately 33. In working conditions, when the measured standard deviation exceeds the set threshold, the algorithm processes the command string to reset the pump. After the reset command is sent, the control unit waits a minimum amount of time to make the system reaching the normal conditions (i.e. standard deviations below the threshold). Every time a control algorithms is activated, the resulting command must be primarily transmitted via the serial communication line from the Controlling PC to the Acquiring PC. The latter communicates via another serial line with the pump controller.

Two simple, intuitive and user-friendly Human-Machine-Interface (HMI), described in the following paragraph, were implemented with the LabView software, respectively for the Acquiring and Control PCs. Aim of this HMIs is to help the final user to understand how the ARU could be used for an efficient control of the LVAD.

Furthermore, it is important to consider that, for patients chronically supported by an intracorporeal VAD, most useful information are related to the prevention and early treatment of VAD-related complications (e.g. device infections and device failure). The intracorporeal VAD is particularly prone to infection. Concerning the incidence of driveline infection, it is low (15%) within the first 30 days after implantation, but it reaches almost 100% at one year [24]. The incidence of LVAD failure is device-specific. Obviously, sudden VAD failure carries an high risk of mortality and complications and require prompt re-hospitalization. The prevention and the early detection of VAD-related complications are of paramount importance in order to have the patients benefit maximally from mechanical support. VAD is a therapy characterized by high burden of complications, invalidating the patients or even resulting fatal, and socio-economic costs.

Unaware, patient can be informed through “alerts”, detectable by controller technician/physician: their resolution can be important for patient’s life before the patient becomes symptomatic.

For this reason, alert signals are implemented in the control algorithm on the Acquiring PC, to advise when one of the four parameters (pump speed, pump current, pressure and flow) exceed its safety threshold.

Then, a preliminary implementation of the implantable platform solution to validate the Auto-Regulation principles was assembled and included:

- external physical sensors:
  - two (pump input/output) commercial pressure sensors,
  - a flowmeter,
- CircuLite Pump with controller,
- National Instruments data acquisition (DAQ) device,
- PC-based graphical user interface.

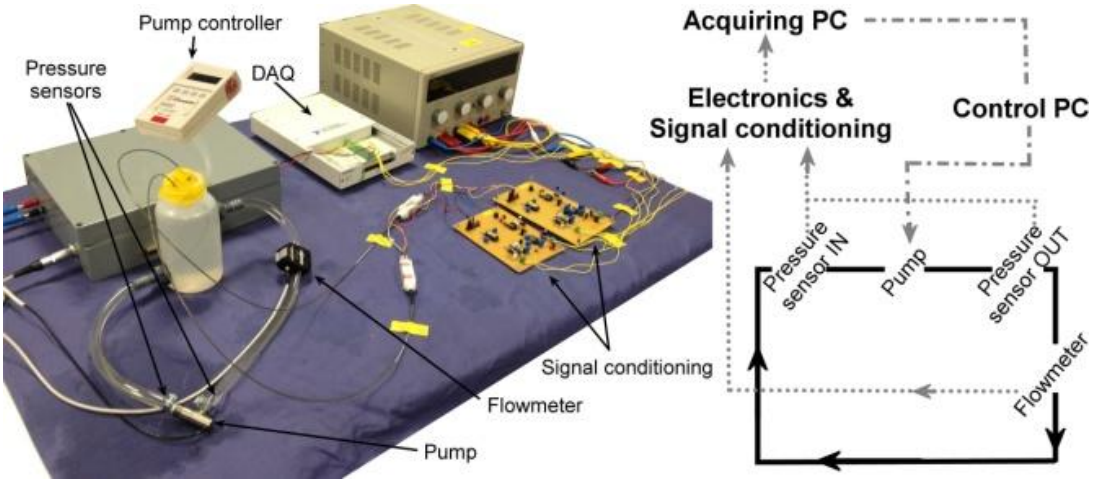

Figure 14 - *In-vitro* implantable platform setup (left) and overall schematics (right).

The ARU functionalities, defined and under verification on the *in-vitro* platform, are:

1. Proportional-Integrative (PI) control of the pump speed in order to achieve the desired flow value,
2. monitoring and acquisition of the pump speed,
3. monitoring of the sensor data (pressure and flow),
4. monitoring and acquisition of the pump current,
5. threshold control of the flow and pressure values by generating alerts,
6. control on the pressure variations with alert generation in case of fast and/or repetitive changes in the pressure value.

As discussed above, primarily all these features have been implemented by using a LabView interface running on two dedicated computers. The step after testing the control algorithm with this simple interface is the conversion in VHDL code, a hardware description language, which will run on an FPGA-based architecture (Figure

15) for the ARU. Thus, system flexibility and efficiency increase, as multiple tasks can run in parallel allowing multiple control task to be executed and tested at the same time.

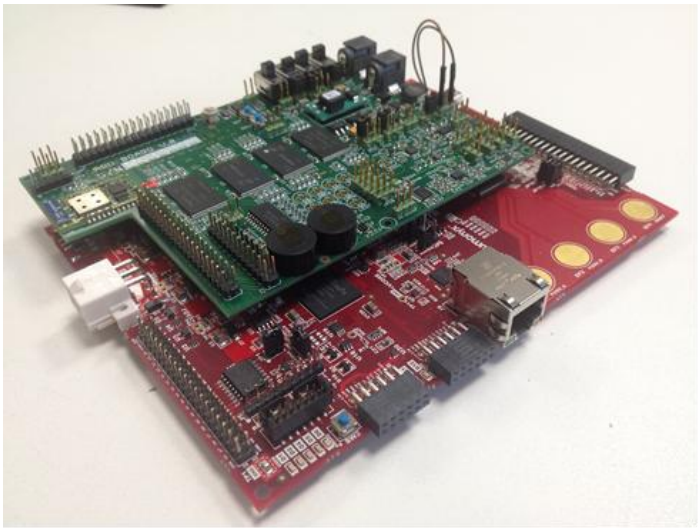

Figure 15 - FPGA of the ARU.

2.2 PC-BASED GRAPHICAL USER INTERFACE: SPLITTING OF THE HMI

In the first prototype of the auto-regulation unit, the control algorithm was implemented on one dedicated PC. But the program results to be too heavy to run properly on only one PC, because the ARU task is not so simple. In fact, it has to monitor the pump and sensors parameters and to actuate a closed-loop control for adjusting flow and pressure parameters on the basis of the physiologic cardiac demand.

For this reason, in order to decrease the overall computational load, the LVAD control has been split on two dedicated PCs. The data acquiring and storing have been implemented on the Acquiring PC, while the data processing for the control of the VAD functionalities has been implemented on the Control PC.

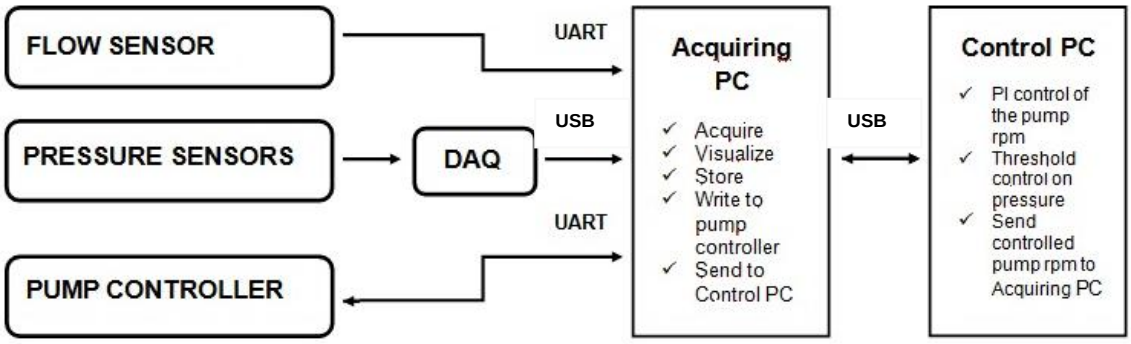

Figure 16 – block diagram of the data flow

In particular, as showed in Figure 16, the data acquired from the platform are flow, upstream and downstream pressures and pump speed and current, obtained from the pump controller for checking the device status. The flow data from the ultrasonic transducer and the two pump parameters are transferred to the Acquiring PC by two different serial communication lines, while pressure data are acquired using the National Instruments data acquisition (DAQ) board and transferred to the PC via USB. Thus, the hardware components of the platform are connected only to the first PC.

All the data are continuously visualized and stored in the Acquiring PC thanks to the dedicated ARU interface, implemented in LabView, exploiting the National Instrument VISA and DAQmx palettes and functions. After the acquisition, these data are constantly collected and converted into format strings in order to be transmitted to the

Control PC, and to be elaborated by the control algorithms. In particular, as described above, a Proportional-Integrative (PI) control of the pump rpm has been implemented in order to achieve the desired flow value, set by the user, by dynamically changing the pump speed. Thus, depending on the desired and actual flow value, the PI control create the command for the setting of the new pump rpm value, that have to be send back to the pump controller. The threshold control on pressure data has been implemented also on the Control PC.

The two control algorithm have been realized using the LabView development environment (for further details see Appendix A), thus to be able to design a simple controller and a user-friendly interface associate to it.

The HMI has been developed to allow the final user, that is the physician or the caregiver, to a simpler and better manage the implanted pump and to understand how the ARU could be used for an efficient control (Figure 17).

The Acquiring PC interface allows the user to visualize in real-time the parameters. It is also provided with LED based visual alarms that are switched on if the input parameters (pump speed and current, flow, pressure difference, i.e. P_{out} - P_{in}) exceed the safety thresholds.

The Controlling PC interface is the most critical and important, since it allows the user inserting the desired flow value, thus activating the PI controller. At the same time, this interface is provided with a reset button that the user has to push in case of high, fast and/or repetitive changes in the pressure value which are alarms for LVAD malfunctioning, resetting the pump status.

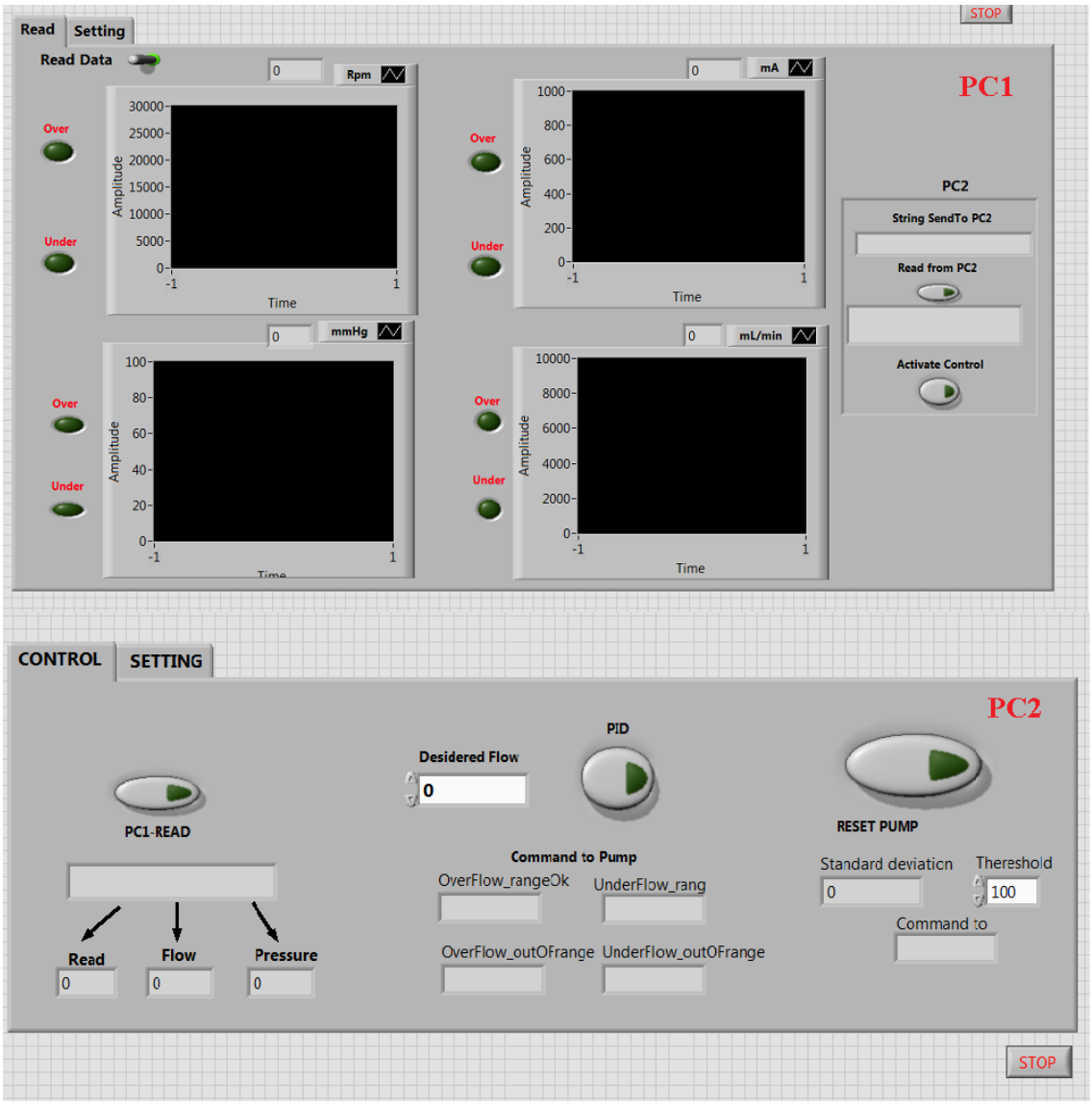

Figure 17 - Human-Machine-Interfaces of the ARU

2.3 Implementation of an UART in VHDL code

2.3.1 Universal Asynchronous Receiver/Transmitter

As discussed in the first paragraph, the final embedded ARU will be FPGA-based, the main reasons are that this architecture increases system flexibility and efficiency, as multiple tasks can run in parallel. These features will become essential when the auto-regulation algorithms will be implemented, thus allowing multiple control tasks to be executed and tested at the same time.

For this reason, the ARU functions have to be translated in VHDL, *Very High Speed Integrated Circuit Hardware Description Language*, in order to program the FPGA (for further details see Appendix B).

As showed in Figure 18, the FPGA that will implement ARU functions will communicate with the extracorporeal part of the implantable platform; in particular, it will interact with the extracorporeal control unit (ECU), in order to acquire pump and sensors data and to send its commands. ECU is an external communication controller, which regulates the communication between the external part of the TET and the ARU.

Finally, the FPGA will communicate optionally with the telemetry system.

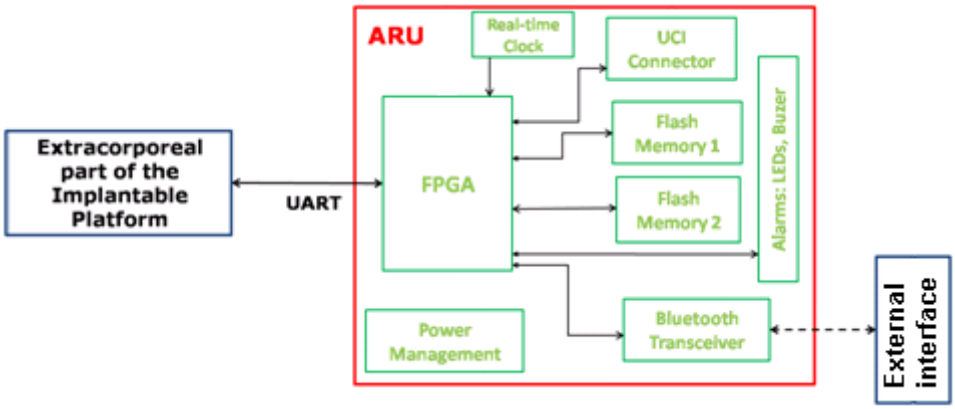

Figure 18 – ARU and platforms interaction

In all the three cases considered, a serial communication line is used, with the communication standard RS–232, but the requirements for each UART (*Universal Asynchronous Receiver/Transmitter*) are different:

- Read,
- Read/Write , CRC16-CCITT,
- TELEMETRY (optional): Read/Write , CRC16-CCITT, control of Rx/Tx flow .

In serial communication process, the data are sent one bit at a time, sequentially, over a communication channel. In a serial line, the transfer time is eight times longer but fewer wires are required than a parallel port.

Instead, a parallel port sends and receives data eight bits at a time over 8 separate wires. In this way, data are transferred very quickly; on the other hand, the cable required is more thick because of the number of individual wires it must contain.

Serial communication is completed using 3 transmission lines: ground, transmit and receive. Since it is asynchronous, the port is able to transmit data on one line while receiving data on another. The serial port contains a electronic chip called a Universal Asynchronous Receiver/Transmitter (UART) which is responsible for the conversion of the bytes in stream of ones and zeroes.

RS-232 is one of the most widely used standards for sending serial data (fur further details see Appendix D). It has the advantages of simplicity while still offering a high level of capability. Data on RS232 is normally sent using ASCII.

2.3.2 UART IMPLEMENTATION FOR ARU INTERACTIONS

The UART responsible for the communication between the ARU and the implantable platform has been implemented.

```
3  USE ieee.std_logic_unsigned.all;
4  USE ieee.numeric_std.ALL;
5  use std.textio.all;
6  use IEEE.std_logic_arith.all;
7
8  entity miniuart_tb is
9  end entity;
10
11 architecture behavioural of miniuart_tb is
12
13
14 component UART
15    generic(BRDIVISOR: INTEGER range 0 to 65535 := 130); -- Baud rate divisor
16    port (
17  -- Wishbone signals
18       WB_CLK_I : in  Std_Logic;  -- clock
19       WB_RST_I : in  Std_Logic;  -- Reset input
20       WB_ADR_I : in  Std_Logic_Vector(1 downto 0); -- Adress bus
21       WB_DAT_I : in  Std_Logic_Vector(7 downto 0); -- DataIn Bus
22       WB_DAT_O : out Std_Logic_Vector(7 downto 0); -- DataOut Bus
23       WB_WE_I  : in  Std_Logic;  -- Write Enable
24       WB_STB_I : in  Std_Logic;  -- Strobe
25       WB_ACK_O : out Std_Logic;  -- Acknowledge
26  -- process signals
27       IntTx_O  : out Std_Logic;  -- Transmit interrupt: indicate waiting for Byte
28       IntRx_O  : out Std_Logic;  -- Receive interrupt: indicate Byte received
29       BR_Clk_I : in  Std_Logic;  -- Clock used for Transmit/Receive
30       TxD_PAD_O: out Std_Logic;  -- Tx RS232 Line
31       RxD_PAD_I: in  Std_Logic);  -- Rx RS232 Line
32 end component;
```

Figure 19 – VHDL code of the specific UART

The communication standard is the RS–232 with a baud rate of 155200 bps and a transmitted packet of 8n1. The data can be only sent from the wearable platform to the ARU and the exact acquisition is checked by the implementation of a LED that is switched on when the desired packet is read.

Its correct behavior has been tested by the simulation software ModelSim. From the simulation results, as in Figure 20, it is possible to see an example of the UART implementation: the LED is switched on when a byte made up of 1 is received.

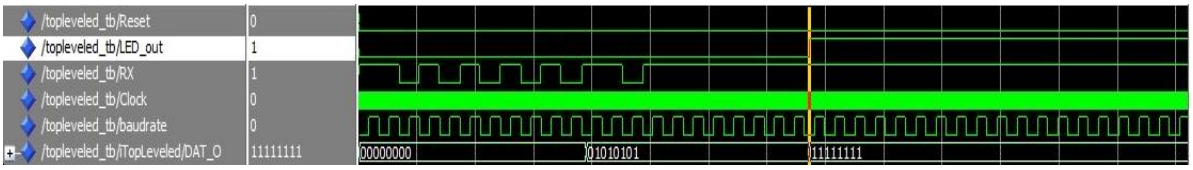

Figure 20 – Simulation results by ModelSim

2.4 DEVELOPING TEST SOFTWARE

The ARU receives data from the implanted part of the platform through the ECU.
A communication protocol between ARU and ECU was defined. Thanks to this protocol, it is possible to transfer, wireless, in real time, data related to the pump speed, the motor current and status information to the ARU.
When ARU requests data, the implantable control unit transmits the requested data in frames from the implantable TET (ITET) to an external TET (ETET) and then from ETET to ECU, which communicates with the ARU by an UART. If the Detach command is sent by the ARU, the data stream between the ETET and the ARU shall be terminated.
The communication principle can be described by the following steps:

1. when the ARU wants data, it has to communicate with the ECU. Therefore, the first action is to send the ARU_Attach() command to the ECU,
2. after receiving the ARU_Attach() command from the ECU, the ETET initializes and prepares the data stream. When the ETEL is ready to send data, the ECU transmits ARU_Update() to the ARU,
3. after the ARU received the command ARU_Update(), it can request data sending the command ARU_GET_Data(),
4. after the ECU received the ARU_GET_Data() command, the ETET transmits the data-frame, composed of startbyte + Data[60 Bytes] + CRC16-CCITT + endbyte,
5. if the data are updated again, the ECU transmits ARU_Update(),
6. then the ARU shall respond with ARU_GET_Data(),
7. then the next data-frame will be transmitted,
8. ... (this continues in a typical repetition rate of 1 second),
9. if the ARU wants to terminate the communication, it transmits the ARU_Detach() command and the data stream between the ETET and the ARU terminates.

Furthermore, the ARU, implementing the control algorithm, has to send to the pump the speed value resulting from the control loop; for this reason, it can send also the ARU_Set_Suggest_Speed command. The pump speed can be varied by the ARU from 20000 rpm to 28000 rpm in the real clinical scenario but it is possible to vary it also

from 0 rpm to 28000 rpm in the experimental scenario, in order to test critical work conditions.

Obviously, the ARU have to send a command to switch the pump on at the beginning, ARU_VAD_On, but also the ARU_VAD_Off command is supported by the control unit in order to switch the VAD off during the experimental phase.

The downstream and upstream commands are defined by 8 bytes consisting:

- P0: start of frame (SOF) = 0x02, ASCII startbyte,
- P1: command number, different for each command to allow the ARU to recognize each data block,
- P2: reserved,
- P3 + P4: parameter value,
- P5 + P6: CRC16-CCITT,
- P7: end of frame (EOF) = 0x0D, ASCII endbyte.

Byte from P1 to P6 have to be converted from hexadecimal to ASCII, e.g. 0x45 → 0x34 0x35.

The data-frame starts with SOF and ends with CRC16- CCITT and EOF. It contains a lot of parameters related to:

- the VAD: speed, current, internal suction, bus voltage, ICU board temperature, pump status,
- the sensors: inlet and outlet pressure and temperature, pressure reference, flow and board temperature of the flowmeter, sensors status,
- the ARU, like suggested motor speed and state,
- the temperature of the implanted coil.

The checksum of the CRC is calculated considering the bytes from P0 to P4 for the commands while, for the data-frame, from SOF to CRC16–CCITT – 1, i.e. all the frame without CRC itself and EOF.

In order to simulate the communication between the ARU and the ECU, to test each unit and to facilitate their integration, a Graphical User Interface (GUI) has been developed. The simulators for the two systems are written in the script language Python extended by the PyQt modules of the Qt-C++ library (for further details see Appendix C).

2.4.1 PYTHON SIMULATOR FOR THE ECU INTERFACE

The tool "ECU simulator" simulates the ECU controller and, in particular, only the communication between the ARU and the ECU which are components of the extracorporeal part of the implantable platform. The following picture (Figure 21) shows a screenshot of this GUI.

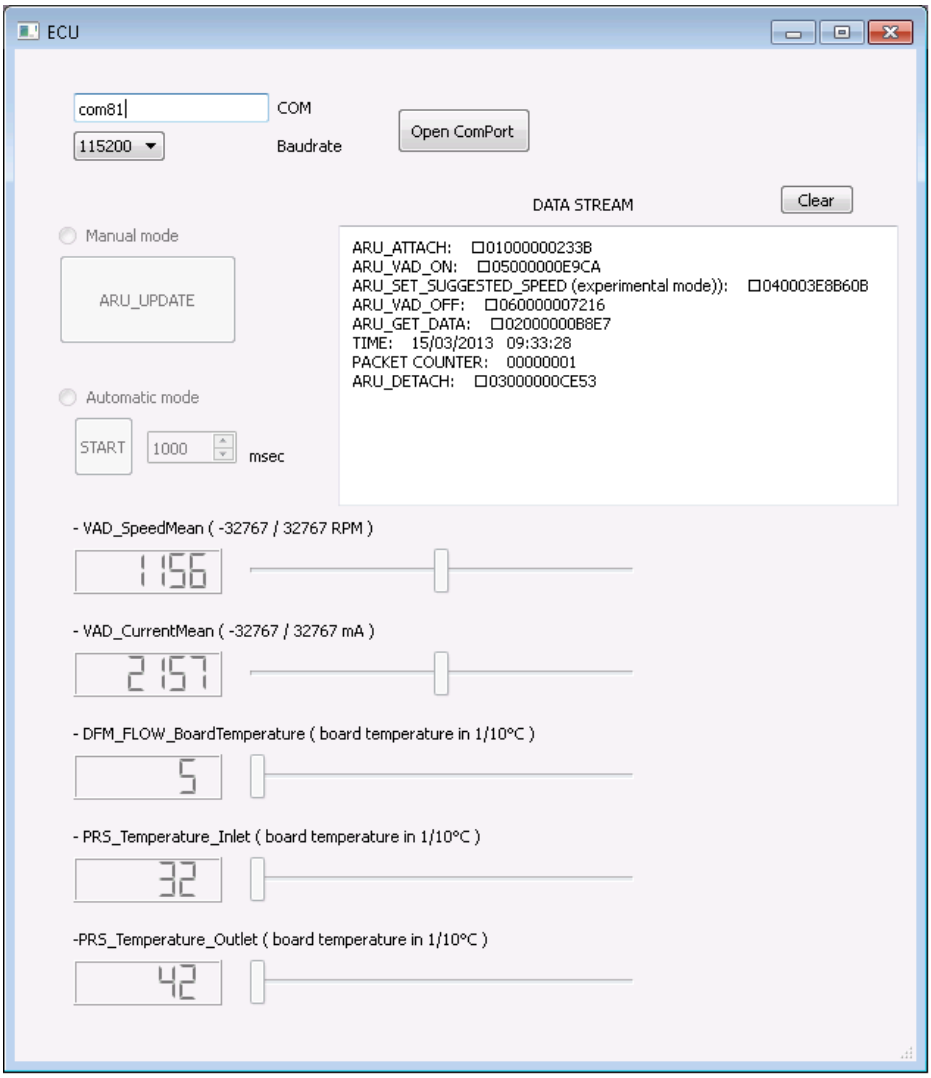

Figure 21 – Screenshot of the ECU interface

The communication between the ECU simulator and the ARU simulator is established over a serial port (RS232) which is part of many PCs.

To connect the ECU, the following steps are necessary:

1. input the name of the serial port (e.g. "COM3"),
2. choose the proper baud rate, which has to be the same on the ARU simulator,

3. click the button "Open ComPort".

After receiving the ARU_Attach() command from the ARU, the ARU_Update() command has to be sent from the ECU to the ARU when the ETEL is ready. It is possible to transmit this command manually by clicking the button "ARU_UPDATE" or in automatic mode. If the automatic mode is chosen, after choosing the time interval in msec between two transmissions by the dedicated box, clicking the button “START” the ARU_Update() is sent continuously.

As soon as it happens, the ECU receives the ARU_GET_Data() command and sends automatically the data-frame. If data is updated again, the ECU transmits ARU_Update(), by clicking again the respective button.

The ECU can also receive the ARU_VAD_ON(), the ARU_VAD_OFF() and the ARU_Set_Suggested_Speed() commands from the ARU.

After having received the ARU_Detach() command, ECU cannot send data to ARU anymore and the data stream between ECU and ARU terminates.

Every reception from the ARU is logged in the textbox on the upper part of the GUI. After the data-frame is sent, a timestamp is generated, which will be displayed together with the packet number in the textbox.

By clicking the button "Clear" above the textbox it is possible to erase the content of the textbox.

In the lower part of the GUI, the value of some parameters of the data-frame can be set and are displayed. VAD_SpeedMean, VAD_CurrentMean, DFM_FLOW_BoardTemperature, PRS_Temperature_Inlet and PRS_Temperature_Outlet are chosen in this case.

The VAD_SpeedMean can range from -32767 rpm to 32767 rpm and the VAD_CurrentMean range is -32767 to +32767 mA. For the other three parameters, the range goes from 0 to 65535 (0x00 to 0xFFFF). To set one of these values, the user has to move the corresponding slider.

After setting the value of these parameters, the data-frame is updated and, when the ECU receives the ARU_GET_Data() command, it sends the new data block.

The CRC16-CCITT checksum is calculated from the python script itself.

2.4.2 PYTHON SIMULATOR FOR THE ARU INTERFACE

The tool "ARU Simulator" simulates the ARU controller and in particular the only communication to the ECU module. The following picture (Figure 22) shows a screenshot of this GUI.

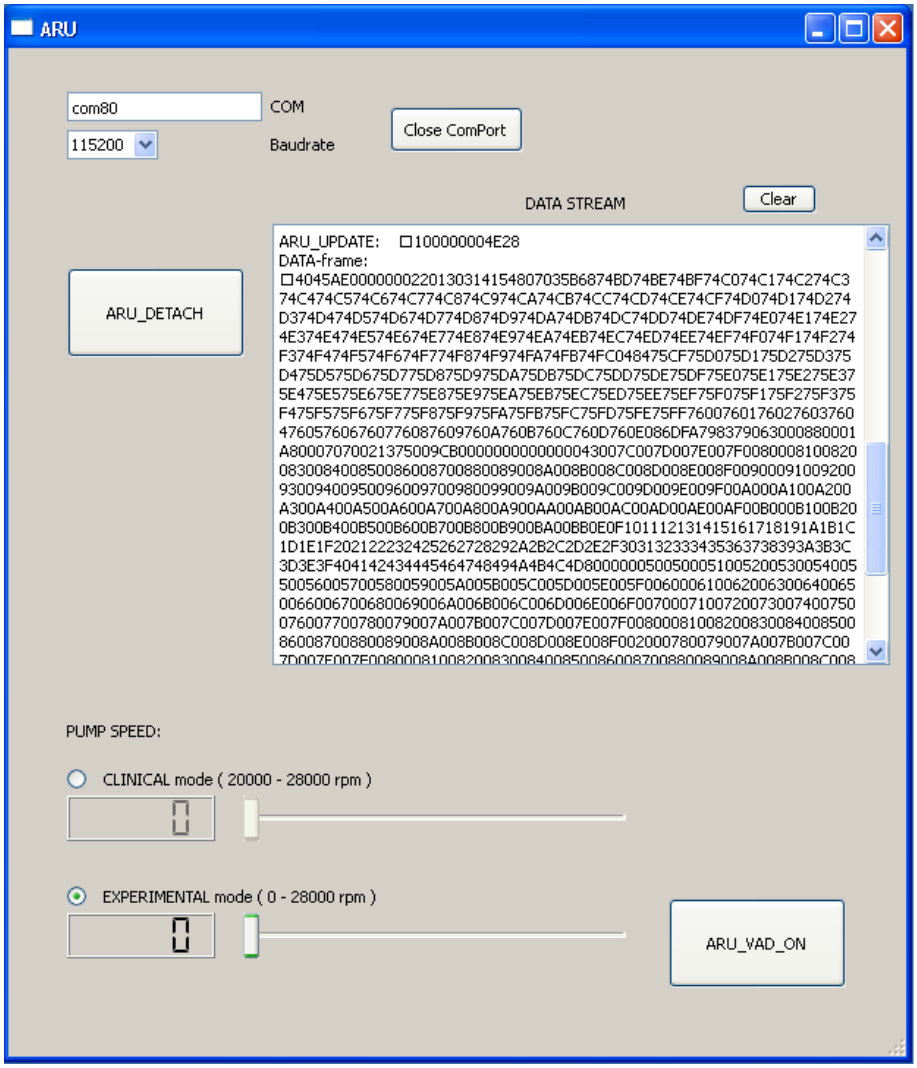

Figure 22 - Screenshot of the ARU interface

To connect the ECU, the following steps are necessary:

1. input the name of the serial port (e.g. "COM3"),
2. choose the proper baud rate, which has to be the same on the ECU simulator,
3. click the button "Open ComPort".

If the ARU wants to communicate with the ECU, the first action is to send the ARU_Attach() command to the ECU, by clicking the button "ARU_ATTACH".

After transmitting this data block, the button becomes automatically the "ARU-DETACH" which allows to send the ARU_Detach() command to terminate the communication.
After clicking the button "ARU_ATTACH", the ARU waits for the ARU_Update() command from the ECU. When it happens, the ARU requests data by sending automatically the ARU_GET_Data() command. The ECU answers sending the data-frame.
If the data are updated again, the ECU transmits ARU_Update(), the ARU shall respond again with ARU_GET_Data(), then the next data-frame will be transmitted.
This loop can be repeated until the button "ARU_DETACH" is clicked.
Every reception from the ECU is logged in the textbox on the right side of the GUI. By clicking the button "Clear" above the textbox it is possible to erase the content of the textbox.
In the lower left corner of the GUI, the value of the speed can be set, moving the corresponding slider, and is displayed. Two cases are considered:

- the clinical mode in which the pump speed can range from 20000 rpm to 28000 rpm, in order to protect patient´s health,
- the experimental mode in which the range is 0-28000 rpm.

If the radio button of the clinical mode is chosen, the ARU_VAD_ON() command is sent automatically to the ECU. This event cannot be repeated and it is clear that, in this case, it is impossible to switch the pump off.
If the experimental mode is chosen, it is possible to switch the pump on and off any time. By clicking the button "ARU_VAD_ON", the ARU_VAD_ON() command is sent and the button becomes automatically the "ARU_VAD_OFF" one. By clicking this button, the ARU_VAD_OFF() command is transmitted. Therefore, the ARU_VAD_OFF() command is supported in experimental mode only.
After setting the suggested pump speed, the ARU transmits automaticaly the ARU_Set_Suggested_Speed() command to the ECU with the speed in rpm as parameter.

CHAPTER 3

3.1 SENSORIZED PLATFORM

One of the important goals in designing LVADs control system is the selection of the most appropriate sensors, responsible for the detection of the changes in the body's metabolic demands.

A sensorized platform would lead to the monitoring not only of the status of the LVAD but also of the patient health, supplying the auto-regulation unit with the physiological signals acquired by the set of sensors.

Thus, the sensors data are essential for the implementation of the control algorithm since they provide an important feedback.

The proposed implantable platform has been equipped with commercially available pressure and flow sensors. According to the design of the *in-vitro* scenario, two pressure sensors have been positioned upstream and downstream at 1 mm distance with respect to the pump ends. Moreover, a flowmeter has been positioned downstream the pump, at 15 cm distance.

Figure 23 - DIGIFLOW-MINI with an ultrasonic clamp-on transducer

In order to measure the flow, a non-invasive clamp-on transducer provided by em-tec (Finning, Germany), the DIFIFLOW-MINI, has been integrated. It is based on the

principle of the transit time difference between ultrasonic acoustic waves in up and downstream direction. The DIGIFLOW-MINI, in combination with an ultrasonic clamp-on transducer (Figure 23), is indicated for the contactless volumetric measurement of liquid flowing through extracorporeal tubing systems.

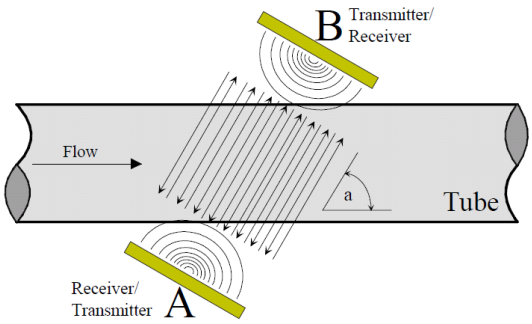

Figure 24 - Measurement principle of the DIGIFLOW-MINI

About the measurement principle (Figure 24), a piezoceramic crystal (A) is stimulated by a high frequency burst and sends out ultrasound to a second piezoceramic crystal (B), the receiver. The crystals are arranged by a certain angle α with respect to the flowing medium. The transit time is influenced by the medium. The flow speed of the medium can be calculated via the measured transit-time differences. The flow volume, in liters per minute, can be attained by calculating in the inner cross-sectional area of the tube.

This ultrasonic flowmeter is characterized by an excellent accuracy and stability; moreover it has been calibrated for flow measurement in Polyvinyl Chloride (PVC) and silicone tubes upon custom request. The transducer is able to measure a maximum flow of 10000 ml/min, that matches with the application flow range, that is typically around 3000-5000 ml/min.

For the measurement of pressure, two sensors have been evaluate: the TruStability NSC sensor made by Honeywell and the Mikro-Tip® pressure catheter made by the Millar Instruments. After the evaluation, the Mikro-Tip® pressure catheters (Figure 25) have been chosen and settled in input and output of the pump. They have been employed because of their specifications that are suitable to be used in an implantable platform. In particular, the SPR-350S model of the Mikro-Tip® pressure catheters has been integrated.

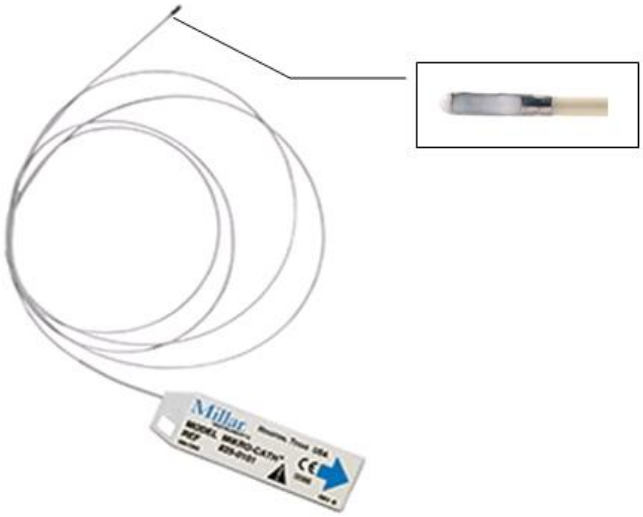

Figure 25- Mikro-Tip® Pressure Catheter with the sensing tip

In fact, the piezoresistive sensor, located at the tip of the catheter, provides optimal data for monitoring high-fidelity cardiovascular pressures at the source. As reported in the datasheet [16], it presents high linearity and sensitivity (up to 5 µV/V/mmHg). The catheter has a straight tip, an effective length of 140 cm and a 2F polyurethane catheter body.

Furthermore, the implantable platform has been provided with all the needed electronic components for signal conditioning. These are mandatory in order to ensure a first phase of data processing both for pressure and flow sensor data.

Regarding the flowmeter, a conditioning board has been provided together with the DIGIFLOW-MINI, for the signal generation and analysis and for sending and receiving ultrasonic signal from/to the piezo-elements of the flow sensor. The zero flow offset adjustment is also expected.

About the pressure sensors, considering their characteristics, a pre-processing of the output voltage is necessary in order to amplify and filter the signal. So, a pressure amplifier system has been realized, according to the pump specifications. As showed in the following, the electronic hardware is based on two amplification stages, through which the desired gain can be selected.

3.2 PRESSURE SENSOR REPLACEMENT

In the first prototype of the implantable platform, the TruStability NSC sensor made by Honeywell was integrated (Figure 26) [17].

Figure 26 - TruStability NSC Series-Uncompensated/Unamplified by Honeywell

It is a piezoresistive silicon pressure sensor offering an analog output for reading pressure over the specified full scale pressure span and temperature range.
It is unamplified and uncompensated, thus it is perfect for own compensation, calibration, and amplification in order to make use of the maximum resolution of the bare sensor output. This leads to the possibility of developing a custom algorithm for the specific application, as required in this study.
The sensor operates in a range between -40° C and 85° C, which includes the temperature range typical for the case application (human body average temperature: ~ 37°C).
Additionally, it provides excellent repeatability, high accuracy, reliability and long-term stability, leading to an alternative-to-transplant use of the LVAD.
On the other hand, the TruStability sensors have two big disadvantages that brought to the later replacement in the *in-vitro* platform.
First of all, as showed in Figure 27, their working pressure range goes from 1 psi (pressure per square inch) to 150 psi (equivalent to 45 mmHg to 7500 mmHg), which is very wide with respect to the typical range of interest for the specific application case. In fact, the blood pressure for healthy people is below 120 mmHg and over 90 mmHg. Even though people with heart disease have higher blood pressure, the measured values are too small to be read and to return an accurate output voltage.

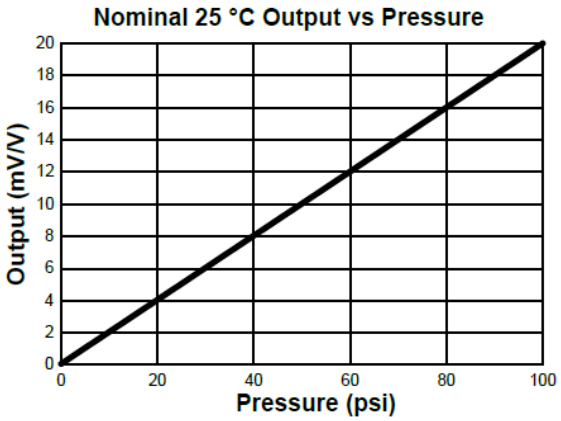

Figure 27 – Honeywell pressure sensor characteristic

Another problem is that this sensor type is intended for use with non-corrosive, non-ionic gases, such as air and other dry gases and for non-corrosive, non-ionic liquids.

All TruStability sensors are also dead-ended devices, thus they are not compatible with liquids containing particulates. Particulates can accumulate inside the sensor, causing damage or affecting the sensor output.

It is worth mentioning that the pressure sensors of the implantable platform have to be in contact with the blood, that is composed of cells, among which the red ones are relatively big, and plasma, a fluid rich in ions.

For these reasons, the Honeywell sensors turned out to be unsuitable for this application and the SPR-350S model of Mikro-Tip® pressure catheters made by Millar Instruments has been chosen to replace them.

They have been employed because of their specifications that are suitable to be used in the implantable platform. In fact, this catheters present high linearity and the pressure range, that is between -50 mmHg and +300 mmHg, is compatible with the range of interest for the application.

For cardiovascular applications, Mikro-Tip catheters may be introduced into the cardiovascular system percutaneously or through the wall of a surgically exposed artery or vein. Thus, it provides flexibility and minimal obstruction of the vessels or valves during insertion.

Another advantage, compared to the TruStability sensors by Honeywell, is that these catheters is for use on large animals, like dogs, pigs and ships. This is an important requirement for the *in-vivo* testing of the implantable platform.

3.3 SIGNAL CONDITIONING FOR THE PRESSURE SENSOR

A first phase of data processing for the pressure sensors data is mandatory, thus all the electronic components for signal conditioning are needed.
Signal conditioning is utilized for data acquisition: sensor signals must be amplified and filtered to levels suitable for the data plotting on the graphical user interface. Filtering is a very important signal conditioning function because usually not all the signal frequency spectrum contains valid data. While, signal amplification performs other two functions, fundamental to read the output: increasing of the resolution of the input signal and increasing of its signal-to-noise ratio. If the output of the pressure sensor is in the mV range, as in the real case, it results too low for the following process phases. Consequently, it is necessary to bring the voltage level up to the required one.
Considering the characteristics of the Mikro-Tip pressure sensors, a pre-processing of the output voltage is necessary and a pressure amplifier system has been designed and realized. In particular, the electronic hardware is based on two amplification stages.

3.3.1 ZERO OFFSET SETTING

The first step of the sensor integration concerns the electronic circuit (Figure 28) and in particular the zero setting of the offset.

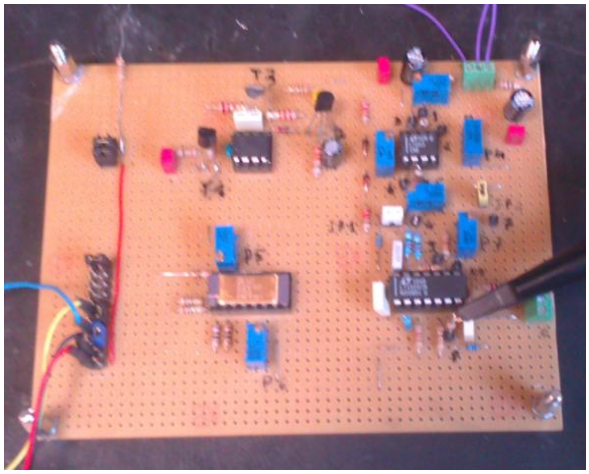

Figure 28 – Signal conditioning circuit

As cited in the previous paragraph, the hardware is composed by two different amplification stages: in the first one, it is possible to choose between three values of gain G_I, that are 10, 100, 1000; while, the second stage is characterized by a gain G_{II} of 10.
In order to cancel the offset of the circuit, one of the potentiometers (the P1 blue box in Figure 28) has been tuned in unloading conditions, until the circuit output has been reset to zero.

3.3.2 CHARACTERIZATION FOR THE PRESSURE SENSOR

The second step is the most important one and its objective is to plot the real characteristic of the Mikro-Tip catheter. In fact, to ensure reliable results a calibrated pressure transducer must be used.
The analysis of a sensor characteristic requires the study of the relationship between the inputs and the response of the device, without investigating the energy transformation process inside it. Therefore, the sensor will be modeled like a black box and the relationships between the input and the output will be analyzed.
Each sensor is characterized by an ideal out-in relationship, that could be written in mathematical form like an equation or like a theoretical curve, able to relate the input and the output in the working range of the device (Figure 29). In real operation, the sensor has a characteristic that is different from the ideal one. In order to take into account the inaccuracy of the device, it must be measured the deviations of the real from the ideal values. The difference between the indicated value and the real one is the error of the sensor.

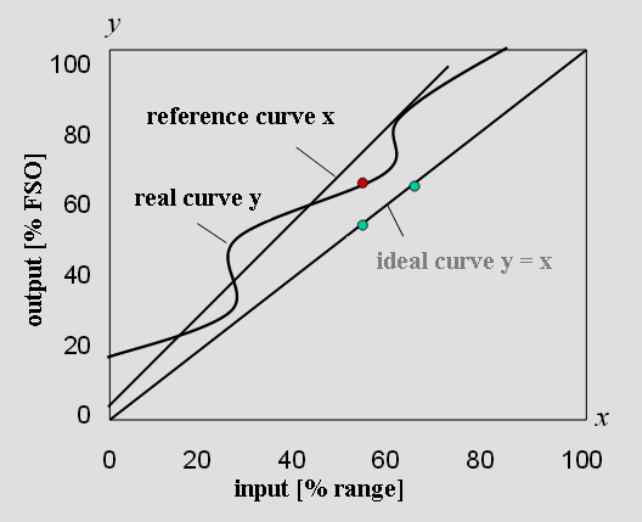

Figure 29 – Sensor characteristic

Thus, in order to obtain the Mikro-Tip real characteristic, a self-made setup of measurement has been used.

Calibration experiments have been performed by using a column with incremental levels of de-ionized water. The level of the fluid has been increased from 0.5 cm to 14.5 cm, by step of 1cm. The corresponding values of the pressure at the different heights of the column have been obtained referring to the Stevin's law:

$$P_h = \rho \cdot g \cdot h + P_A$$

where P_h is the pressure at the level of water, ρ is the density of the water (998.21 Kg/m^3) in normal conditions, g is the gravity acceleration (9.80 m/s^2), h is the eight of the column and P_A is the atmosphere pressure (101.33 kPa) which is the reference pressure for the sensors.

The catheter tip has been placed on the bottom of the baker, with the sensitive area in contact with the water, and the output voltage of the signal conditioning circuit has been read through both the oscilloscope and the multimeter.

The test has been repeated twice, with both the electronic circuits of the two pressure sensors, positioned upstream and downstream with respect to the pump.

During the measurements, also the gain of the first amplification stage G_I has been tested and the sensor characteristic has been plotted for each of the three possible values.

The collected data were plotted and processed by MatLab, in order to adjust the transfer function coefficient. The transfer function has been calculated by a linear fitting and the slope or gradient of the obtained line represents the sensor sensitivity in working conditions.

As showed in Figure 30, the sensitivity value resulted in ~ 0.2 mV/Pa.

Furthermore, a gain of 100 has been chosen because, in this way, the total gain of the signal conditioning circuit results to be 1000 ($G_T = G_I * G_{II} = 100 * 10 = 1000$) and the amplified voltage magnitude is big enough for a good data management (it has been increased from the range of mV to V). In fact, as it is possible to see in Figure 30, in the pressure range of interest that goes from 12 KPa to 16 KPa (90 - 120 mmHg), the output voltage is in the order of 2.5 - 3.5 V.

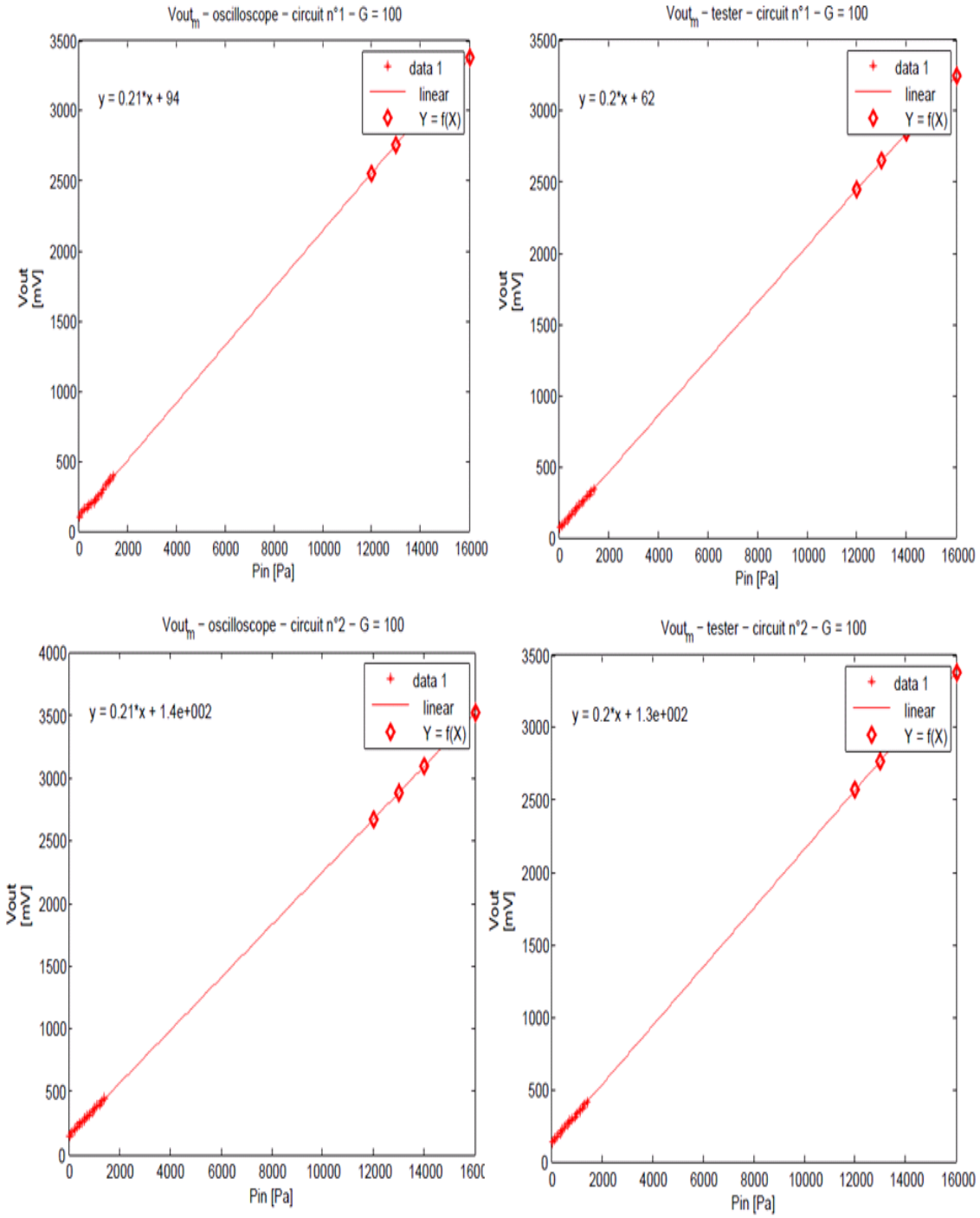

Figure 30 – Mikro-Tip real characteristic

3.4 HUMAN MACHINE INTERFACE UPGRADE

In the first prototype of the *in-vitro* platform, Honeywell sensors data were acquired and processed by a digital signal conditioning. In particular, a dedicated Labview program elaborated the voltage output, amplifying and filtering it, and plotted the collected pressure data on the home-made HMI.

Since, in the new scenario, the Millar sensor signal is conditioned by an analog circuit, the Labview program had to be upgraded. Thus, the output data processing block was deleted and another block has been created in order to obtain the input pressure values from the read output voltage. The sensitivity value, ensued from the sensor characterization, has been used to rich this aim. The sensitivity represents the relation between the output and the input of a sensor, thus the voltage signal has been multiplied by the sensitivity and the resulted pressure signal has been plotted on the HMI.

CHAPTER 4

4.1 TRANSCUTANEOUS ENERGY TRANSFER SYSTEM

As previously said, the TET is a system that transmit energy to the LVAD and the sensors wireless, leading to a decrease of the amount of cable through the skin.

Regarding the power requirements for the specific TET system of the proposed implantable platform, the CircuLite Synergy™ device needs an average of 10 W (Figure 31), with a voltage supply of 12 V and a maximum current consumption of 850 mA. Other VAD systems have very similar power requirements, thus guaranteeing interoperability of the platform, once successful application to the CircuLite unit will be demonstrated. Furthermore, the consumption of the monitoring system and the auto-regulation unit can be roughly estimated in a few hundreds of mW and should be added to the above mentioned 10W.

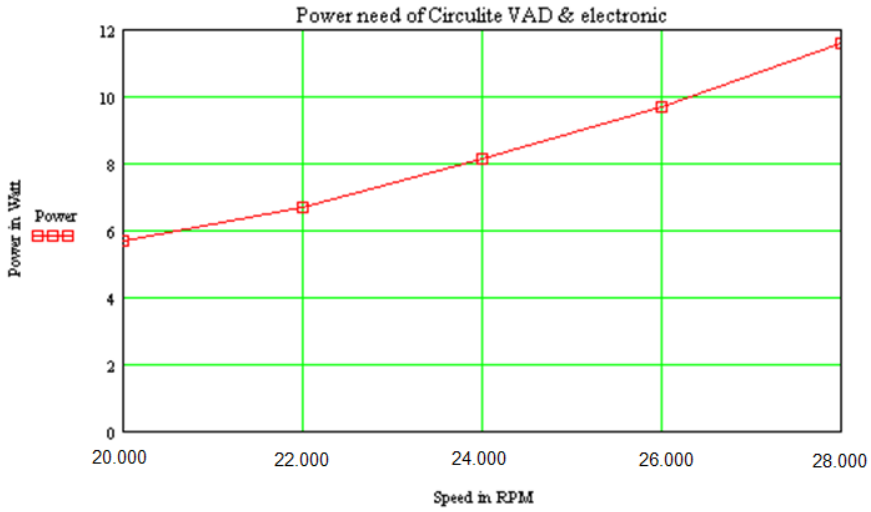

Figure 31 - Power need of the target VAD

The implanted part of the system shall be called ITET, the extracorporeal part ETET. The ETET implements the following functions:

- to drive the external TET coil,

- acquisition and conditioning of inductive voltage and current of the implanted coil,
- measurement of the temperature of the external coil,
- zero voltage synchronisation,
- zero derivative synchronisation,
- power regulation,
- generate pulse width modulation (PWM) signal for MOSFET-Driver.

While, the ITET implements the following functions:

- power compensation,
- synchronous rectification,
- acquisition and transfer of regulation data.

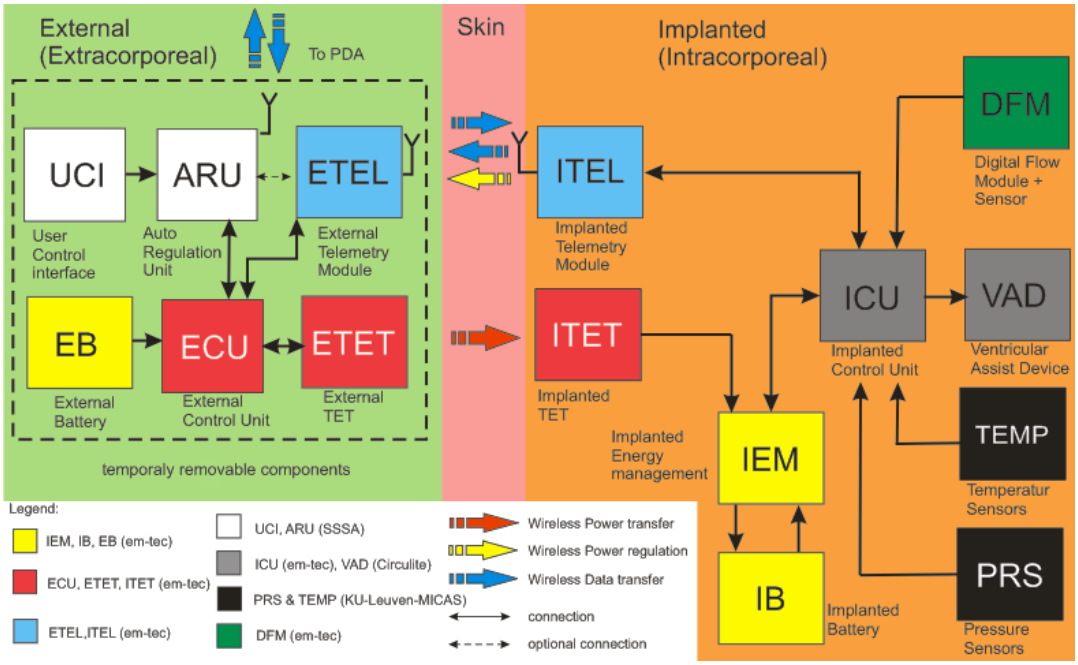

Figure 32 - Overview over the external and implanted parts of the system

As showed in Figure 32, the power received by the ITET must be converted, regulated and delivered over the implanted energy management system to all the intracorporeal components and should additionally charge an implanted energy storage unit. The control of the VAD is the main objective of the Implanted Control Unit (ICU), which controls the device internal control loop. Another task is the data collection from the implanted sensors and wireless transmission to the ARU. It is worth mentioning that it

was ruled out during the development that it is an advantage to hold symmetry between the extra- and the intra-corporeal parts. Therefore, the ECU has been introduced in the architecture. It is an external communication controller, necessary because the power regulation controller of the ETET had to be unloaded from the complex communication tasks.

About the coil, the chosen type must satisfy some requirements such as compact size, high link efficiency, high coil quality factor (low dc resistance, low influence of the skin and proximity effect), low heat dissipation, biocompatible enclosure. For these reasons, the spiderweb coils were applied; for an medical transcutaneous power transfer, they are unique and have the following advantages, over the application of a classical flat coil:

- only low proximity effect which leads to low resistances and therefore to a high coil quality factor Q (the high quality factor of the flat coils is based on ferrite cores, which is due to the high sensitivity of lateral and vertical movements),
- oblate shape,
- flexible design,
- place for extracting the wire endings and introduction monitoring thermistors.

For protection from the ionic conductive body fluids, the implantable coils were encapsulated in a flat silicon enclosure, as showed in Figure 33. Furthermore, to avoid movements of the implanted coils, the enclosure has four fixing eyelets that allow the surgeon to fix the TET coils under the skin with a sawing material. For applications in humans, only approved and unrestricted medical grade silicon, as MED4211 (shore A25) or equivalent, has to be used.

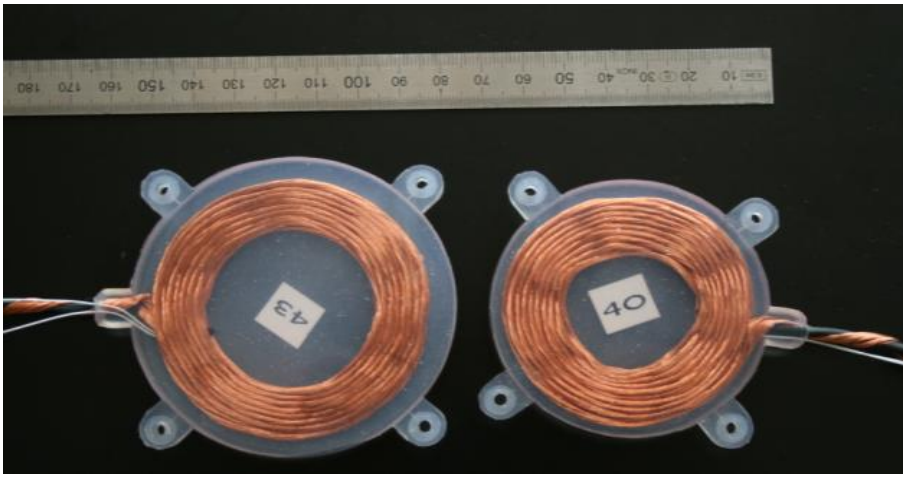

Figure 33 - The extracorporeal (left) and implantable (right) TET coils

It is demonstrated that the spiderweb coil has a better thermal dissipation characteristic then a classical flat coil. To demonstrate, also, that the TET coil could be implanted and the ISO14708-1 (no outer surface of an implantable part of the active implantable medical device shall be greater than 2 °C above the normal surrounding body temperature of 37 °C when implanted, and when the active implantable medical device is in normal operation or in any single-fault condition) [25] is respected, in this work of thesis specific measurements, described in the following paragraphs, have been done.

The most critical power component of the implantable part of the transcutaneous power transfer is the rectifier. An efficient rectification of the received alternate current (AC) is an essential part for the power transfer capability of the system.

The conversion efficiency is directly related to the thermal dissipation of the rectification circuit and, for this reason, it needed to be optimized.

After the realization and evaluation of three prototypes, a synchronous full-bridge MOSFET rectifier was chosen as power rectifier (Figure 34).

The reduction of the power loss at the level of the wireless power receiver is important to avoid thermal design issues. In many cases passive full-bridge rectifiers are used. Despite its simplicity, the drawback of this rectifier is that there are always two diodes conducting at the same time. The forward voltage drop of these diodes causes the majority of the power loss. The drop issue can be resolved using synchronous rectification. Typically, the timing of the synchronous rectifier is optimized to maximize the conduction time of the MOSFETs.

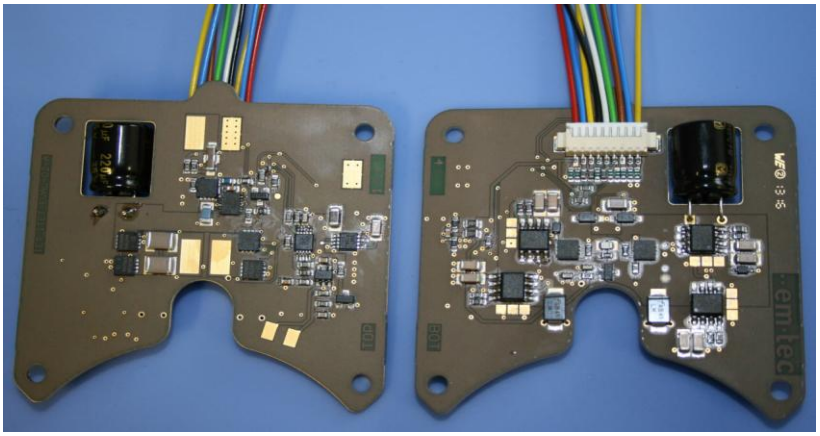

Figure 34 - ITET rectifier (top (left) and bottom (right) layer)

Furthermore, an important goal is to simulate and design the external and internal TET by paying special attention to the avoidance of too much heat especially on the internal components and too high magnetic field strength between the coils. In order to avoid too high temperatures, that will harm the human tissue, special electronic circuits must be designed, since common techniques cannot be used.

Also the operating frequency has to be chosen carefully in order to achieve the lowest possible heating of the tissue and to fulfill the requirements of the standards, which define the maximum tolerable magnetic field strength on humans.

The choice of the operating frequency is also a difficult step because the selected value has to cope with the conflict between the body absorption and the data transmission: a low frequency can better penetrate the human body, but lowers the bandwidth for data transmission. Taking into account of:

- proximity effect,
- influence of stray parameter, bigger for smaller coils,
- losses (switching losses, attenuation of electromagnetic waves in body, ...) and skin effect, proportional to frequency,
- higher frequencies allow smaller coil size,

the chosen working frequency is 150 KHz.

All the hardware developed for this unit drives the TET system in open loop. The result is a stable, high efficient coil driver which functions properly in the open loop operation at the fixed frequency.

The optimal TET coil separation gap for this auto-regulation behavior is between 10 mm and 20 mm. But, it is expected that a regulations by a closed loop operation will further optimize the TET performance versus load and misalignment and will improve possible coil gaps. It is worth mentioning that for developments on the close loop operation the availability of a telemetry unit is necessary.

4.2 COIL TEMPERATURE MEASUREMENTS

As discussed above, the TET uses an external and an implantable coil which are responsible for the energy transfer through the body. For this reason, it is necessary to test the coil temperature while all the TET system is running.

For the time being, only the ETET coil of the proposed system is provided with a thermistor (thermally conductive Epoxy coated thermistor 3K3A340I, Betatherm), placed between the windings. Thus, the measurements have been done on this coil but it is considered that the implantable coil temperature trend is the same as the external coil one.

The most interesting aspect to discover is how much the implantable coil surface becomes hot, because, if the temperature is higher than 37° C, the body tissues, near the implant, can be damaged. In fact, for example, results of in vivo measurements [27] show that for muscles power densities of 60 mW/cm^2 and 80 mW/cm^2 increase the baseline tissue temperature by 4-7°C. Thus, the absolute temperatures range from 43°C to 46° C, with necrosis occurring at the upper end of this range. While, for a power density of 40 mW/cm^2, the tissue temperature increase is limited to a range of 2-3° C, with absolute temperatures remaining below 42°C.

In these tests, first of all, the temperature of the ETET coil has been monitored under dependency of the VAD load. The other experiments have tested how the temperature trend changes varying the ITET coil position with respect to the external one. In particular, the vertical, horizontal and angular misalignment between the external coil and the implantable coil have been varied.

The main purpose of this measurements is to understand which is the most safe and efficient position to implant of ITET coil, so that the body internal movements don't cause an interruption in the energy transfer between the two coils.

About the measurement procedure, the temperature of the ETET coil has been monitored by the following measurements: the inner temperature, reading the thermistor output, the environmental and surface temperature, by both thermography (with the Fluke TiS Thermal Imager) and a measuring instrument (Almemo 2690).

In these tests, it is mandatory to consider that the thermal processes are very slow. Therefore, it is necessary to wait, before acquiring data, until the coil temperature has reached the stable phase, becoming constant. In fact, as showed in Figure 35 and Figure

36, the TET system has to run about one hour and half before the coil reaches a constant temperature value.

In the plots below, it is possible also to notice the efficacy of the silicon enclosure of the coils, which spreads heat from the inner part to the surface, allowing the coil implantation. In fact, the coil by itself becomes very hot (~52° C) and, if it is implanted without cover in the human body, it burns the tissues it is in contact with. While, in the covered coil, the temperature doesn't exceed the safety threshold of 37° C.

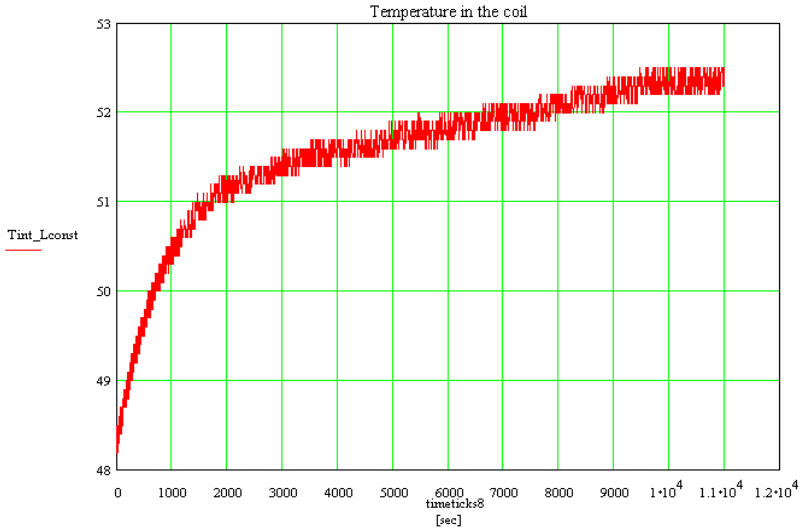

Figure 35 - Trend of the temperature (Absolute value [°C]) measured by the thermistor in the inner part of the coil with a constant current load of 800mA.

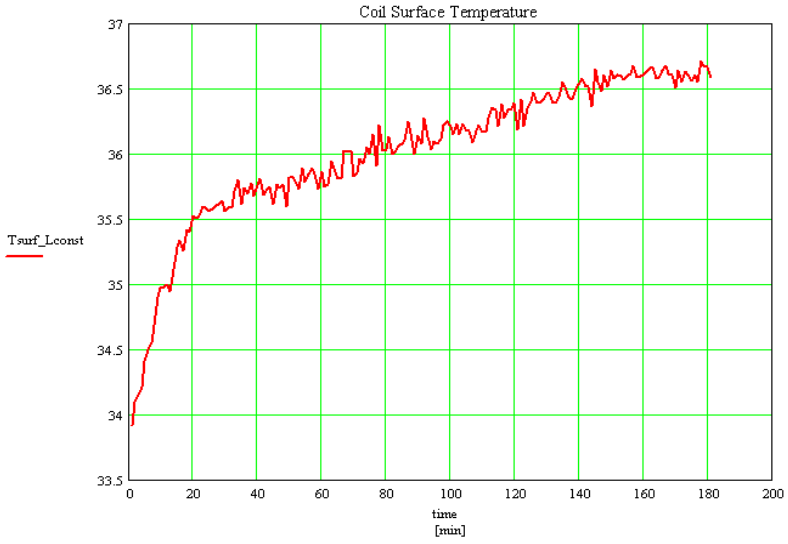

Figure 36 - Trend of the temperature (Absolute value [°C]) of the silicone surface of the coil with a constant current load of 800mA.

4.1.1 TEMPERATURE MONITORING OF THE ETET COIL DEPENDING ON THE VAD LOAD

The setup includes the extracorporeal and intracorporeal TET modules, the pump and its controller and the external and implantable power coils (Figure 37).

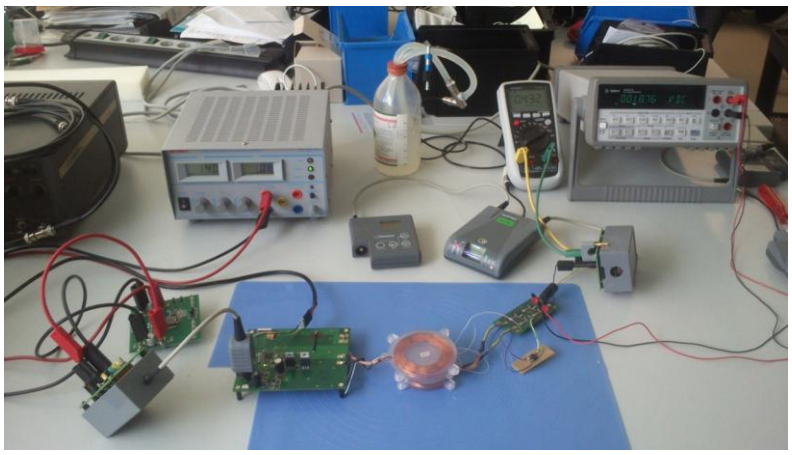

Figure 37 – Setup for the temperature monitoring depending on the VAD speed.

During the test, the load has been increased from 20.000 rpm to 28.000 rpm, by steps of 2000 rpm, and the temperature trend has been measured.

Plotting the relation between the coil inner temperature difference, with respect to the environmental temperature, and the VAD speed (Figure 38), it is possible to notice the minor relevance of the motor speed over the efficiency. The small temperature increase, when the VAD load goes from 24000 to 26000 rpm, could be an artifact, since the results are based only on one measurement.

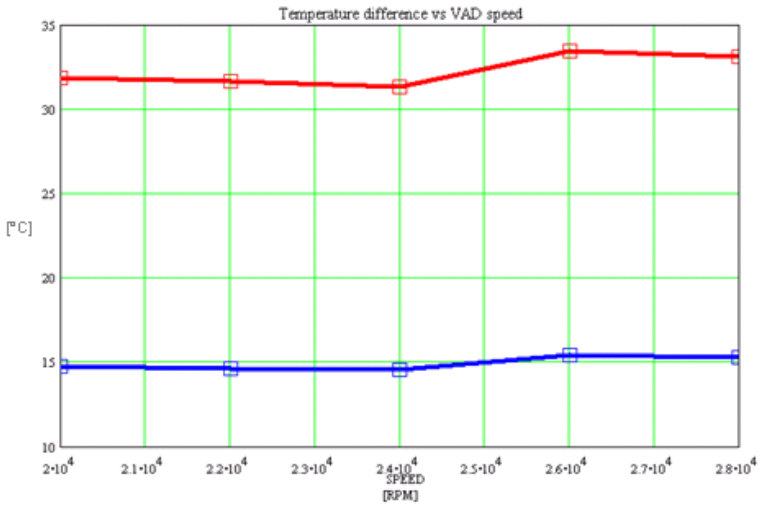

Figure 38 - Red broken line: relation between the coil inner temperature difference, with respect to the environmental temperature [°C], and the VAD speed [rpm]. Blue broken line: relation between the coil surface temperature difference, with respect to the environmental temperature [°C], and the VAD speed [rpm].

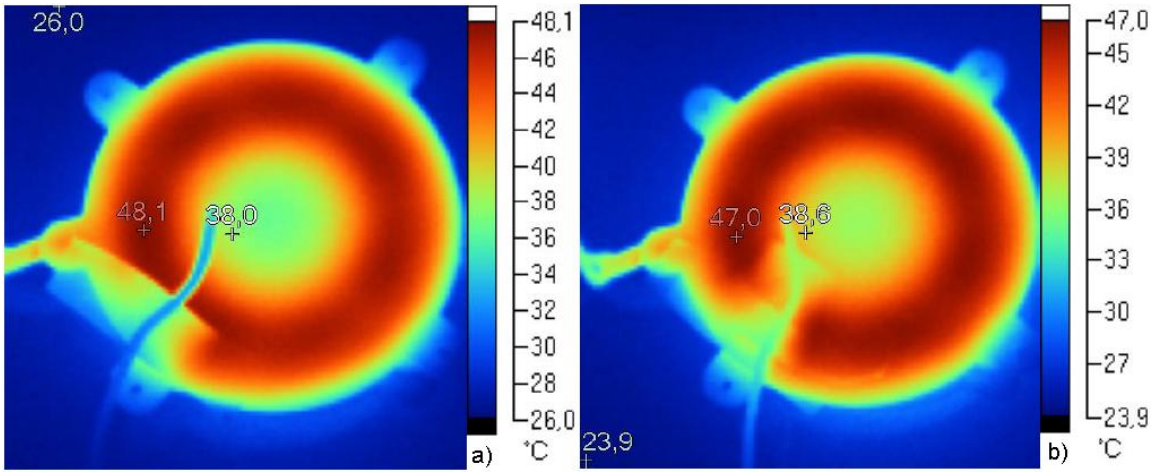

Figure 39 - Thermal image of the extracorporeal coil by infrared thermography at 20000 RPM (a) and 28000 RPM (b)

The surface temperature trend is the same as the inner temperature one, but the heat is spread through the silicon so the surface is 15° C colder than the inner part. In this way, with a 0.8 A load (that is the current consumption of the VAD at full speed, i.e. 28000 rpm) and an environmental temperature of 24°C, the coil surface temperature reaches 36.5°C that is acceptable for an implantable device.

It is also possible to notice from the infrared thermografy images, in Figure 39, the hottest areas in the coil at two different pump speeds (the lowest and highest rpm values).

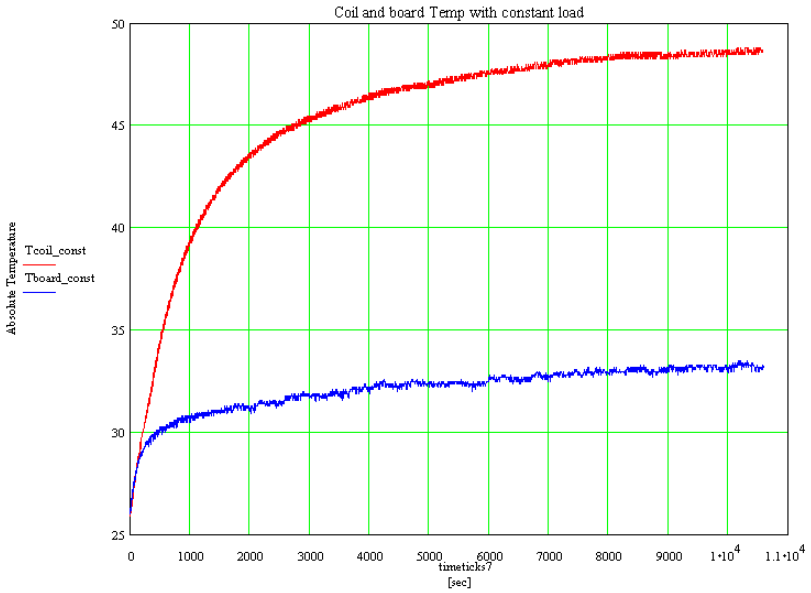

Figure 40 - Red curve: trend of the temperature (Absolute value [°C]) of the inner part of the coil with a constant current load of 800mA. Blue curve: trend of the temperature (absolute value [°C]) of the ETET board with a constant current load of 800mA.

Obviously, also the ITET board warms up while it is running, thus the PCB temperature has been acquired too, by a voltage output temperature integrated circuit from Microchip. In Figure 40 the board temperature trend in extreme working condition over time (800 mA) is plotted, it reaches the stable phase very quickly and doesn't exceed the safety threshold of 37°C.

4.1.2 TEMPERATURE MONITORING UNDER VERTICAL MISALIGNMENT

In this test, the same setup of the above measurement has been exploited. The VAD load is 24000 rpm and the distance between the coils is increased from 0 mm to 18 mm, by steps of 3 mm.

It is possible to notice (Figure 41) a inner temperature increase of 27° C and a surface temperature increase of 11° C. In this case, the two temperature trends are different: in the range between 0 mm and 9 mm, the inner and surface temperature difference

becomes more and more bigger, then in each case there is a stable phase in which the temperature is constant and at 15 mm the temperature stars to raise again.

The measurements have been stopped when the vertical distance between the two coils reaches 18 mm because at a greater distance there isn't any energy transmission. In fact, as showed in Figure 42, the TET system efficiency falls rapidly to zero.

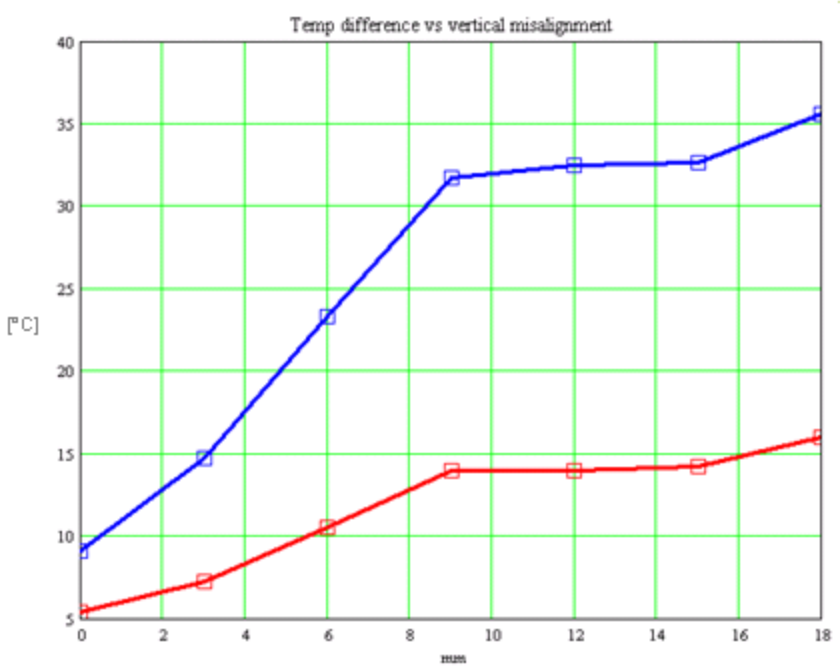

Figure 41 - Red broken line: relation between the coil surface temperature difference with respect to the environmental temperature [°C] and the vertical misalignment [mm]. Blue broken line: relation between the coil inner temperature difference with respect to the environmental temperature [°C] and the vertical misalignment [mm].

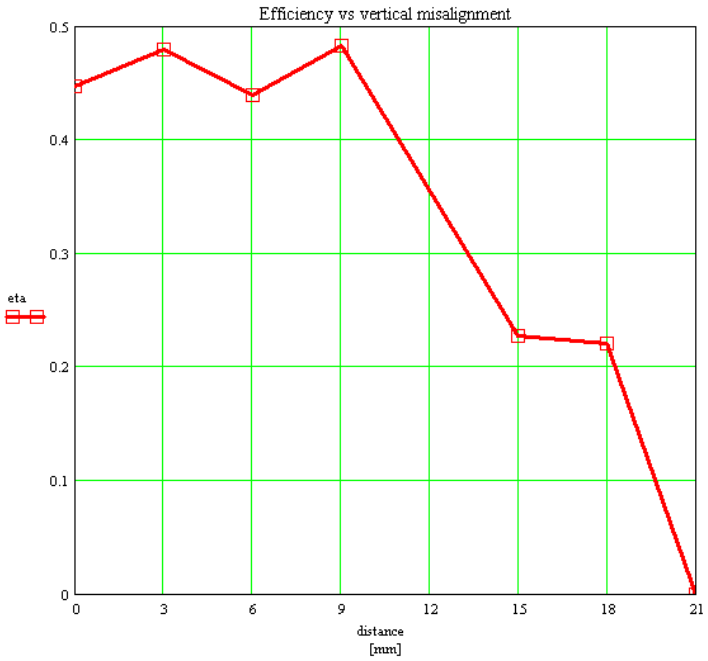

Figure 42 - Relation between the efficiency and the vertical misalignment [mm].

4.1.3 TEMPERATURE MONITORING UNDER HORIZONTAL MISALIGNMENT

The test setup is composed of the extracorporeal and intracorporeal TET modules, the external and implantable power coils. Additionally, a programmable DC electronic load is used to simulate the current consumption of the VAD at full speed. The current load is set to 0.8 A. The distance between the coil centres is increased from 0 mm to 15 mm, by steps of 5 mm. The origin of the x axis is located in the coil geometric centre.

It is possible to notice a inner temperature increase of 11° C and a surface temperature increase of 5° C. The trend reaches the smallest value at 10 mm misalignment and then there is a fast big increase.

In this case, the TET system doesn't work anymore over 15 mm horizontal distance between the two coils.

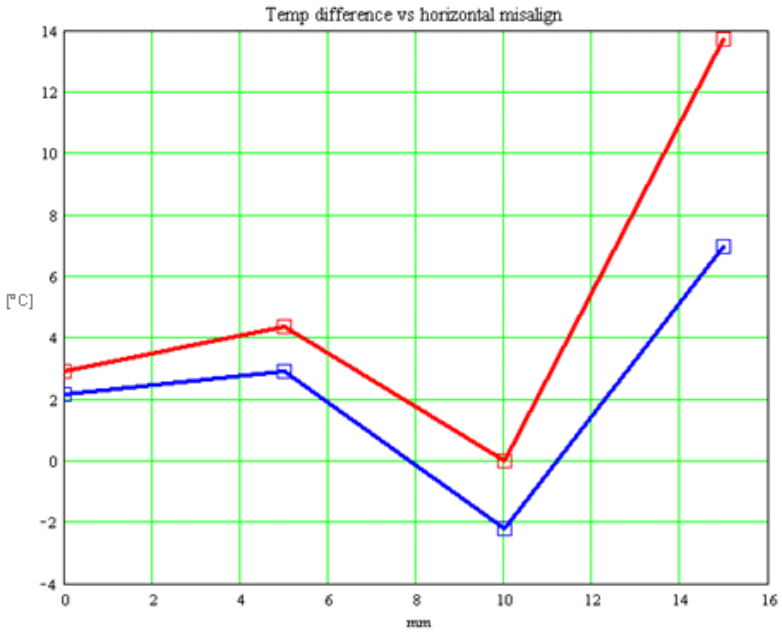

Figure 43 - Red broken line: relation between coil inner temperature difference, with respect to the environmental temperature [°C], and the horizontal misalignment [mm]. Blue broken line: relation between the coil surface temperature difference, with respect to the environmental temperature [°C], and the horizontal misalignment [mm].

4.1.4 TEMPERATURE MONITORING UNDER ANGULAR MISALIGNMENT

The setup is the same of the temperature monitoring under horizontal misalignment.

The current load is 0.8 A and the angular misalignment between the coils is increased from 0° to 40°, by steps of 10°.

For these measurements, a plastic test bench was designed and manufactured completely with non-magnetic materials (plastic, aluminum and V2A screws) to avoid magnetic influences.

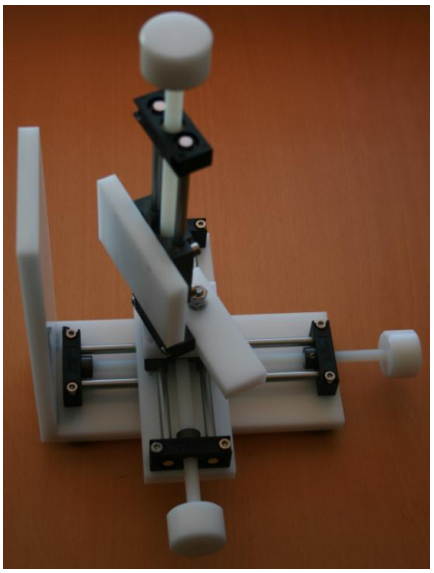

Figure 44 - Test bench for misalignment measurements of inductive power coils.

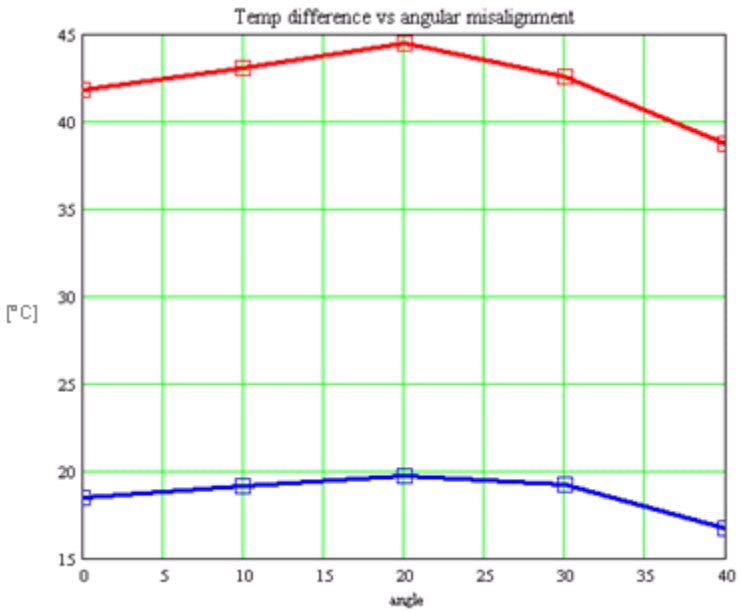

Figure 45 - Red broken line: relation between coil inner temperature difference, with respect to the environmental temperature [°C], and the angular misalignment. Blue broken line: relation between the coil surface temperature difference, with respect to the environmental temperature [°C], and the angular misalignment.

In this case, the temperature increase is minimum, in fact it is possible (Figure 45) to notice only a little pick of 3° C at 20° misalignment.

4.3 ITET RECTIFIER EFFICIENCY

The most critical power component of the implantable part of the TET is the rectifier. An efficient rectification of the received AC is fundamental for the power transfer of the TET. But, the conversion efficiency is directly related to the thermal dissipation of the rectification circuit, thus, in order to develop an implantable ITET, it was necessary to optimized the circuit.

The first rectifier circuit for the laboratory prototype ITET was a self-controlled rectifier. The advantage of this circuit is that the rectification is controlled by the alternating power current itself, not by an active controller. On the other hand, there is one schottky diode for each half-wave in the power path which lead to power dissipation. The loss over the diodes causes a voltage drop in the range of 0.3-0.6 V which is responsible, with a maximum current of 3 A, of a maximal thermal dissipation of 0.9 to 1.8 W.

In Figure 46, it is possible to notice the worm big area results from the thermal dissipation of the schottky diodes with two hot spots of nearly 60°C .The application of heat spreading material reduces clearly the hot spots by dissipating the heat over a bigger area, but this solution did not result sufficient.

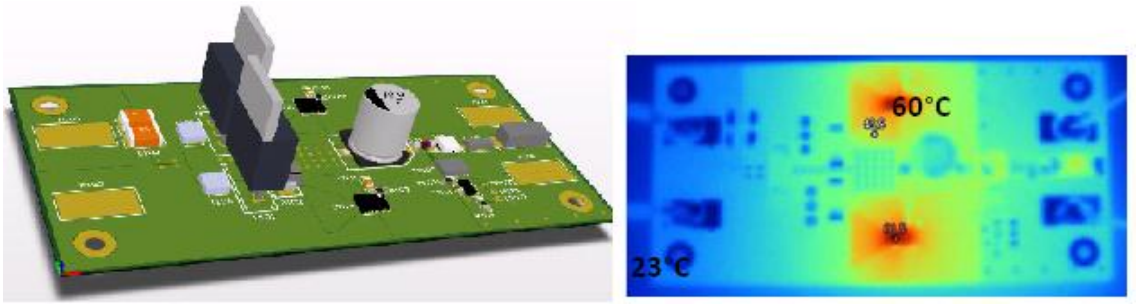

Figure 46 - Semi-active rectifier with ideal diodes and its thermography image at 12 W.

It was obvious that such high temperatures are not acceptable for implantable electronics. Therefore other rectifier solutions, without diodes, had to be investigated.

Then, a regulated synchronous full-bridge MOSFET rectifier was realized and tested. This type is a digitally controlled MOSFET rectifier, based on a digital signal controller, which drive actively the MOSFETs and was proposed by Huwig *et al* [28].

This circuit is characterized by an overall efficiency increase of around 3% with respect to a semi-active rectifier and 7% to a passive diode rectifier. The disadvantage is the high development effort and reliability issues based on firmware (functional safety aspect).

This circuit was originally designed to work at 50-60 Hz, thus a compensation network was realized in order to extend the operating frequency to 150 kHz.

The thermography image (Figure 47) demonstrates that the hot spot temperature is under 37°C and that most of the surface remains in the range of the environmental temperature (25°C).

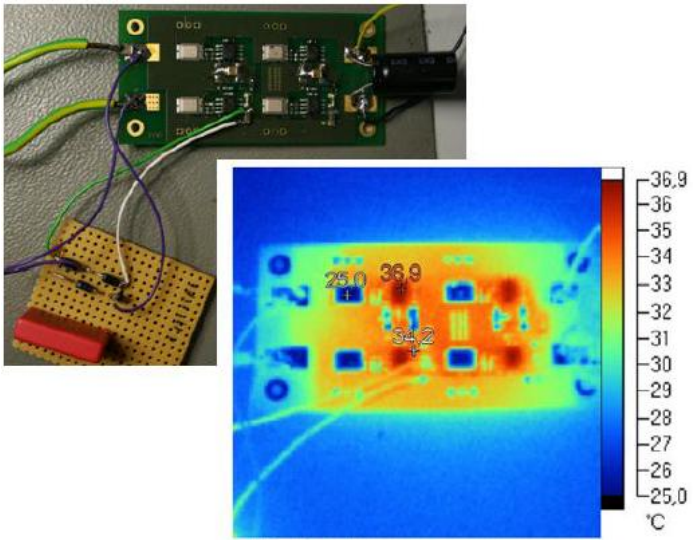

Figure 47 - Thermography of a Full-bridge MOSFET rectifier able to transfer 20 Watt of power.

Afterwards, an improved power rectifier was developed. A special PCB layer stack was designed and manufactured in order to spread effectively the generated heat from the power rectifier over a huge area avoiding hot spots in the implant.

Furthermore, the ITET should be placed as much closed to the power coil as possible. This optimal location will reduce interferences, avoid that the high AC voltages need to be transferred inside the body over a long distance and will help to minimize thermal dissipation loss.

The thermography of the improved ITET is showed in Figure 48 for 12 W, which is the maximum power requested by the CircuLite LVAD, running at a speed of 28.000 rpm. With this final solution, an acceptable surface temperature for implantable electronic is guaranteed.

A task of this thesis was to evaluate the three different power synchronous rectifier solutions, the pure AC(RMS)-DC efficiency of the power rectifiers has been measured as function of the frequency.

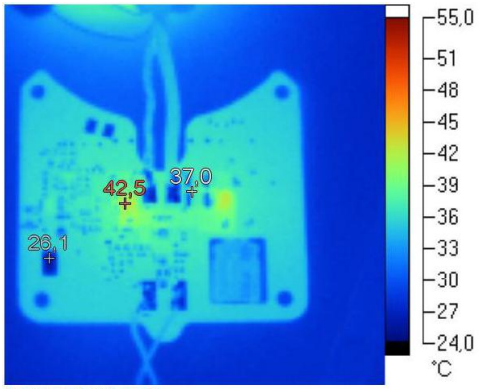

Figure 48 - Thermography of the ITET for an output power of 12 Watt.

First of all, the AC-DC efficiencies of the power rectifiers have been measured directly by a power amplifier (non-resonant case) over a wide frequency range that goes from 80 kHz to 200 kHz, in a constant 10 Ohm load (Figure 49).

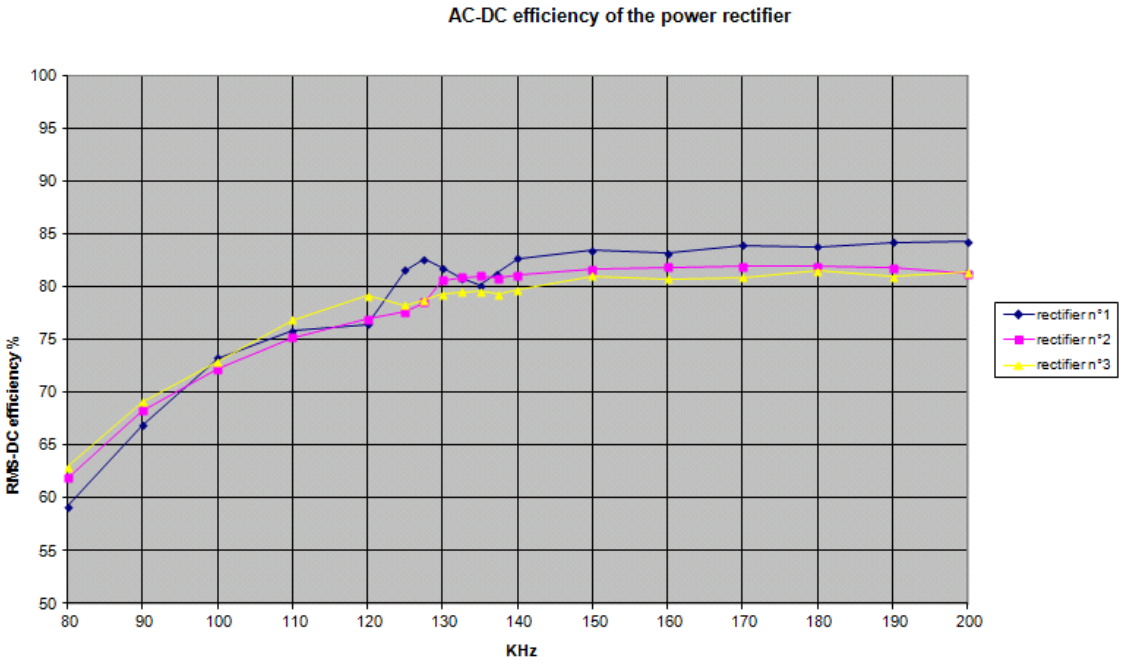

Figure 49 – Efficiency (RMS-DC) of three MOSFET power rectifier as function of the frequency.

The RMS-DC efficiency is always higher than 80 % at the intended operating frequency of 150 kHz. In detail, at 150 kHz, the first prototype, self-controlled rectifier, is characterized by an efficiency of 80.9% while in the second, full-bridge MOSFET rectifier, the efficiency reaches 81.6%. Finally, the advanced fully-synchronous power rectifier has an efficiency of 83.4%. Thus, this improved ITET, not only can be implanted thanks to its heat dissipation strategies, but presents also a very high efficiency.

Furthermore, the efficiency of the improved power rectifier has been measured (Figure 50), in the operating frequency range, for four different loads: 7.2 Ω, 10 Ω, 14.9 Ω and 20.1 Ω, in order to simulate different VAD loads, i. e. different speed values.

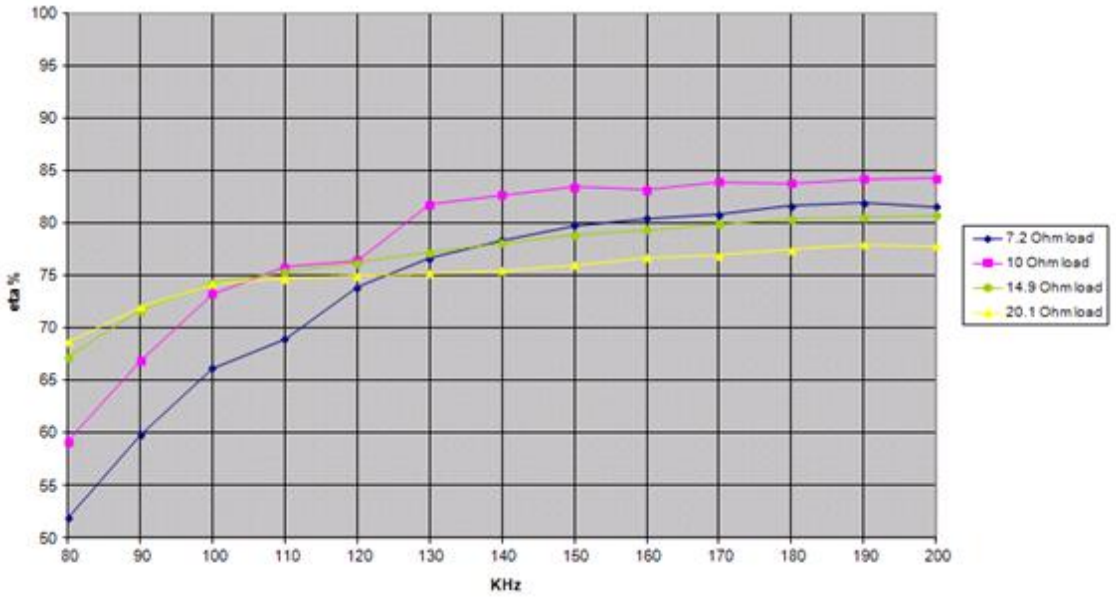

Figure 50 – Improved ITET efficiency, for different loads, in function of the frequency.

CHAPTER 5

5.1 MEDICAL IMPLANT COMMUNICATION SERVICE – TELEMETRY

The need of a biomedical telemetry in the proposed system is for the acquisition of physiological signals from the pump and the sensors at a distance, through wireless communication technologies.

In order to develop the telemetry system of the proposed platform, several different antenna types with specific characteristics have been tested. But not all types are perfectly suitable for an implantable antenna and each solution has advantages and disadvantages.

To find a good solution for implantable antenna, a set of antennas was selected by modifying commercially available samples and developing other particular types. Their performance in free-air, *ex-vivo* and in simulating tissue matter have been compared.

The needed bound-rate is estimated by an evaluation of the data-rate of each component of the implantable platform and are reported in Figure 51.

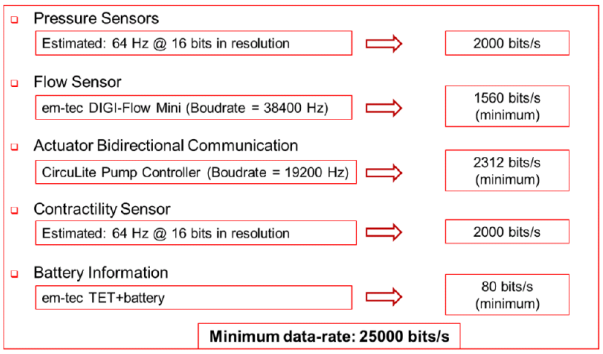

Figure 51 - Data Rates of implantable platform components

The following considerations have been done in order to make a choice about the operating band:

- ISM bands offer many frequent choices but are heavily to be used,
- lower frequency are less attenuated in the body (losses are proportional to frequency),
- higher frequency allow smaller antenna size,

- MICS band has low interference and employs clear channel assessment and listen before talk.

From these considerations, the MICS band was chosen because of:

- FDA, FCC approval for implantable devices (as pacemakers) and endoscopic capsule (es. Pillcam) without causing interference to other users in the electromagnetic radio spectrum,
- good propagation characteristics for medical implants,
- reasonable sized antennas,
- worldwide availability.

Thus, the main objective in this section is the development of a bidirectional telemetry (TEL) operating in the MICS frequency range from 402 to 405 MHz. The components ETEL (external TEL) and ITEL (implantable TEL) are the important wireless communication bridge between the implantable platform and the extracorporeal system components.

5.1.1 IMPLANTABLE TRANSCEIVER MODULE

The MICS telemetry system of the platform is based on the implantable transceiver module ZL70321 from Zarlink (Microsemi). This transceiver is an ultra low power chip that provides high speed communications between the IMD and an external device over the MICS band.

This transceiver was chosen thanks to its main features:

- MICS Band with 800 kbps data-rate,
- highly reliability: automatic media access controller and cyclical redundancy check,
- low size-consuming,
- extremely low power consumption and three possible power wake up circuits,
- biomedical certification (ISO9001 [32]).

To support a quick startup, Zarlink provides an evaluation and Application Development Kit (ADK). This development kit (Figure 52) is designed with clearly separated hardware and software layers. The software of the ADK is intended to operate in conjunction with a personal computer and it provides separated GUI for base station

and for the implanted part. On this basis, all the features of this MICS telemetry system can be evaluated and analyzed by the usage of the GUI.

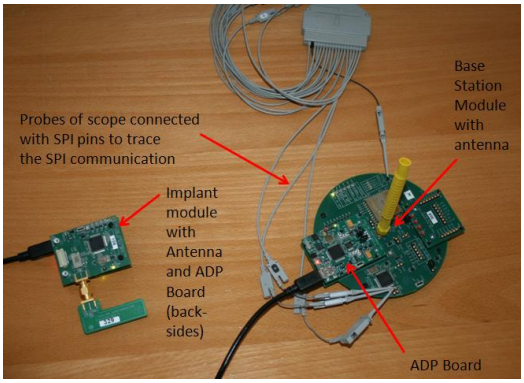

Figure 52 - Startup with Evalkit from Zarlink

To have access to the registers of the telemetry module two standalone software have been developed. They are able to control the ETEL and the ITEL. These programs could be used for the parameter optimization of the telemetry link and are helpful for the characterization of MICS telemetry modules, implantable antenna and unit testing.

Based on the implantable module ZL70321 from Zarlink, a universal telemetry board with an additional MSP430 microcontroller was developed. In contrast to the evaluation kit from Zarlink, this board is intended to be applied on both the extra- and intra-corporeal side. This concept simplifies the RF matching and integration, but requires the application of a MICS in-band wake-up.

Furthermore, a LC pre-matching circuit was designed in order to adapt the implantable antenna, that will be chosen, to the ZL70321. Impedance matching is the process of removing mismatch loss. It minimizes the reflection coefficient, reducing the power reflected from the load, i.e. the antenna, and maximizing the power delivered to the antenna.

With this matching circuit the RF impedance of the implantable antenna prototypes will be transformed to 50 Ohms. This results in optimized transmission and receiver characteristics and leads to a minimized RF exposition of the human tissues, thus minimized SAR.

5.2 ANTENNA MEASUREMENTS IN TISSUE (EX-VIVO AND IN-VITRO)

5.2.1 MEASUREMENTS WITH IMPLANTABLE DIPOLE AND PRINTED LOOP ANTENNA

5.2.1.1 Measurements with Dipole antenna

The device under test is a dipole antenna (for further details see Appendix E) with a 3 mm diameter and without ground plane. A spectrum analyzer, a magnetic field probe and a broadband amplifier have been used in the setup. The procedure consists in shortening (tuning) the antenna for in-body measurements, by step of 5 mm, from 19.5 cm to 13.5 cm (Figure 53). The transmitter is 0,65 m from the receiver (the magnetic field probe), at the same height as the receiving antenna.

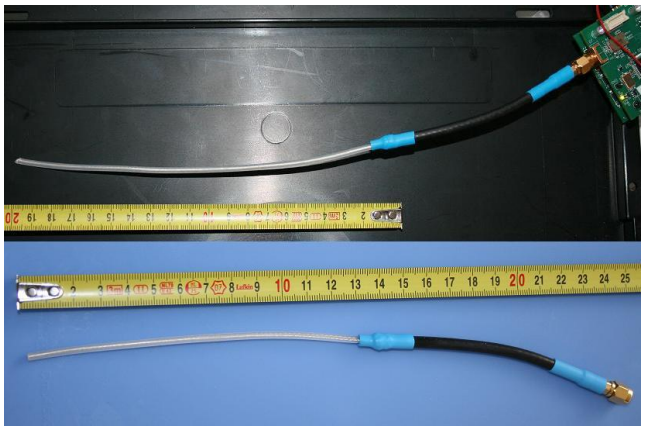

Figure 53 - Dipole antenna before and after the measurement procedure (shortening from 19.5 cm to 13.5 cm)

Four different setups have been used. As described in Figure 54, in the “free air” setup (setup 1), the antenna is on a layer of meat (pork); in the “in contact with skin” setup (setup 2), the antenna is on two different layers of tissue, one of pork skin and one of meat; in the “transcutaneous” setup (setup 3), the antenna is on a layer of meat and covered with skin; in the “deep implantable” setup (setup 4), the antenna is on a layer of meat and covered with two different layers of tissue, one of pork ribs and one of skin. For each setup, the radiated power has been measured for the different antenna lengths, as showed in Figure 55.

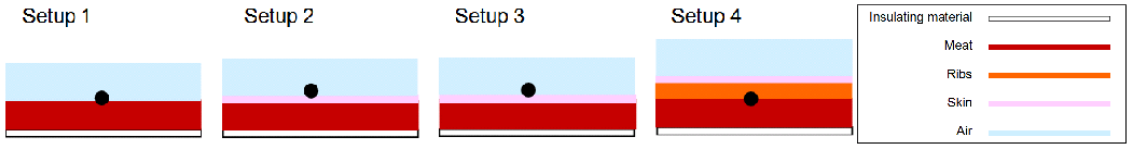

Figure 54 - Description of the four used setups.

F [MHz]	L=λ/4 [mm]	Setup 1 [dBm]	Setup 2 [dBm]	Setup 3 [dBm]	Setup 4 [dBm]
384,6	195	- 12,4	- 12,0	- 14,4	--
349,7	190	- 11,2	- 12,4	- 14,0	--
405,4	185	- 12,4	- 11,2	- 13,6	--
416,7	180	- 13,6	- 10,8	- 13,2	--
441,2	170	- 12,4	- 10,4	- 12,8	--
468,8	160	- 11,6	- 10,8	- 11,2	--
500	150	- 12,4	- 10,4	- 10,8	--
517,2	145	- 12,0	- 10,4	- 9,2	--
535,7	140	- 11,8	- 10,8	- 8,8	- 6,8
555,6	135	- 11,2	- 9,2	- 7,8	- 7,2

Table 1 - Measurement results.

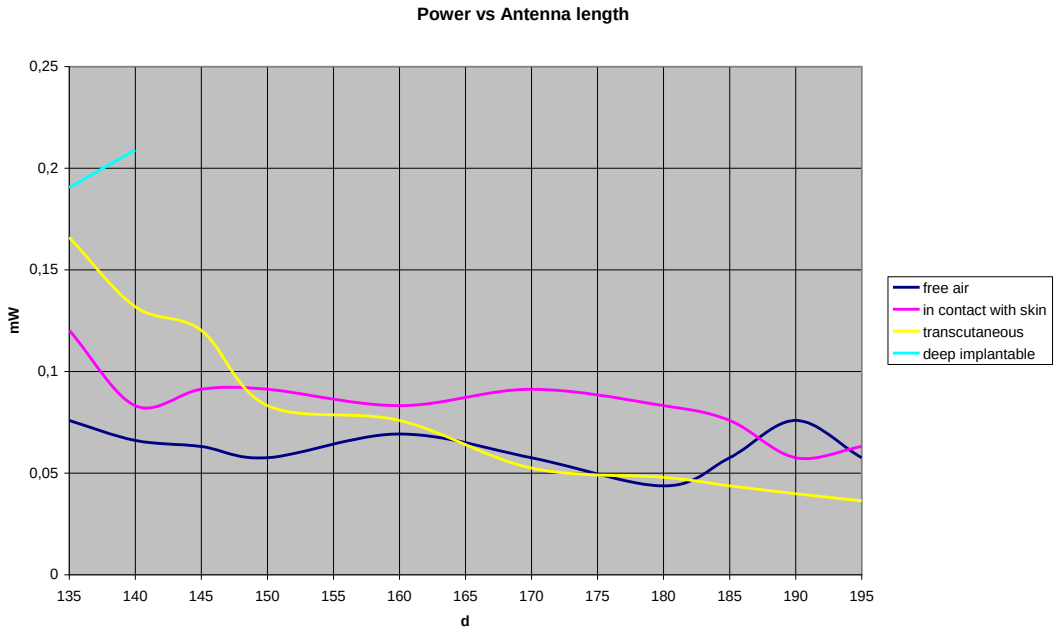

Figure 55 - Relation between radiated power [mW] and antenna length [cm] for the four different setups.

5.2.1.2 Measurements with implantable printed loop antenna

The device under test is the implantable printed loop antenna (for further details see Appendix E) PLA100 Rev C (by Zarlink) optimized for MICS 402 – 405 MHz band (Figure 56). It has an added tuning camp which improves the ground to SMA connection and changed antenna shape to match better the 50 Ohm impedance. The specified antenna gain in air: -16 dBi @ 403.5 MHz (max.), approximate a loop length of 80 mm.

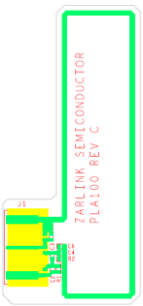

Figure 56 - PLA100 Rev C by Zarlink.

Two *ex-vivo* measurement procedures have been followed:

- in the former, the transmitted power is measured (Figure 57) by varying the value of the power code in the register "reg_rf_txrfpwrdefaultset" of the AIM200 (implantable device from the ADK of Zarlink, used in this setup). The transmitter is 0,65 m from the receiver (magnetic field probe), at the same height of the receiving antenna. The antenna is covered by a silicon sheet and placed between two layers of meat (pork);

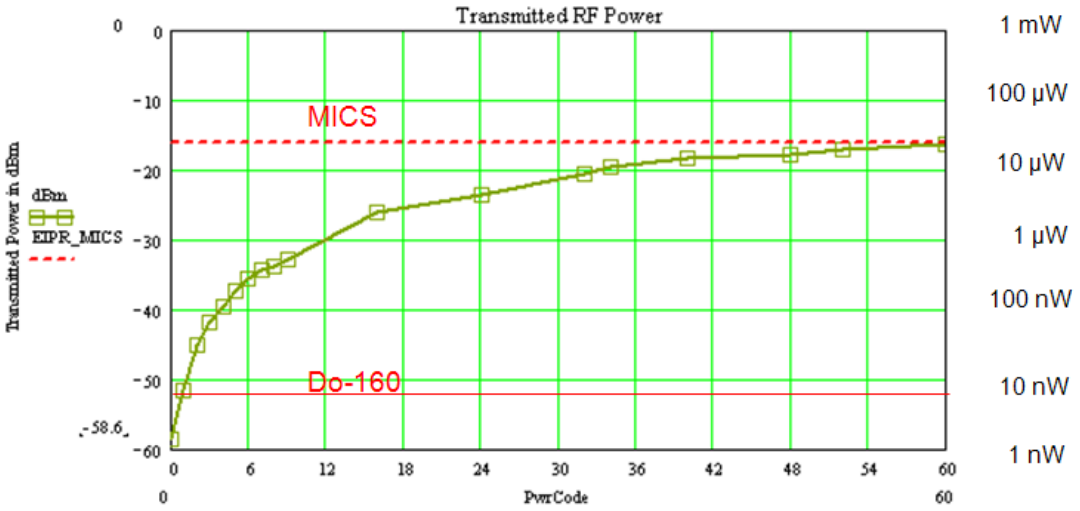

Figure 57 - Transmitted Power measured at a distance of 0.65 m from the magnetic field probe with HM5530, in-Vivo Modell: 3 cm meat, antenna in silicon sheet, 5 – 8 cm meat (pig)

- in the latter, the measurement procedure consists in increasing the thickness of the meat (pork) on the antenna for in-body measurements. The value of the power code in the register "reg_rf_txrfpwrdefaultset" of the AIM200 is set at 0x30. The transmitter is 0,65 m from the receiver (magnetic field probe), at the same height of the receiving antenna. The antenna is covered by a silicon sheet (Figure 58).

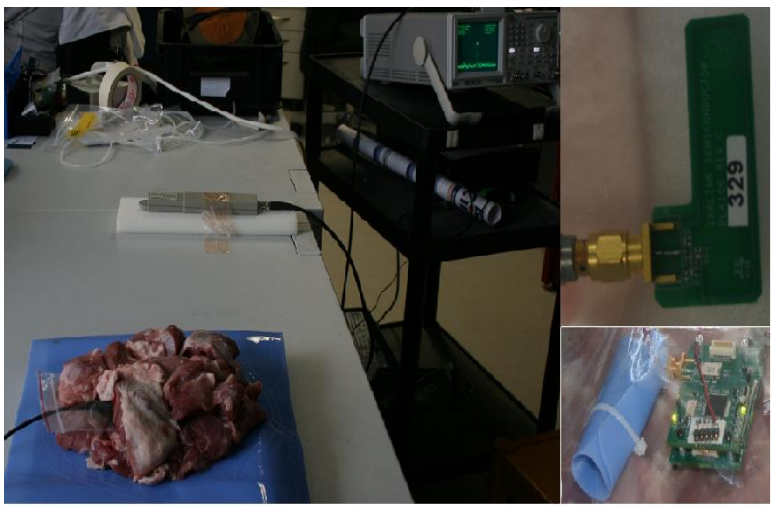

Figure 58 - Implantable antenna PLA100 (Zarlink) and setup for *ex-vivo* measurements, with antenna in silicon sheet

Four tests have been done with different setups, increasing the meat thickness on the antenna. In the first two setups (Figure 59), the thickness of the meat under the antenna is 5 cm while in test 3 and 4 (Figure 63) it is 2 cm. In test 1 and 3 the pork ribs and skin have been placed in parallel to the antenna, while in test 2 and 4 the pork ribs and skin have been placed perpendicular to the antenna.

The radiated power, measured in these tests, in mW and dBm, are showed in the following Figures.

The result that better shows accordance with data reported in literature [29] is that obtained in test 3, pork ribs and skin placed in parallel to the antenna. In literature, the penetration of the radiation in biological tissue is calculated at 433 MHz (which is closed to MICS). The relative attenuation of the radiated power is 0.1 at 3.5 cm in depth and ~0.01 at 7.0 cm. Instead, in test 3, at 403 MHz, the relative attenuation is ~0.5 at 3.5 cm (Figure 66).

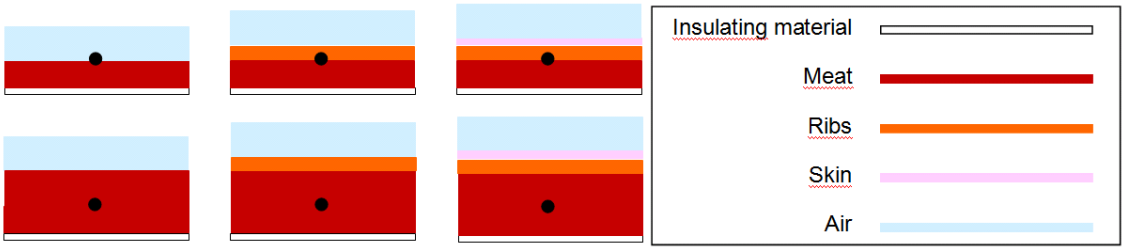

Figure 59 - Described of the used setup in test 1 and 2

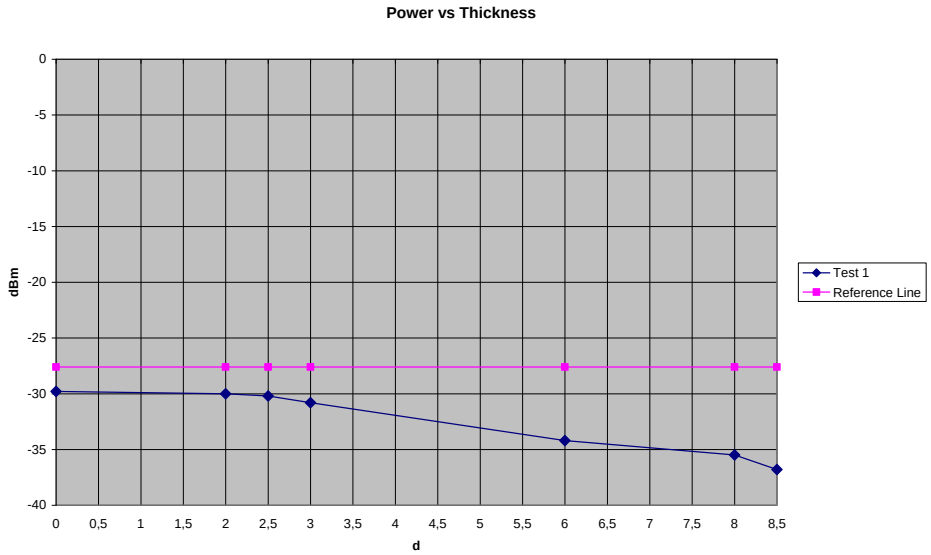

Figure 60 - Blue broken line: relation between radiated power [dBm] and thickness [cm] of the meat on the antenna in Test 1. Pink broken line: radiated power of PLA100 operating in air (reference line).

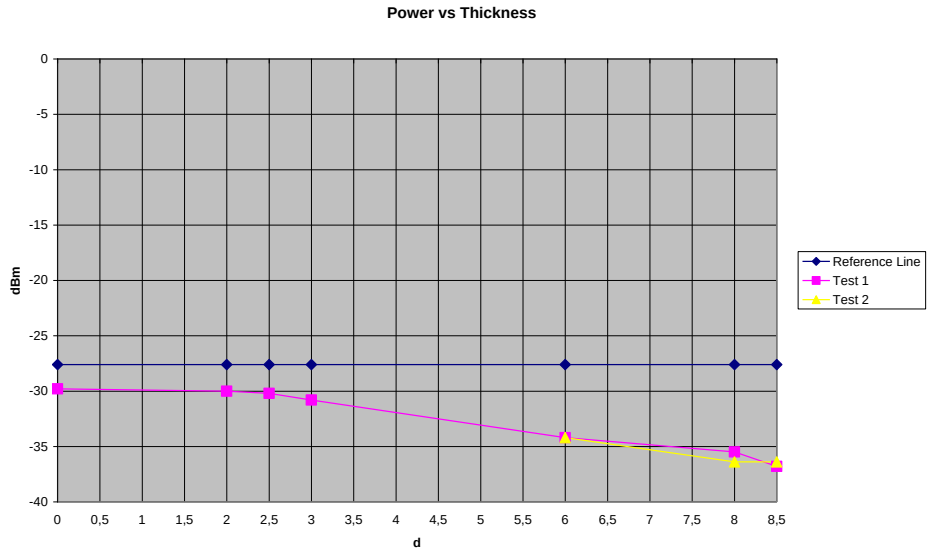

Figure 61 - Pink broken line: relation between the radiated power [dBm] and thickness [cm] of the meat on the antenna in Test 1. Yellow broken line: relation between the radiated power [dBm] and thickness [cm] of the meat on the antenna in Test 2. Blue broken line: radiated power of PLA100 operating in air(reference line).

Figure 62 - Pink curve: relation between the radiated power [mW] and thickness [cm] of the meat on the antenna in Test 1. Yellow curve: relation between the radiated power [mW] and thickness [cm] of the meat on the antenna in Test 2. Blue line: radiated power of PLA100 operating in air (reference line).

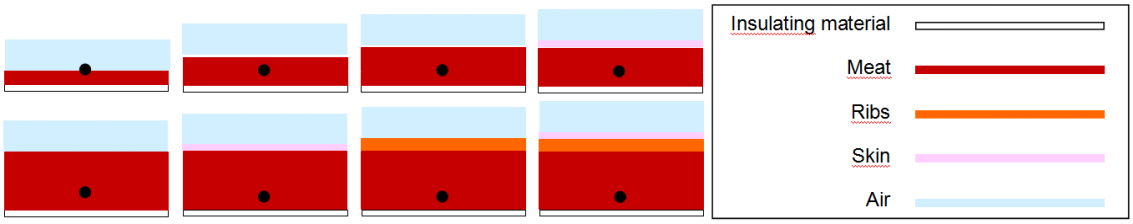

Figure 63 - Description of the used setup in test 3 e 4

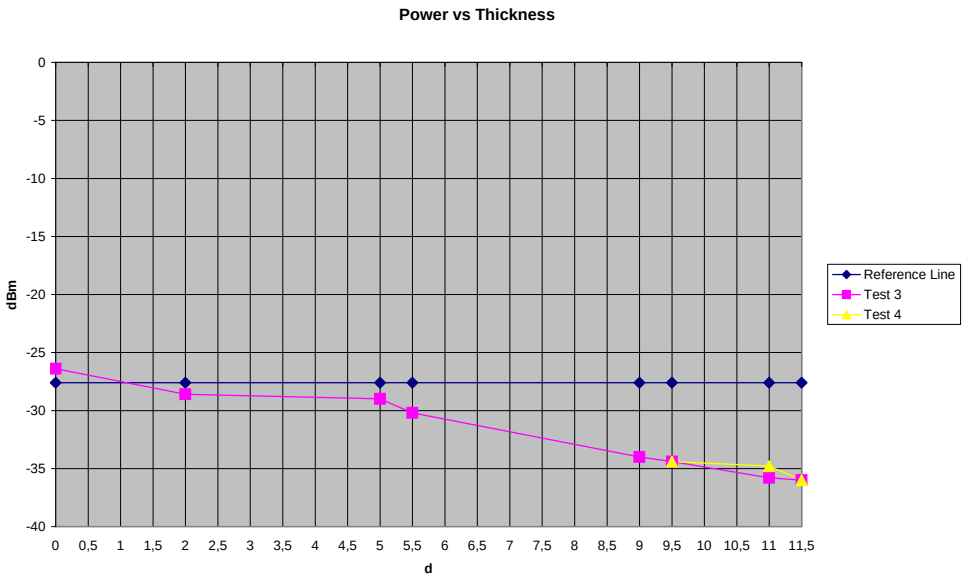

Figure 64 - Pink broken line: relation between the radiated power [dBm] and thickness [cm] of the meat on the antenna in Test 3. Yellow broken line: relation between the radiated power [dBm] and thickness [cm] of the meat on the antenna in Test 4. Blue broken line: radiated power of PLA100 operating in air (reference line).

Figure 65 - Pink curve: relation between the radiated power [mW] and thickness [cm] of the meat on the antenna in Test 3. Yellow curve: relation between the radiated power [mW] and thickness [cm] of the meat on the antenna in Test 4. Blue line: radiated power of PLA100 operating in air (reference line).

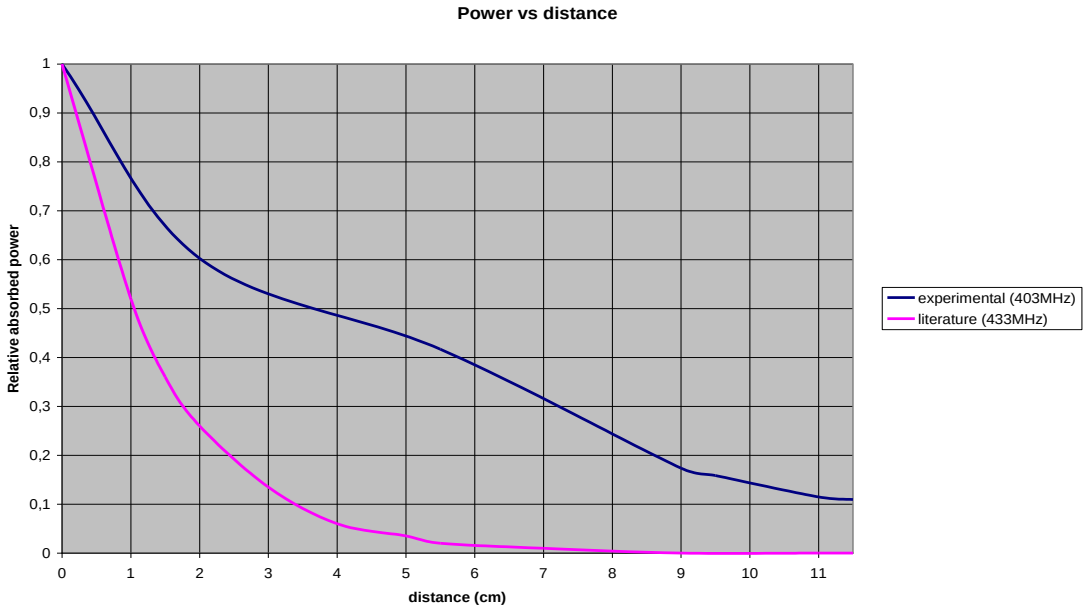

Figure 66 - Pink curve: Relative power absorbed as a function of the tissue depth at 433MHz (Vorst et al., p.43). Blue curve: Relative power absorbed as a function of the tissue depth at 403MHz, obtained with this *ex-vivo* measurements.

5.2.2 Antenna Measurements in the German Aerospace Center (DLR)

For the antenna characterization, specific tests have been done at the German Aerospace Center (DLR) with the Agilent/HP E8363C PNA Series Microwave Network Analyzer.
In this measurements, the device under test is the implantable printed loop antenna PLA100 Rev C (Zarlink).
The plot of S11 parameter (for further details see Appendix F) has been measured with the Network Analyzer at different thicknesses of the meat (pork) on the antenna, to simulate in-body measurements.
The antenna is protected with an antistatic bag and different setups has been tested to simulate: a subcutaneous implant, an intercostal implantable antenna and a deep implanted antenna. The maximal resonance is reached when PLA100 operates with ribs placed on the antenna at 45 degrees with respect to the direction of the antenna.

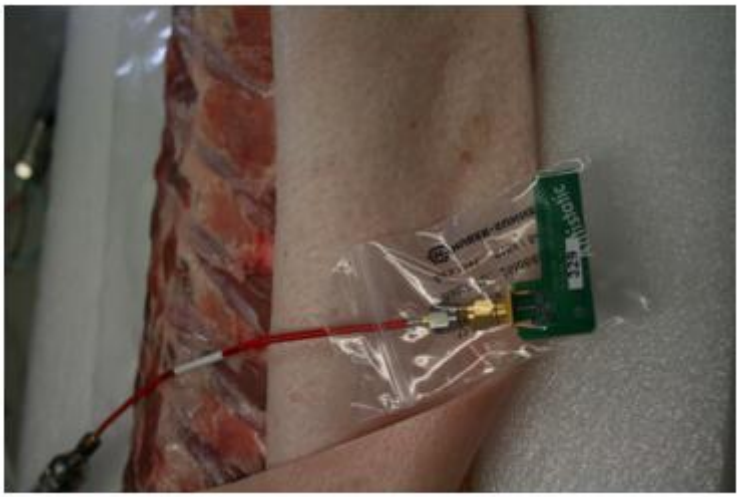

Figure 67 - Reference setup with PLA100 operating in air protected with an antistatic bag

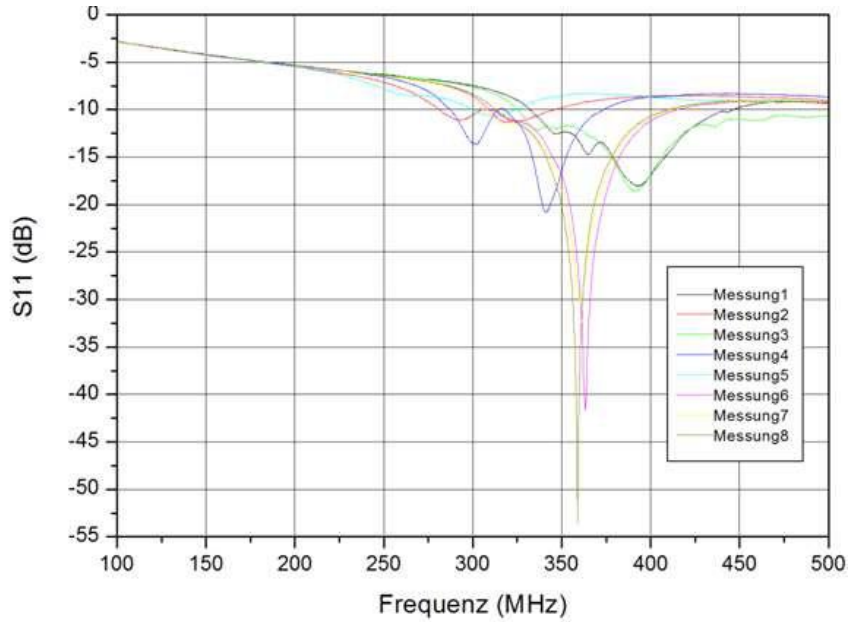

Figure 68 - Comparison of the S11 diagrams for PLA100 operating in 8 different setups

The Figure 68 implies that the antenna radiates best at ~360 MHz, where S11=-55,36 dB, in the maximal resonance case (green line, messung 8). Further, near 100 MHz the antenna will radiate virtually nothing, as S11 is close to 0 dB (so all the power is reflected).

The antenna bandwidth can be determined from the plot of S11. The bandwidth is defined as the frequency range where S11 has to be less than -6 dB, then the bandwidth, in the maximal resonance case, would be roughly 40 MHz, with 380 MHz the high end and 340 MHz the low end of the frequency band.

These measurements have showed that the loop antenna was tuned by Zarlink as an air-antenna: S11 = - 16 dB at 402.5 MHz (Messung 1, Figure 68). This could be maximized in air between -18 and -22 dB by a proper tuning. Furthermore, with different tissue types, the measured MICS values are between -8 dB (PLA100 deep in meat, Messung 4) and -16 dB (subcutaneously, Messung 3).
It is worth mentioning that the maximal seen resonance is due to ribs orientation. This demonstrate that the PLA100 has a strong undesirable dependence on the configuration.

5.2.3 DIELECTRIC ENCLOSURE INFLUENCE

Because of biocompatibility issues, the implantable antenna needs to be embedded in a dielectric enclosure.
The advantage of a dielectric enclosure are that the length of the antenna can be shorter and the implantable antenna will be partly decoupled from the variable tissue characteristic.

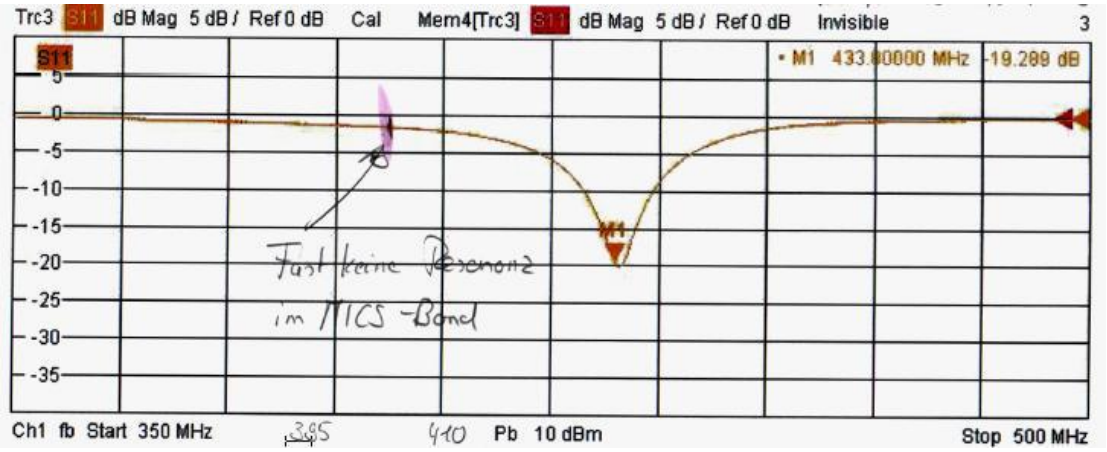

Figure 69 - Stub-Antenna at 433 MHz without silicone.

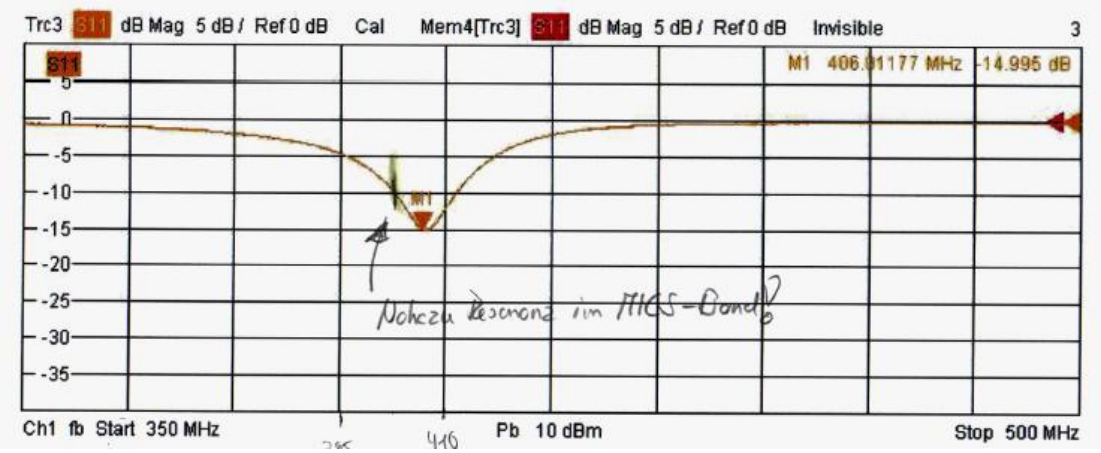

Figure 70 - Stub-Antenna at 433 MHz enclosed in silicone (d=1.35 mm).

Enclosing implantable antennas in dielectric materials (e.g. silicone) cause a decreasing of the resonance frequencies, as showed in Figure 69 and Figure 70. This leads to suitable implantable antenna solutions, but the decoupling effect with surrounding tissue and the implantation depth have also to be considered and investigated in *ex-vivo* and *in-vivo* experiments.

5.2.4 EX-VIVO AND IN-VITRO MEASUREMENTS

5.2.4.1 Test environment

In order to verify the performances of an implanted antenna in the human body, it is indispensable to evaluate the interactions between the human body and the electromagnetic waves radiated from the devices. In these types of investigations, instead of a real human body, tissue-equivalent phantoms are usually used.

This method guarantees more repeatable and reproducible tests than recurring to animal tissue samples (e.g. pork meat).

Thus, a phantom has been developed and tested in accordance with [31]. It has properties similar to the human body tissues. Its dielectric permittivity, conductivities and mass density are an average of the different tissues values.

The gel consists of de-ionized water, sugar, salt and a TX-151 powder and is formed by adding the powder to the liquid solution, which is obtained dissolving sugar and salt in hot water.

TX-151 (The Oil Research Centre, Lafayette, LA, USA) is a gelling compound consisting mostly of polysaccharides. After being mixed with the liquid solution, it solidifies into a material with the consistency of a rubber. It can be formed into various shapes using molds.

The benefit of this procedure is that phantoms of different parts of the body can easily be generated because conductivity and permittivity can be adjusted using different concentrations of salt and sugar. Sugar added to the solution reduces the permittivity while additional salt is used to increase conductivity.

To formulate a recipe of the mimicking gels, measurements are performed by Pichitpong Soontornpipit [30]. Different recipes are given for MICS and ISM bands because using a single formula it is not possible to produce a valid approximation to human skin performance for the entire spectrum, from 300 MHz to 3 GHz. The given concentrations of the ingredients of the liquid solution in the MICS gel are: 3.2% salt, 50.6% sugar, 46.2% de-ionized water.

The original recipe suggests also the usage of TX151 with 1 g/100 ml but, according to this experience, the given relationship is incorrect because in this way the solution didn´t solidify. In fact, as reported in the datasheet, the mixing instructions of the TX powder suggests a ratio by weight (Tx product to water) of 1 to 5 for a hard consistency, 1 to 10 for a medium consistency and 1 to 15 for a soft consistency.

Three samples have been produced with the three different ratios and compared with the meat consistency in order to reproduce the muscle tissue.

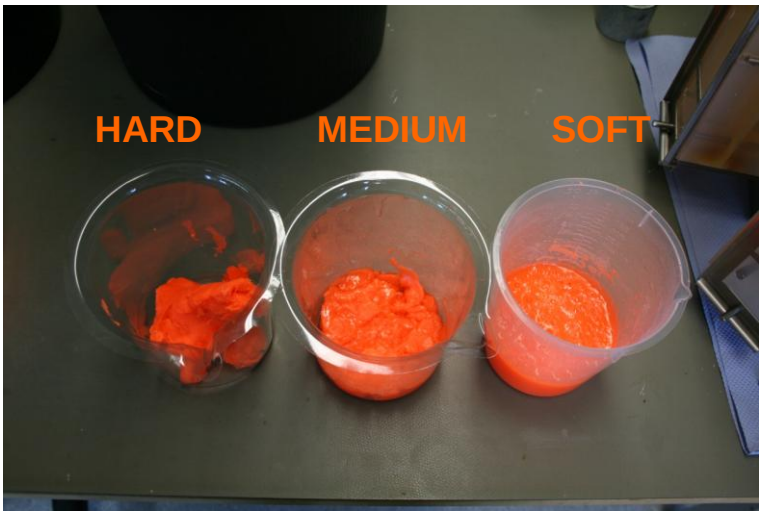

Figure 71 - Three different mimicking gels.

In Figure 71, it is possible to notice that the medium and soft material are too liquid for this specific application, thus 1:5 ratio has been chosen in order to realize the phantom.
An appropriate phantom for testing medical implant antenna is defined in EN301 489-27 [31] : "a cylindrical Plexiglas container with a size of 30 cm ± 0,5 cm by 76 cm ± 0,5 cm with a sidewall thickness of 0,635 cm ± 0,05 cm. The implant antenna shall be mounted no further than 6 cm ± 0,5 cm from the sidewall and centred vertically within the container."
Before testing the antenna with the normative phantom, some measurements have been done to compare all the potential antenna, in order to choose primarily the best implantable one. Thus, two cylinders of mimicking gel with a size of 22 cm by 4 cm have been prepared and, during the measurements, each antenna has been placed at 6 cm from the cylinder border (Figure 72). In this way, the performance of an abdomen implanted antenna is simulated.

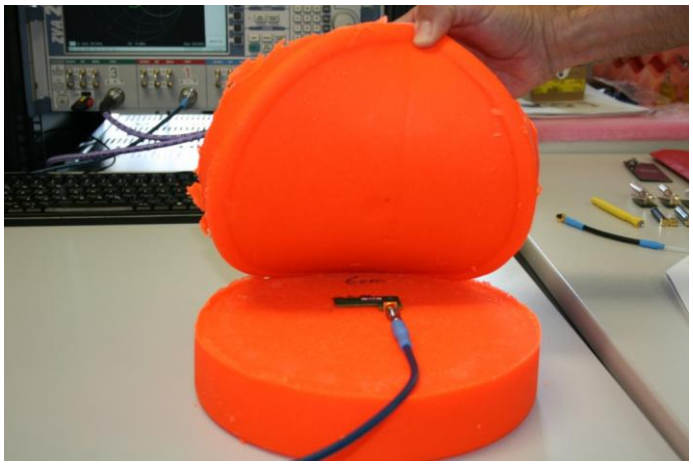

Figure 72 - Phantom for *ex-vivo* measurements.

5.2.4.2 Test methods

Antenna measurements have been made in the German Areospace Center (DLR) with a vector network analyzer (Rohde&Schwarz ZVA24, 10-240MHz). This instrument provide the Smith diagram, S11 plot and S21 plot and the reference antenna used with that VNA is a log-period antenna.
The goal of the measurements is to evaluate the matching impedance of the antennas to 50 Ω, so that it will be equal to the source impedance to get a decent input return loss (S11).

Three test methods are used: in air, inside the phantom and between two pieces of porcine tissue, but without any voids. In both of them, the plots about the impedance and the S11 and S21 parameters (for further details see Appendix F) have been obtained.

The antennas under test are (Figure 73):

1. dipole antenna with a 3 mm diameter and without ground plane,
2. printed loop antenna: the PLA100 Rev C (Zarlink),
3. dual-band antenna: designed to interact with implantable medical devices (Zarlink),
4. stub antenna: a electrically short $\lambda/4$ monopole antenna embedded in dielectric enclosure,
5. stub antenna embedded in silicone,
6. stub antenna without the dielectric enclosure but embedded in silicone,
7. em-tec Helix antenna with 9 turns embedded in silicone and the matching network,
8. em-tec Helix antenna with 5 turns embedded in silicone and the matching network,
9. em-tec Helix antenna with 2 turns embedded in silicone and the matching network.

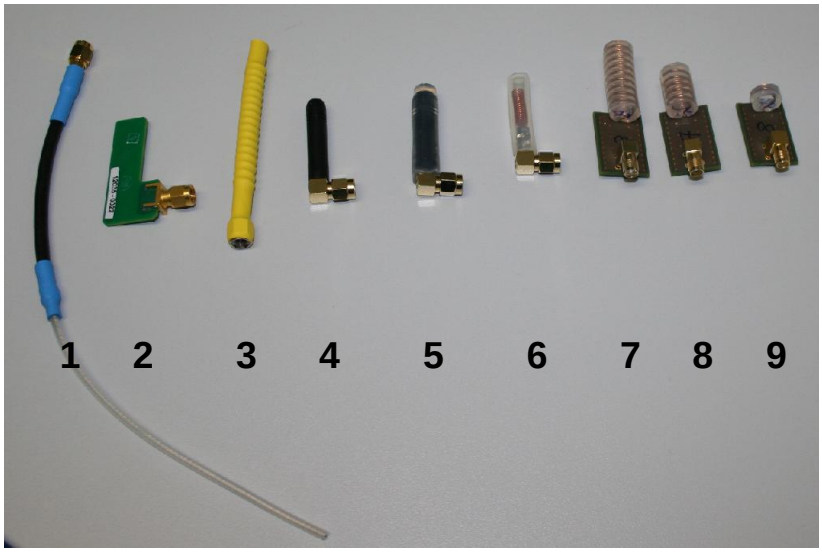

Figure 73 - Antennas under test

The behaviour of each antenna is observed comparing the plots (Smith, S11 and S21) for all the methods.

5.2.4.3 Test results

First of all, the Zarlink RF transceiver has been tested. The default impedance is measured in two cases, in a box and outside. The integrated matching network is optimized for a nominal antenna impedance of 100 + j150 Ω at 403.5 MHz and the board is connected to the network analyzer by a 50 Ω RF adaptor (Figure 74).

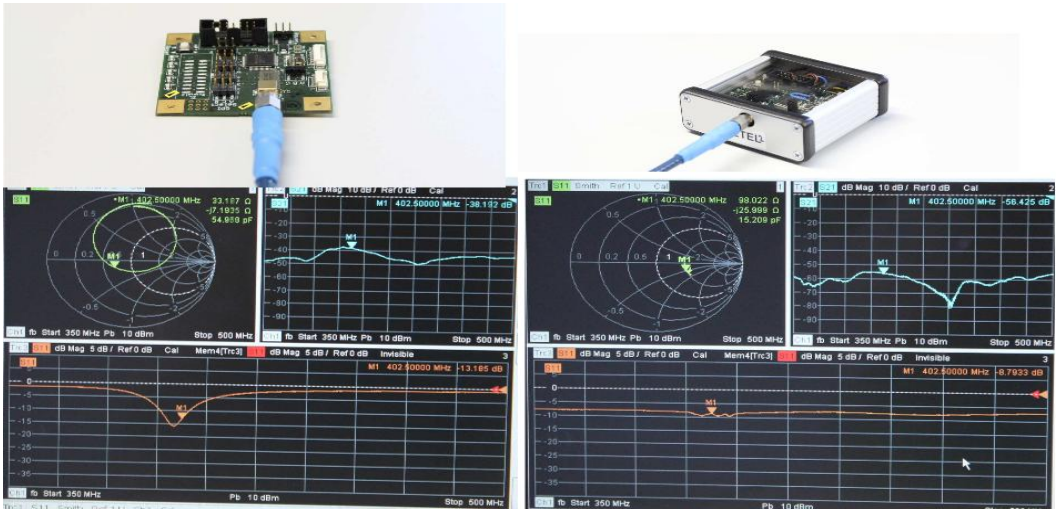

Figure 74 - Input Impedance measurement of the telemetry module (TEL)

In the sample without housing, the real part of the impedance is nearly 50 Ω. Whereas, it was evident that something was not working properly for the case with the board in the box, probably the connector was not soldered correctly. Therefore, it was impossible to have clear results and it will be necessary to repeat the measurement with three samples. The future goal will be to reach a good matching of the antenna because it is important for the tuning to have a constant impedance.

About the Zarlink printed loop antenna, the result was that it is a good free air antenna but in the phantom and meat the S11 plot becomes flat and the S21 goes down (Figure 75).

Furthermore, also not considering that it is tuned from Zarlink to work in air, other disadvantages of the PLA100 antenna are that it is not packed in biocompatible

enclosure which would lead to an huge feedback effect on the antenna performance and its size is not compact.

Figure 75 - Results for the PLA100 loop antenna in a) air b) phantom c) meat

The possibility to use the dipole antenna has been also rejected because its impedance is out of the range of interest and the S11 is quite flat even in free air (Figure 76).

Figure 76 - Results for a dipole antenna in a) air b) phantom c) meat

Comparing the plots of the stub antenna with the dielectric enclosure, the stub antenna embedded in silicone and the stub antenna without the dielectric enclosure but embedded in silicone, it was clear that the second type is the best one and an excellent solution for MICS extracorporeal air-antenna.

It is possible to notice that, at 402,5MHz, S21 is very high and the S11 plot has a resonance peak (Figure 77). The impedance value is in the range of interest and is also similar to the transceiver value.

The next goal is to embed the stub antenna without any dielectric protection in the silicon, and to test its behaviour inside the phantom and meat.

Figure 77 - Results for a stub antenna covered by silicone in a) air b) phantom c) meat

About the three types of helix antenna, the best one is certainly that with 9 turns. Only with this antenna it is possible to notice a little S11 resonance peak also when it is inside the phantom or in the meat (Figure 78).

With the antenna in the meat, the S21 parameter raises from -50 dB to -40 dB when S11 reaches its peak. This value is considered as a receivable signal, because the receiver is able to detect up to – 110 dB (maximum sensitivity).

If the antenna is completely covered by meat a second resonance point in the S11 appeared but not in the MICS band. This behavior have to be investigated further.

Figure 78 - Plot for 9 turn helix antenna in a) Air b) phantom c) meat

In conclusion, this helix antenna shows an excellent performance in spite of its compact size and has the advantage that part of the electromagnetic field is established within the coil. As a result, this part is not disturbed so much by the organic tissue variations. Furthermore, the circular polarization is substantially immune to interference by multi-path propagation as a linear polarization.

For these reasons, actually, the em-tec helix antenna with 9 turns embedded in silicone was considered as the best solution for the implant but it is not yet fully optimized to work embedded in meat.

CONCLUSIONS AND OUTLOOK

In this work of thesis, a contribution to the development of an *in-vitro* sensorized platform for LVAD- implanted patients has been performed.

The main purpose of this intelligent platform will be assuring to heart failure patients a higher life quality and support the physician to easily monitor the LVAD.

The last generation of heart pumps allows the patient to leave the hospital because the VADs are provided with a belt that contains the motor controller and the battery.

Whit respect to this recent solution, the advantage of the new platform is that it provides innovative tele-control services allowing the patient and the healthcare professional to keep under control the performance of the VAD.

To this aim, the platform is provided with two types of physiological sensors commercially available, a non-invasive clamp-on transducer provided to measure the blood flow and two pressure catheters. But, the core of this system is the ARU which monitors the pump and sensors parameters, implements control algorithms and actuates a closed-loop control for adjusting the pump speed to obtain the desired flow and pressure values on the basis of the physiological cardiac demand. Thus, this control offers the patient a more normal and safe life because it will be not necessary anymore a continuous check from the specialist.

Furthermore, the implementation of a transcutaneous energy transfer system and a telemetry system will decrease the amount of cables through the skin. This cables are very stiff and they cause discomfort, limited range of motion and many health risks to the patient, because the exposure of the tissue to the cable increases the risk of infections. For these reasons, the capacity of time varying magnetic fields to transfer power across the skin has been exploited in order to charge the implanted components of the platform. Additionally, wireless communication have been used to acquire data from the pump and the sensors and to send to the pump the controlled speed.

The first task of this work deals with the HMI of the ARU, described by the LabView development environment and the conversion of the control algorithm in VHDL code. In particular, for problem of overall computational load, the control has been split on two dedicated PCs and alert signals have been implemented.

Later, an UART, used by the ARU to communicate with the extracorporeal part of the platform, has been implemented in VHDL code.

Furthermore, in order to simulate the communication between the ARU and the ECU, to test the defined protocol and to facilitate their integration, a GUI has been developed. The simulators for the two systems have been written in the script language Python extended by the PyQt modules of the Qt-C++ library.

The second thesis task regards the integration of the pressure sensors. Then, the Mikro-Tip® pressure catheters by Millar Instruments has been selected and integrated. Consequently, the characterization of these sensors have been done and the analog circuit for signal conditioning has been realized and tested.

About the TET, the aim was to evaluate the biocompatibility of the implantable part of the system and, in particular, to demonstrate that the ITET coil could be implanted by respecting the ISO14708-1 norm. Temperature measurements have been done, to discover how much the implantable coil surface becomes hot; indeed, if the temperature is higher than 37° C, the body tissues, near the implant, would be damaged. The temperature of the coil has been monitored under dependency of VAD load and also the temperature trend has been measured varying the ITET coil position with respect to the external one. The results show that, thanks to the silicon enclosure of the coil, the temperature of the surface doesn't exceed the safety threshold, even in extreme working condition, with a VAD speed of 28000 rpm. It is also possible to notice a surface temperature increase when the internal coil is moved away from the external coil, along the vertical axis, while, varying the horizontal and angular misalignment the temperature increase is minimum.

Moreover, the AC-DC efficiencies of the three prototypes of the TET power rectifier have been measured and the advanced full-synchronous power rectifier has been chosen because it results implantable thanks to its heat dissipation strategies and has the highest efficiency at the intended operating frequency of 150 kHz.

Finally, a contribution for the developing of the telemetry system of the proposed platform has been given. In particular, to find a good solution for implantable antenna, different antenna types with specific characteristics have been tested and their performance in free-air, *ex-vivo* and *in-vitro* have been compared. The Smith chart and the S11 and the S21 diagrams (for further details see Appendix F) have been acquired for each antenna and the best results have been obtained with the helix antenna with 9

turns embedded in silicone. Actually, it is the best solution for the implant but it is not yet fully optimized to work embedded in the human body.

The first following step will be to test the system made by the telemetry module and the transcutaneous energy transfer blocks on animals, in order to evaluate if the transmission through the body really works properly. Then, the integration of all the components in an unique platform would follow, together with the check of the right communication between all the parts and the correct implementation of the control algorithm.

Once successful application of the platform to the used LVAD and sensors will be demonstrated, another outlook would be to test the interoperability of each component, in order to reuse them separately for other applications.

After these steps, the new proposed platform would be ready to be produced and certified for real implant, offering a better life to the heart failure patients. Therefore, thanks to all its benefits, the LVAD implant would be considered as an optimal alternative to transplantation.

REFERENCES

[1] “European Cardiovascular Disease Statistics 2012 edition”, European Heart Network and European Society of Cardiology, 2012.

[2] http://www.sensorart.eu/.

[3] Mattias Stenberg, “Concept Design and In Vitro Evaluation of a Novel Dynamic Displacement Ventricular Assist Device”, thesis in Technology and Health, University of Florida, 2006.

[4] “Organ Donation and transplantation, an invitation of the European Commission”, october 2012.

[5] John Henderson, “Starling’s Law and Related Matters”, A life of Ernest Starling people and ideas series, pp 77-98, 2005.

[6] Douglas J. Hirsch, John R. Cooper, “Cardiac failure and left ventricular assist devices”, Anesthesiology Clin N Am, vol. 21, pp. 625–638, 2003.

[7] Daniel G. Tang, Philip E. Oyer, Hari R. Mallidi, “Ventricular Assist Devices: History, Patient Selection, and Timing of Therapy”, J. of Cardiovasc. Trans. Res., vol. 2, pp. 159–167, 2009.

[8] Michael M. Givertz, “Ventricula Assist Devices: important imformation for patients and families”, Circulation, vol. 124, pp. e305-e311, 2011.

[9] C D Bertram, “Measurement for implantable rotary blood pumps”, Physiol. Meas., vol. 26, pp. R99–R117, 2005.

[10] Parnis *et al,”* Progress in the development of a transcutaneously powered axial flow blood pump ventricular assist system”, ASAIO J., vol. 43, pp. M576–80, 1997.

[11] C. A. Giridharan, M. Skliar, D. B. Olsen, G. M. Pantalos, "Modeling and control of a brushless DC axial flow ventricular assist device," vol. 48, pp. 272-289, 2002.

[12] Bullister E, Reich S, Sluetz J, “ Physiologic control algorithms for rotary blood pumps using pressure sensor Input”, Artif. Org, vol. 26, pp. 931–8, 2002.

[13] K. Ogata, Y. Yang, “Modern control engineering”, Prentice Hall, pp. 669-703, 1990.

[14] Wu Yi, “Physiological Control of Rotary Left Ventricular Assist Device”, Proceedings of the 26th Chinese Control Conference, 2007.

[15] http://apexmedtech.com/.

[16] Millar Instrument, “Mikro-tip catheter pressure transducer, animal use only, instructions for use”.

[17] Honeywell, “TruStability® Board Mount Pressure Sensors: NSC Series–Uncompensated/Unamplified”, http://honeywell.com/Pages/Home.aspx.

[18] Sara Carr, Carl Hoge, Robert McGregor, Keith Lesser, Oxana Petritchenko, “Transcutaneous signal and power transmission for ventricular assist device”, Multi-Disciplinary Engineering Design Conference, 2010.

[19] T. Dissanayake, D. Budgett1, A.P. Hu, S. Malpas, L. Bennet, “Transcutaneous Energy Transfer System for Powering Implantable Biomedical Devices”, ICBME 2008, Proceedings 23, pp. 235–239, 2009.

[20] ICNIRP, International commission on non-ionizing radiation protection, “Guidelines for limiting exposure to time-varying electric, magnetic, and electromagnetic fields (up to 300 GHz)”, Health Physics 74, pp. 494-522, 1998.

[21] Vivek Shirvante, Fabien Todeschini, Xiaoyu Cheng, Yong-Kyu Yoon, “Compact Spiral Antennas for MICS band Wireless Endoscope toward Pediatric Applications “, IEEE, 2010.

[22] Asimina Kiourti, Konstantina S. Nikita, “A Review of Implantable Patch Antennas for Biomedical Telemetry: Challenges and Solutions”, IEEE Antennas and Propagation Magazine, vol. 54, no. 3, 2012.

[23] Anders J Johansson , “Wireless Communication with Medical Implants: Antennas and Propagation”, 2004.

[24] McHugh M., “In-Body communications”, Zarlink Microelectronics, Healthy Aims

[25] ISO 14708-1:2000, “Implants for surgery - active implantable medical devices - part 1: general requirements for safety, marking and for information to be provided by the manufacturer”.

[26] G. M.Wieselthaler, H. Schima, A. M. Lassnigg, M.Dworschak, R. Pacher, M. Grimm, E.Wolner, “Lessons learned from the first clinical implants of the DeBakey ventricular assist device axial pump: A single center report”, Ann. Thorac. Surg., vol. 71, pp. S139–143, 2001.

[27] C. R. Davies, F. Fukumura, K. Fukamachi, K. Muramoto, S. C. Himley, A. Massiello, J. Chen, H. Harasaki, “Adaptation of tissue to a chronic heat load”, ASAIO Journal, vol. 40, pp. M514-7, 1994.

[28] Huwig D., Wambsganß P., “Digitally Controlled Synchronous Bridge-Rectifier for Wireless Power Receivers”, IEEE, 2013.

[29] A.V. Vorst, A. Rosen, Youji Kotuska, “RF microwave interaction with biological tissues”, 2006.

[30] Pichitpong Soontornpipit, “Effects of Radiation and SAR from Wireless Implanted Medical Devices on the Human Body”, J Med Assoc Thai, vol. 95, suppl. 6, 2012.

[31] EN 301 489-27 V1.1.1 (ETSI).

[32] ISO 9001:2008, “Quality management systems - requirements “.

APPENDIX A

LabVIEW

LabView (*Laboratory Virtual Instrument Engineering Workbench*) is a system-design platform and development environment for a visual programming language from National Instruments. It runs on a variety of platforms including Microsoft Windows, Linux, and Mac OS X.

It is commonly used for data acquisition, industrial automation and instrument control and the programming language, named G, is a dataflow programming language.

The structure of a graphical block diagram, on which the programmer connects different function-nodes by drawing wires, facilitates the execution. The nodes execute their function when all their input data become available and the wires propagate the variables from one node to another. Obviously multiple nodes can work simultaneously, since G is capable of parallel execution.

LabView put together the created user interfaces (called front panels) into the development cycle. Its programs or subroutines are called Virtual Instruments (VIs). Each VI is compost of three components: a block diagram, a front panel and a connector panel.

The last leads to represent the VI in the block diagrams of other, calling VIs.

The front panel needs controls and indicators to be built. Controls represent the inputs, since they supply information to the VI, while indicators are the outputs, because they indicate, or display, the results based on the given inputs.

The block diagram that contains the graphical source code is the back panel. It supplies a different representation of the front panel in which all of the objects appear as terminals. The back panel also contains structures and functions which perform operations on controls and supply data to indicators. The structures and functions are found on the Functions palette and can be placed on the back panel.

Collectively controls, indicators, structures and functions will be referred to as nodes. For example, two controls and an indicator can be wired to the addition function so that the indicator displays the sum of the two controls.

Thus, a VI can either be run as a program, with the front panel used as a user interface, or, when dropped as a node onto the block diagram, the front panel defines the inputs

and outputs for the given node through the connector panel. In this way, each VI can be easily tested before being embedded as a subroutine into another larger program.

LabView is an inherently concurrent language, so it is very easy to program multiple tasks that are performed in parallel by means of multithreading. This is, for instance, easily done by drawing two or more parallel while loops.

One of the biggest advantages of LabView is that it offers an extensive support for accessing instrumentation hardware. Drivers and abstraction layers for many different types of instruments and buses are included or are available for inclusion.

Many libraries are provided in several LabView package options. They supply a large number of functions for data acquisition, signal generation, mathematics, statistics, signal conditioning, analysis, etc..

In particular, there are a lot of instruments for data capture from hardware sensors. It provide, in fact, a multitudinous of advanced mathematic blocks for functions such as integration, filters, and other specialized capabilities.

Furthermore, LabView includes a text-based programming component called MathScript with additional functionality for signal processing, analysis and mathematics.

Another benefit of LabView is related to the fully modular character of its code that allows code reuse without modifications.

APPENDIX B

VHSIC Hardware Description Language

VHDL (*Very High Speed Integrated Circuit Hardware Description Language*) is a versatile hardware description language which is useful for modeling electronic systems at various levels of design abstraction. It was developed during the United States Government's Very High Speed Integrated Circuits program, when it became clear that there was a need for a standard language for describing the structure and function of integrated circuits (ICs). Subsequently VHDL was adopted as a standard by the Institute of Electrical and Electronic Engineers (IEEE) in the US.

It is designed to fill a number of needs in the design process. First of all, it allows description of the structure of a design, in particular the sub-designs and their interconnections. It is also possible to use familiar programming language forms to implement the specification of the function of designs. Another advantage is the opportunity of simulating the design before being manufactured, so that designers can quickly compare alternatives and test for correctness without the delay and expense of hardware prototyping.

In detail, VHDL has many features appropriate for representing the behavior of electronic components ranging from simple logic gates to complete microprocessors and custom chips. These features allow electrical aspects of circuit behavior to be precisely described.

It is also a general-purpose programming language, since it allows the behavior of complex electronic circuits to be captured into a design system for automatic circuit synthesis or for system simulation.

Just as high-level programming languages like Pascal, C and C++, VHDL includes features useful for structured design techniques and for control and data representation. Unlike these other languages, the hardware described using VHDL is inherently concurrent in its operation, thus it provides features allowing concurrent events to be described.

One of the most important benefit to using VHDL is the possibility to test the logic design using simulation models to represent the logic circuits that interface to the design. This collection of simulation models is commonly called a test bench.

Test benches are VHDL descriptions of circuit stimuli and corresponding expected outputs that verify the behavior of a circuit over time. Test benches should be an integral part of any VHDL project and should be created in tandem in order to test the circuit step by step.

APPENDIX C

Python and PyQt

Python is a general-purpose, dynamic, object-oriented programming language. It was initially developed by Guido van Rossum and first released in 1991. Python was inspired by ABC, Haskell, Java, Lisp, Icon and Perl programming languages. Python is a high level, general purpose, multiplatform, interpreted language. It incorporates modules, exceptions, dynamic typing, very high level dynamic data types, and classes. One of its most visible features is that it does not use semicolons nor brackets but uses indentation. Python combines remarkable power with very clear syntax. The language comes with a large standard library that covers areas such as string processing (regular expressions, Unicode, calculating differences between files), Internet protocols (HTTP, FTP, SMTP, XML-RPC, POP, IMAP, CGI programming), software engineering (unit testing, logging, profiling, parsing Python code), and operating system interfaces (system calls, file systems). It has interfaces to various window systems, and is extensible in C or C++. It is also usable as an extension language for applications that need a programmable interface. Finally, Python is portable: it runs on many Unix variants, on the Mac and on Windows 2000 and later.

The Python code resides in files, ending with .py suffix. These files can be grouped in modules, in the form of directories with an indexfile called __init__.py, and it is possible to import elements from modules and files in other files. Thus, during the implementation of an application, it is necessary to import all the modules in the main function. Python is, like Java, a language that is compiled to byte-code and it uses a virtual machine to run the byte-code. This virtual machine is written in C and interprets each byte-code instruction, translates it to real machine code and finally runs it. The translation from Python code to byte-code is done only once: Python saves a compiled version of the code in another file with the extension .pyc.

For creating graphical user interfaces, there are many GUI libraries available for Python — examples are wxPython, Tkinter, PyGTK, PyFLTK, FoxPy, and PyQt.

PyQt is based on Qt, an advanced GUI library for Windows and Unix, written in C++ by Eirik Eng and Arnt Gulbrantsen of Trolltech in Norway.

PyQt brings together the Qt C++ cross-platform application framework and the cross-platform interpreted language Python. PyQt combines all the advantages of Qt and Python. A programmer has all the power of Qt, but is able to exploit it with the simplicity of Python. Qt library is one of the most powerful GUI libraries. PyQt is implemented as a set of Python modules. It has over 400 classes and almost 6000 functions and methods.

Because there are a lot of classes available, they have been divided into several modules.

- QtCore, contains the core non-GUI functionality; used for working with time, files and directories, various data types, streams, threads or processes.
- QtGui, contains the graphical components and related classes; include for example buttons, windows, status bars, toolbars, sliders, bitmaps, colors, fonts etc..
- QtNetwork, contains classes for making the network programming easier and more portable.
- QtXml, contains classes for working with XML files.
- QtSvg, provides classes for displaying the contents of SVG files. (SVG is a language for describing two-dimensional graphics and graphical applications in XML.)
- QtOpenGL, used for rendering 3D and 2D graphics.
- QtSql, provides classes for working with databases.

Qt also includes Qt Designer, a layout and forms GUI builder. PyQt is able to generate Python code from Qt Designer. It is also possible to add new GUI controls written in Python to Qt Designer. Qt Designer is the Qt tool for designing and building graphical user interfaces. It allows you to design widgets (buttons, lists, tables, menus, inputs etc.), dialogs or complete main windows using on-screen forms and a simple drag- and-drop interface. It has the ability to preview your designs to ensure they work as you intended, and to allow you to prototype them with your users, before you have to write any code.

Qt Designer uses .ui files to store designs while the C++ code, that creates the user interface, is generated by the uic utility. Qt also includes the QUiLoader class that allows an application to load a .ui file and to create the corresponding user interface dynamically.

APPENDIX D

RS-232 PROTOCOL

The important serial characteristics are baud rate, start bit, data bits, stop bits, and parity (Figure 79). For two ports to communicate, the following parameters must match:

1. **Baud rate**. It is a speed measurement for communication, in particular it indicates the number of bit transfers per second (bps). In the UART case, the baud rate indicates the clock cycle. For example, if the protocol requests a 4800 baud rate, then the clock is running at 4800 Hz. Greater baud rates are possible, but these rates reduce the distance by which devices can be separated. In fact, these high baud rates are used for device communication where the devices are located together, as in the case of study.
2. **Start bit**. It is transmitted at the beginning of each transmission, indicating to the receiver that a byte of data is about to follow. The start bit is intended to make the receiver synchronize to the data bits. This means that the receiver can create its own sample clock at the middle of each bit. Once the start bit is found, the receiver understands where the following bits are, as it is given the sample period (derived from the baud rate) as part of the initialization process.
3. **Data bits**. They are the actual data bits in a transmission, bringing the information. In data transmission, the amount of actual data may not be a full 8 bits. Standard values for the data packets are 5, 7, and 8 bits, with the LSB (least significant byte) transmitted first. For example, standard ASCII has values from 0 to 127 (7 bits). If the data being transferred used standard ASCII, then sending 7 bits of data per packet is sufficient for communication. A packet refers to a single byte transfer, including start/stop bits, data bits, and parity. This saves a bit and increases transmission speed when transmitting large blocks of data.
4. **Stop bits**. They represent the end of the communication for a single packet. Typical values are 1, 1.5, and 2 bits. Since the data is clocked across the lines and each device has its own clock, it is possible for the two devices to become slightly out of synchronization. For this reason, the stop bits are very important, they not only indicate the end of the transmission but also give the computers

some room for the detection of errors in the clock speeds. The more bits that are used for stop bits, the greater the difference in synchronization between the two clocks, but the slower the data transmission rate.

5. **Parity bits**. It is a simple form of error checking, used in serial communication. The types of parity are four: even, odd, marked, and spaced. Obviously, it is possible also the option of using no parity. For even and odd parity, the parity bit is set by the serial port to a value which ensure that the transmission has an even or odd number of logic high bits. It simply evaluates all the data bits and for odd parity returns a logic one if there is an odd number of data bits that are set. For even parity, an even number of data bits set the parity bit. Marked and spaced parity does not actually check the data bits, but simply sets the parity bit high for marked parity or low for spaced parity. In this way, the receiver knows the state of a bit, then it is able to determine if noise is corrupting the data or if the transmitting and receiving devices clocks are out of synchronization. On the other hand, the problem with error detection using the parity bit is that if two bits are in error then the parity check fails. This is because each error cancels the effect of the other, in terms of the parity calculation. Any even number of errors causes a failure in error detection. For this reason, in a noisy environment, a better system should be used, like adding a cyclic redundancy check to the data stream before and after it is sent over the RS-232.

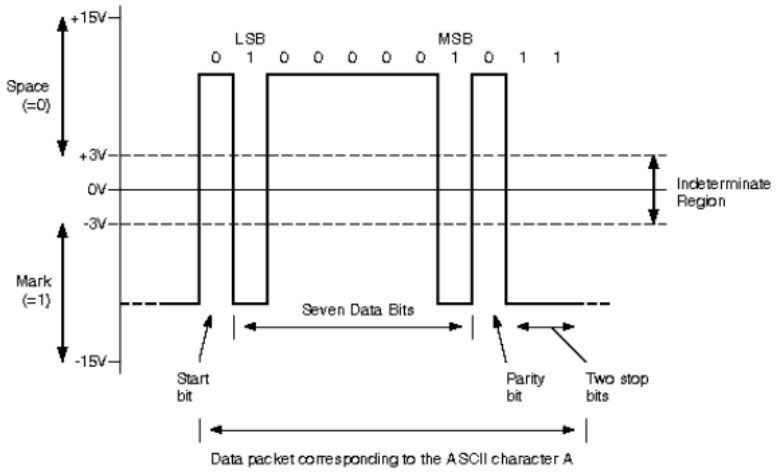

Figure 79 – one byte of async data

The output voltage specification is from +5V to +25V (transmitting a logical zero) and -5V to -25V (transmitting a logical one). Meanwhile, the receiver can accept minimum signal levels of ±3V.

Generally, the kind of the transmitted packet is indicated by an abbreviation made up on the basis of an alphanumerical code, for example like 8n1 and 7e2: the first number indicates how many bits are transmitted (in the example 8 and 7 bits), the letter the parity type (in the first example none, in the second an even parity) and the second digit the number of the stop bits (1 and 2 in the two examples).

Serial communication can be half duplex or full duplex. In the full duplex communication, a device can receive and transmit data simultaneously. While, in the half duplex communication, the device can both send and receive, but not at the same time. Consequently, half duplex serial communication requires a minimum of two wires, one for signal ground and one for the data line. Instead, full duplex serial communication needs at a minimum three wires for signal ground, transmit data line and receive data line.

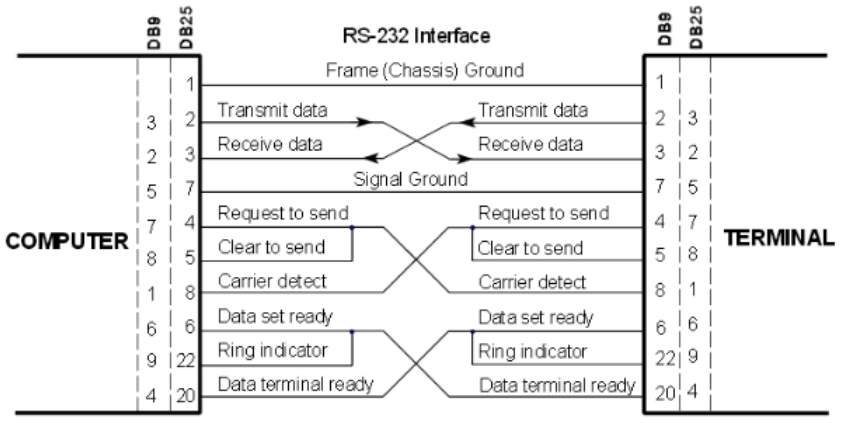

Figure 80 – RS-232 pinout

About the interface pinout, the RS-232 specification defines several additional signals that are asserted for information and control beyond the data signals. These signals are represented in Figure 80. Data Set Ready (DSR) is an indication from the Data Set (i.e., the modem) that it is on. Similarly, Data Terminal Ready (DTR) indicates to the Data Set that the terminal is on. Carrier Detect (CD) indicates that a good carrier is being received from the remote modem, so signals a successful connection. Pins 4 RTS (Request To Send - from the transmitting computer) and 5 CTS (Clear To Send - from

the Data set) are used to control, to indicate that the modem is ready to receive. The Ring Indicator is used by the Data Set to indicate to the Data Terminal that a ringing condition has been detected.

A cyclic redundancy check (CRC) is an error-detecting code that allows to detect accidental changes to raw data. It is commonly used in digital networks and storage devices. CRCs are so called because the check value for data verification is a redundancy, since it expands the message without adding information, and the algorithm is based on cyclic codes. The entire message is treated as a binary number, which both the sender and receiver divide by the same divisor. The quotient is discarded and the remainder is sent as the CRC value. If there isn't any error in the received message, the receiver's calculation will match the sender's calculation and the CRC values will agree. In particular, the polynomial used for the CRC16-CCITT has highest degree 16:

$$f(x) = x^{16} + x^{12} + x^5 + 1$$

The CRC checksum is popular because it is simple to implement in binary hardware and easy to analyze mathematically. It is particularly good at detecting common errors caused by noise in transmission channels.

Finally, in data communications, flow control is the process of managing the rate of data transmission between two nodes. Its task is to prevent a fast sender from overwhelming a slow receiver. The flow control mechanism allow the receiver to control the transmission speed, so that the receiver is not overwhelmed with data from transmitting node.

Transmit/Receive flow control can either be stop-and-wait or use a sliding window.

Stop-and-wait flow control is the simplest form of flow control. In this method, when the receiver indicates that it is ready to receive data for each frame, the message is broken into multiple frames. After every frame, the sender waits for an acknowledgement (ACK) signal in order to ensure that the receiver has received the frame correctly. Then the next frame is sent by the sender only after the ACK has been received.

When the buffer size is limited and pre-established, it is better to use the sliding-window flow control. During a typical communication between a sender and a receiver,

the receiver allocates buffer space for a number of frames equal to the buffer size, n. In this method, the sender can send n frames and the receiver can accept them without having to wait for an acknowledgement. The receiver acknowledges a frame by sending an ACK signal that includes the sequence number of the next frame expected. This acknowledgement indicates to the sender that the receiver is ready to receive those n frames that begin with the number specified. In this way, both the sender and the receiver maintain what is called a window, the size of which is less than or equal to the buffer size.

Sliding window flow control performance is certainly better than stop-and-wait flow control one. This is because, in a wireless environment, waiting for an acknowledgement for every transferred packet is not very feasible, as data rates are very low and noise level is very high. Therefore, transferring data as a unique block guarantees a better performance in terms of higher throughput.

APPENDIX E

Antennas under test

Four different antenna types are briefly described. The antenna prototypes, selected as possible implantable antennas, belong to these types.

- Dipole antenna

The dipole antenna is one of the most important and commonly used types of RF antenna. It consists of a conductive wire rod that is half the length of the maximum wavelength the antenna can generate. This wire rod is split in the middle, and the two sections are separated by an insulator. Each rod is connected to a coaxial cable, at the end closest to the middle of the antenna. Radio frequency voltages are applied to dipole antennas at the center, between the two conductors. The current distribution along a dipole is roughly sinusoidal. It falls to zero at the end and it is at a maximum in the middle. Conversely, the voltage is low at the middle and rises to a maximum at the ends. The polar diagram of a half wave dipole antenna has maximum sensitivity or radiation at the right angles to the axis of the RF antenna then the radiation falls to zero along the axis of the RF. If the length of the dipole antenna is changed then the radiation pattern is altered. As the length of the antenna is extended, it can be seen that the familiar figure of eight pattern changes to give main lobes and a few side lobes. The main lobes move progressively towards the axis of the antenna as the length increases.

- Spiral Helix antenna

A helix antenna is a type of antenna that utilizes a conducting wire wound in a spiraling helix shape (constant parallel spaced turns) mounted over a ground plane. It is a type of directional antenna , in which the electromagnetic field typically rotates around the axis of the helix in either a clockwise or counterclockwise direction.

A helix antenna is a travelling wave antenna, which means that the current travels along the antenna and the phase varies continuously.

The radiation pattern is omni-directional, with maximum radiation at the right angles to the helix axis. Then, it provides consistent uniform radiation as a reduced sized equivalent to the standard quarter-wavelength antenna.

The advantages of spiral helix antennas are: excellent performance at compact size, circular polarization in z-direction (if 3/4 λ < C < 4/3 λ with C = pi * Diameter), only real part of impedance: Zin = 140 C/λ, tuning by shortening. Their disadvantages are: more complex design, high Q factor that leads to narrow bandwidth. The bandwidth could be designed broader by prolonging spirals pitch.

- Loop Antenna

Loop antennas come in a variety of shapes (circular, rectangular, elliptical, etc.) but the fundamental characteristic is that the radiation pattern are largely independent from the loop shape. The far-field electric field of a small loop antenna is identical to the far-field magnetic field of the short dipole antenna and the far-field magnetic field of a small loop antenna is identical to the far-field electric field of the short dipole antenna. Therefore, the radiation patterns are the same. This means that the plane of maximum radiation for the loop is in the plane of the loop.

They are also inexpensive and simple to construct and represent a compromise between repeatability, size and cost. On the other hand, loop antennas are useful only for short range applications, difficult to tune and match and dependent from PCB production process.

- Ducky or stub antenna

The rubber ducky is an electrically short quarter-wave antenna in which the inductor, instead of being in the base, is built into the antenna itself and is sealed in a rubber or plastic jacket to protect the antenna. The antenna is made of a narrow helix of wire like a spring, which functions as the needed inductor.

This type of antenna has lower gain than a full size quarter-wavelength antenna, reducing the range of the radio. Their design is a compromise between antenna gain and small size.

They are difficult to characterize electrically because the current distribution along the element is not sinusoidal as in the case of a linear antenna.

The rubber ducky has a high Q factor and thus a narrow bandwidth. This type of antenna is often used over a wide frequency range, e.g. 100-500 MHz, and over this range its performance is poor, but in many mobile radio applications there is sufficient excess signal strength to overcome any deficiencies in the antenna.

APPENDIX F

5.3 S-parameters and Smith chart

S-parameters refer to the scattering matrix. The scattering matrix is a mathematical construct that quantifies how RF energy propagates through a multi-port network. The S-matrix allows to accurately describe the properties of incredibly complicated networks as well as simple ones.

For an RF signal incident on one port, some fraction of the signal bounces back out of that port, some of it scatters and exits other ports (and is perhaps even amplified), and some of it disappears as heat or even electromagnetic radiation.

The S-matrix for an N-port contains a N^2 coefficients (S-parameters), each one representing a possible input-output path. S-parameters are complex (magnitude and angle) because both the magnitude and phase of the input signal are changed by the network. Quite often we refer to the magnitude only, as it is of the most interest, because it indicates the gain (or loss).

S-parameters are defined for a given frequency and system impedance, and vary as a function of frequency. They refer simply to RF relationship between output voltage and input voltage and come in a matrix, with the number of rows and columns equal to the number of ports. For the S-parameter subscripts "ij", j is the port that is excited (the input port), and "i" is the output port. Parameters along the diagonal of the S-matrix are referred to as reflection coefficients because they only refer to what happens at a single port, while off-diagonal S-parameters are referred to as transmission coefficients, because they refer to what happens from one port to another.

For instance, in the case of 2 ports called Port 1 and Port 2, S21 represents the power received at 2 relative to the power input to antenna 1. For instance, S21=0 dB implies that all the power delivered to antenna 1 ends up at the terminals of antenna 2. If S21=-10 dB, then if 1 W (or 0 dB) is delivered to antenna 1, then -10 dB (0.1 W) of power is received by antenna 2.

Instead, S11 represents how much power is reflected from the antenna. S11 is the most commonly quoted parameter in regards to antennas and is known as the reflection

coefficient. If S11=0dB, then all the power is reflected from the antenna and nothing is radiated. If S11=-10 dB, this implies that if 3 dB of power is delivered to the antenna, -7 dB is the reflected power. The remainder of the power is delivered to the antenna. This accepted power is either radiated or absorbed as losses within the antenna. Since antennas are typically designed to be low loss, ideally the majority of the power delivered to the antenna is radiated. The plot of S11 would typically be measured using a Vector Network Analyzer (VNA).

Another important parameter is the impedance of the transmission line. The Smith Chart is a tool for visualizing it as a function of frequency.

This chart can be used to increase understanding of transmission lines and how they behave from an impedance viewpoint.

The Smith chart is plotted on the complex reflection coefficient plane in two dimensions and is scaled in normalised impedance 50 ohms.

It is one of the most useful graphical tools for high frequency circuit applications. The chart provides a clever way to visualize complex functions. From a mathematical point of view, the Smith chart is a 4-D representation of all possible complex impedances with respect to coordinates defined by the complex reflection coefficient.

The Smith chart is used to display the actual antenna's impedance when measured on a VNA. Thus, it results a graphical method of plotting the impedance of an antenna, which can be a single point or a range of points as a function of frequency.

Ringraziamenti

Finalmente… o purtroppo… eccomi qui, giunta al traguardo, a scorrere con la mente questi anni universitari, anni ricchissimi di cambiamenti, di sacrifici, di soddisfazioni. Amo studiare e, come ogni cosa mi piaccia fare, ci metto sempre tutta la passione possibile,senza arrendermi mai. Sono la determinazione e la curiosità la chiave per la vittoria e il mio percorso universitario per me ne è stato la prova. Ora mi sento pronta e preparata ad affrontare il mio futuro e con grinta voglio, nonostante questa triste realtà, continuare a credere nei miei sogni e dare il meglio di me per realizzarli.

Studiare all'università è stata la migliore opportunità che potesse capitarmi e per questo ho da dire grazie a coloro che al mio fianco sono stati protagonisti di questa meravigliosa esperienza.

Innanzitutto, ringrazio la prof.ssa Arianna Menciassi e la Dott.ssa Monica Vatteroni che hanno creduto in me e mi hanno guidata nella parte finale del mio percorso di formazione che ha portato alla realizzazione di questa tesi. Un grazie va anche a Rossella, Michele ed Antonella che mi hanno aiutata a superare le difficoltà iniziali e all'ing. Elmar Huber, mio tutor durante l'esperienza tedesca.

Ma i ringraziamenti non possono essere tali se il più grande pensiero non va a loro, il fulcro del mio cuore: mia madre e mio padre. Perché se davvero esiste qualcosa che è per sempre non può non essere il nostro rapporto. La mia felicità la devo solo a loro che mi hanno cresciuta offrendomi sempre il meglio e soprattutto con un amore infinito. Spero di essere riuscita a renderli orgogliosi di me, questo è il regalo più grande che io possa donare loro (oltre al viaggio promesso, ovviamente!). Un ulteriore grazie va a mia mamma in qualità di mia migliore amica che mi sopporta con una pazienza che solo lei può avere, che mi conosce più di me stessa e di cui mi fido più di me stessa. Grazie anche al mio sosia maschio, Maura con la barba, detto Giulio, perché non smette mai di coccolarmi.

Se oggi sono qui sorridente e felice di aver realizzato il mio primo grande sogno lo devo anche a Peppe, compagno di vita, che sono 12 anni ormai che mi stringe forte la mano, condividendo con me ogni momento in salita ed in discesa. Grazie perché ti prendi cura di me con tanto amore, perché mi sopporti in silenzio e mi supporti con tanta forza ma soprattutto perché mi fai sorridere sempre il cuore.

Un ringraziamento speciale va ai miei amatissimi nonni, ai loro abbracci magici che mi riscaldano l'anima, all'incredibile capacità che hanno di farmi sentire davvero la loro campionessa. Grazie perché mi guardate ancora come se fossi una bambina e mi viziate (e ingrassate!) come nessun altro è in grado di fare .

Un grazie va anche ai miei zii e in particolare alla zia Roberta, che mi ha incoraggiata ad intraprendere questo percorso a Pisa e grazie alla quale non ho mai pagato nessuna

mora per le tasse (!), alla zia Lucia, mia unica vera insegnante d'inglese e alla zia Tiziana e le sue torte al cioccolato!

Non posso non nominare i miei cuginoni per i quali ero già "la dottoressa" ancor prima di diventarlo e i cuginetti Francesca, Federica, Chiara e Fabrizio che ringrazio per quanto mi adorano e mi vogliono bene, che ormai sono diventati grandi (anche troppo!) ma per i quali sarò sempre la mitica "Cuscinotta" che li strapazza di coccole.

Un ringraziamento immenso va ai miei compagni d'avventura che hanno reso l'esperienza universitaria molto più speciale. Grazie a Vero-thebest, con cui ho condiviso ogni gioia e dolore, ogni abbraccio di felicità e ogni lacrima di difficoltà, per le tante cose in comune (la determinazione e l'impegno, la voce alta e la "pagliacciaggine") che insieme ci rendono esplosive! Grazie a Luì, il mio primo grande amico incontrato a Pisa, per tutti i dolci che mi ha preparato, perché è un grande estimatore del mio Salento, perché mi dice sempre che sono la sua soddisfazione! Grazie alla mia patata, Rob, la donna più forte che conosca, alle nostre chiacchierate depressive accompagnate da pranzi dietetici altrettanto depressivi, alle nostre risate stupide! Grazie a Franci, al suo sorriso contagioso e al suo modo così intimo di volermi bene. Grazie a La Vivi, l'unica vera salentina tra le amiche, per la sua grinta e per aver sempre provato a lottare contro la mia pigrizia. Grazie a Mariangela, con cui sono felice di aver condiviso anche le forti emozioni di oggi.

Voglio ringraziare anche i miei amici di sempre, Fabio, Martina, Giorgio, Alberto, Roberto, Francesco, Matteo, Giorgia per la gioia che provo nel riabbracciarli ogni volta e perché non smettiamo mai di divertirci come ragazzini quando siamo insieme.

Dulcis in fundo, grazie al mio grillo parlante, Benedetta (non ti ci abituare al nome per esteso!) che non mi abbandona mai, neanche da lontano, per l'incredibile capacità che ha di ascoltare le mie lamentele e paranoie senza mai stancarsi, per aiutarmi sempre a risolvere i miei pasticci.

Un grazie, infine, va alla Nutella e al mio lettone (è inutile che stropicciate gli occhi, sì, avete letto bene!) perché niente più di loro ha saputo consolarmi e coccolarmi nei momenti più difficili.

Mi pare però che stia dimenticando ancora qualcuno… ah sì, me stessa! Voglio dirmi grazie per la forza che ci ho messo in questi anni e la sicurezza che ho acquisito dalle mie piccole soddisfazioni, perché non esiste né fortuna né destino ma solo la propria volontà nel lottare e poi vincere!!!